POLITECNICO DI MILANO

School of Industrial and Information Engineering

Department of Chemistry, Materials and Chemical Engineering

"G. Natta"

Master degree in Materials Engineering and Nanotechnology

GRAPHENE GROWTH ON ELECTRODEPOSITED POLYCRYSTALLINE COPPER AND RUTHENIUM

Supervisor: Ing. Luca MAGAGNIN

Assistant Supervisor: Prof. Roya MABOUDIAN

Master degree thesis:

Dario PIGLIAFREDDO Mat.: **769950**

Academic Year 2013 - 2014

CONTENTS

ABSTRACT

English text

In the last years graphene has generated a high interest in the scientific and industrial communities due to its peculiar and, in some cases, extraordinary characteristics. The aim of this thesis work is to explore new ways of producing it via chemical vapor deposition on polycrystalline metallic substrates. Specifically, since surfaces used nowadays for graphene growth are synthesized through expensive physical vapor deposition techniques, this thesis work has the purpose to investigate the development of cheap electrodeposited substrates as an alternative to traditional ones. It was possible neither to find any work attesting the feasibility of graphene growth on electrodeposited surfaces nor any previous attempt, through bibliographic researches. It was therefore important to determine a reliable method to produce it and only afterwards to improve its quality. The project is mainly focused on growth of ruthenium-based substrates on copper foil, respectively produced via electroforming for the copper layer and electroplating processes for ruthenium, and the subsequent growth of graphene through high temperature chemical vapor deposition with methane and hydrogen as precursors. Most of the preparation of the samples was carried out at Politecnico di Milano, where electroformed copper foil of about 40 μm in thickness was used as substrate for the electrodeposition of a 500 nm thick ruthenium layer. During the development of the work, the conformation of the described samples evolved to better face the challenges raised through the execution of the various tests. This evolution was also necessary to better comprehend the nature of the processes related to graphene growth and quality with respect to the changes performed on the substrate. Thanks to collaboration between Politecnico di Milano and the University of California, Berkeley, it was possible to develop the second phase of the work (graphene growth) in their laboratories, using a chemical vapor

deposition reactor to obtain a more reproducible and higher quality graphene. In Berkeley it was also possible to characterize both samples and graphene using atomic force microscopy, scanning electron microscopy, Raman and x-ray photoelectron spectroscopy to track the presence and the potential changes in graphene's quality.

Testo in Italiano

Negli ultimi anni il grafene ha generato un elevato interesse nella comunità scientifica e industriale grazie alle sue peculiari, e in alcuni casi straordinarie, caratteristiche. Lo scopo di questo lavoro di tesi è di esplorare nuove modalità di produzione di questo materiale tramite chemical vapor deposition su substrati metallici policristallini. In particolare, poiché i substrati attualmente utilizzati vengono ottenuti attraverso costose tecniche di deposizione fisica da fase vapore, la strada intrapresa in questo lavoro è stata quella di sviluppare substrati elettrodeposti a basso costo da sfruttare per la crescita di grafene. Attraverso ricerche bibliografiche non è stato rintracciato alcun lavoro che attesti l'effettiva possibilità di produrre grafene su superfici elettroformate né tantomeno è stato possibile individuarne tentativi precedenti. E' stato quindi importante determinare un affidabile metodo di produzione e, solo successivamente, il lavoro si è concentrato sul miglioramento della qualità del deposito. Il progetto svolto si fonda principalmente sull'utilizzo di substrati a base di rutenio e rame, entrambi realizzati tramite processo di elettroformatura, e la successiva crescita del grafene attraverso lo sfruttamento di un processo di chemical vapor deposition ad alta temperatura, impiegando metano e idrogeno come precursori. Buona parte della preparazione dei campioni è stata svolta presso il Politecnico di Milano, dove una lamina di rame elettroformato di circa 40 micron di spessore è stata utilizzata come substrato per l'elettrodeposizione di uno strato di rutenio di 500 nm. Durante lo sviluppo del lavoro, la conformazione dei campioni appena descritti si è evoluta per meglio affrontare le sfide incontrate durante l'esecuzione delle varie prove e per aumentare la comprensione della natura dei processi relativi alla crescita del grafene e le cause influenzanti la sua qualità rispetto ai cambiamenti apportati al substrato di crescita. Grazie ad una collaborazione tra il Politecnico di Milano e l'Università della California di Berkeley è stato possibile realizzare la seconda

fase del lavoro (l'effettiva crescita del grafene). nei laboratori di Berkeley si è utilizzato un reattore CVD, che permette il raggiungimento di una migliore riproducibilità e di qualità più elevate del grafene. A Berkeley è stato anche possibile caratterizzare sia i substrati che il grafene prodotto usando tecniche AFM, SEM, XPS e Raman per monitorare la presenza di grafene e le eventuali variazioni riscontrabili dal punto di vista qualitativo.

1 INTRODUCTION

1.1 Graphene

Carbon is the sixth element of the periodic table and the fourth most abundant element in the universe, was identified for the first time 220 years ago as component of both graphite and diamond [1]. Since then, more allotropic forms of carbon have been reported and a large interest has risen about the study of the characteristic properties of this element, that can adopt many structures ranging from diamond and graphite (3D) to graphene (2D), nanotubes (1D) or fullerenes (0D). Among these structures, three-dimensional allotropes have been known and widely used for centuries, whereas fullerenes and nanotubes have been only discovered and studied in the last two decades. With the exception of diamond which has a face-centered cubic crystal structure, it is possible to think of fullerenes, nanotubes and graphite as different structures built from the same hexagonal array of sp^2carbon atoms, that is graphene. Fullerenes and nanotubes can indeed be mentally visualized as a graphene sheet rolled into a spherical and cylindrical shape respectively, and graphite can be described as a stack of alternately shifted graphene sheets. For many years graphene was just a concept used for descriptive approach of more complex forms of aromatic carbon and a simple modelling system for solid state theoreticians. Except for the early

observations of chemically derived graphene sheets and, subsequently, the characterization of graphite monolayers on metals and carbides, very few studies considered graphene of some interest until 2004. However, the direct observation of isolated graphene monolayer on those years has generated a growing interest and just a few years were enough to bring several scientific communities to investigate the properties of this new material. The discovery of graphene takes place in 2004 by physicists Andre K. Geim and Konstantin S. Novoselov of the University of Manchester while they win the Nobel Prize in Physics in 2010[2].

1.1.1 Characteristics of graphene

The term graphene was coined as a combination of graphite and the suffix "ene" by Hanns-Peter Boehm[3], who described single-layer carbon foils in 1962 [4](Figure 1).

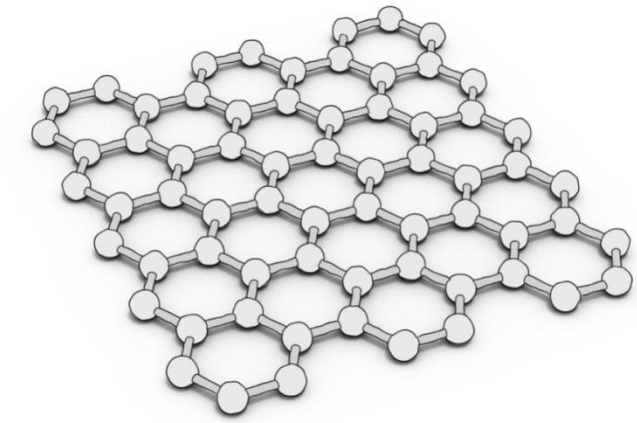

Figure 1 - Schematic representation of graphene structure.

Graphene is an allotrope of carbon whose structure is a single planar sheet of sp^2 hybridization form of carbon atoms, which are densely packed in a honeycomb crystal lattice, which comprises two triangular Bravais lattices. The atoms at the sites of one sub-lattice, (for example A) are at the centers of the triangles defined by the other lattice (in this case B) as shown in Figure 2. The unit cell has two atoms and it is invariant with respect to a rotation of 120° around any atom. The sp^2hybridization between one *s* orbital and two *p* orbitals leads to a trigonal planar structure with the formation of a bond between carbon atoms whit a distance of

1,42 Å. Graphene sheets stack to form graphite with an inter-planar spacing of 0,335 nm.

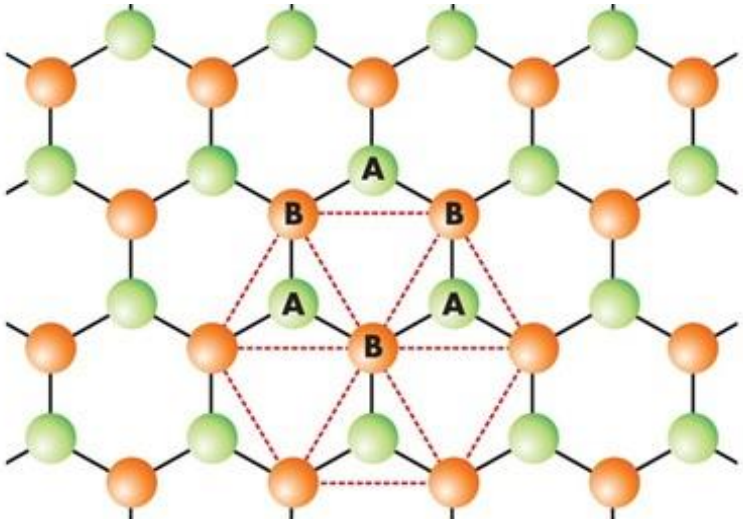

Figure 2 - Graphene lattice consists of two interpenetrating triangular sublattices, each with different colors.

The corresponding reciprocal lattice is again a honeycomb, with two nonequivalent vertices K and K' which in this case are both crystallographic points and Dirac points, because the electronic states relevant for transport are concentrated in two touching cones with the tips at K or K' as illustrated in the right side of figure1.3. The Bloch states corresponding to this reciprocal lattice are formed mainly by the carbon valence p_z orbitals, (considering the z axis perpendicular to the graphene plane) forming the two bands previously approximated as conic. The states in the lower cones are holelike or valencelike, while the upper cone states are electronlike or conductionlike, borrowing this terms from semiconductors vocabulary [5]. Half-filled bands in transition elements play an important role in the physics of strongly correlated systems since, due to their strong bonding character, the Coulomb energies are large, leading to strong collective effects, magnetism, and insulating behavior [6]. The energies of those bands depend on the momentum of the charge carriers within the Brillouin zone. In the low-energy regime, i.e. in the vicinity of the K and K' points, those two bands meet each other producing the previously mentioned conical-shaped valleys, as in Figure 3.

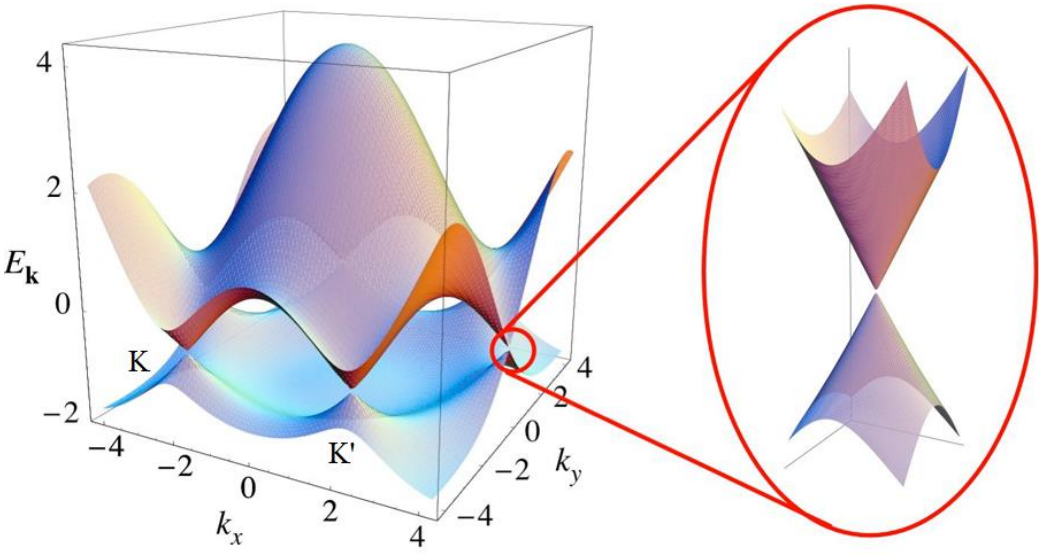

Figure 3 - On the left side the π–π band structure of graphene in the reciprocal lattice with K and K' points and on the right a magnification of the conic-shaped electronic dispersion.*

In this low-energy limit, the energy–momentum dispersion relation is linear and carriers are seen as zero-rest mass relativistic particles with an effective ‘‘speed of light’’ that is the linearity constant between energy and momentum of c* ≈ 106 m/s. The peculiar local electronic structure, thus, allows the observations of several phenomena which are typical of a two-dimensional Dirac fermions gas [7]. In the high-energy limit, the linear energy–momentum relation is no longer valid and the bands are subjected to a distortion leading to anisotropy, also known as trigonal warping [8]. Since carbon have four valence electrons, the other three occupied valence states of carbon form the deep-lying bands by sp^2 hybridization which are responsible for the toughness of graphene structure and due to the Pauli's principle, these bands have a filled shell. Upon stacking layers on top of each other, it can be obtained bilayered graphene, which exhibits its own set of very specific properties. The center of the aromatic rings of the upper graphene sheet sits on top of an atom of the lower sheet, so that the symmetry is trigonal rather than hexagonal. With the inter-plane interaction, the charge carriers acquire a mass and the dispersion recovers a parabolic shape described by the Schrödinger formalism. Nevertheless, bilayer graphene remains gapless if the trigonal distortion is not considered. The interaction of the two π and π* bands of each graphene sheet produces two other bands. A gap can be opened at the K or K' points, in the presence of an external potential [9]. Further generalization of the

perfect stacking results in graphite with alternating (ABAB, Bernal type) or staggered (ABCABC, rhombohedral type) arrangement depending on whether the lateral carbon atom shift changes direction from one layer to the next or not, as shown in Figure 4.

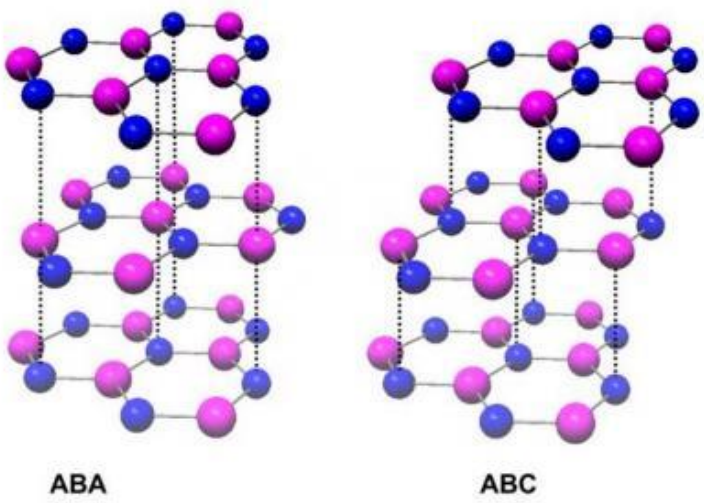

Figure 4 - Bernal and rhombohedral arrangements in grapheme.

The interplanar distance of ideal graphite is 3,45 Å but if successive planes are rotated with respect of each other, this spacing can increase (turbostratic case). While graphene has been known as a structural model to calculate band diagrams and predict electronic properties since the early 1940s, the experimental investigation of graphene properties, as a standalone object, has been almost inexistent until the very recent years because of the difficulty to identify and univocally characterize the single-atom thick sheet.

1.1.2 Properties and applications

The characteristic electronic structure previously reported makes graphene a suitable candidate for a wide range of applications in nanoscience and nanotechnology due to its relevant optical, electronic, mechanical, thermal and biochemical properties. The great potential of graphene in the electronic field derives from the mobility μ of the charge carriers, which can reach interesting values at low and even at room temperatures [10]. Generally, the limiting factor of the carrier mobility are disordered entities such as charged impurities or

microscopic ripples. It has been demonstrated that in single layer graphene (SLG) and in bilayer graphene, if the extrinsic source of disorder (defects) is eliminated, the carrier mobility at 300K can reach the extraordinary value of 200000 $cm^2V^{-1}s^{-1}$, becoming the greatest known value of μ for an existing material [10]. However up to now, the electronic world is based on Silicon, a semiconductor with a band gap of 1,1 eV between conduction and valence band. This band gap plays a significant role in modern device physics and technology and controls the performance of semiconductor devices as well as their transport and optical properties. The fact that graphene owns a zero band gap has, therefore, limited its applications in the electronic world due in some cases to its high leakage current in some devices. It has been possible however, to open and tune the band gap of bilayer graphene by applying an electric field [11], by doping [11], [12], or by hydrogenation of single layer graphene [11], [12]. This possibility to tailor the structure of graphene in order to change its electronic properties as well as its optical properties has therefore led to an increase in its potential applications making possible its use in solar cells and transistors (an example of graphene based transistor is shown in Figure 5). The interest in graphene does not stop with electronics, since another unique property of this two-dimensional material is its transparency.

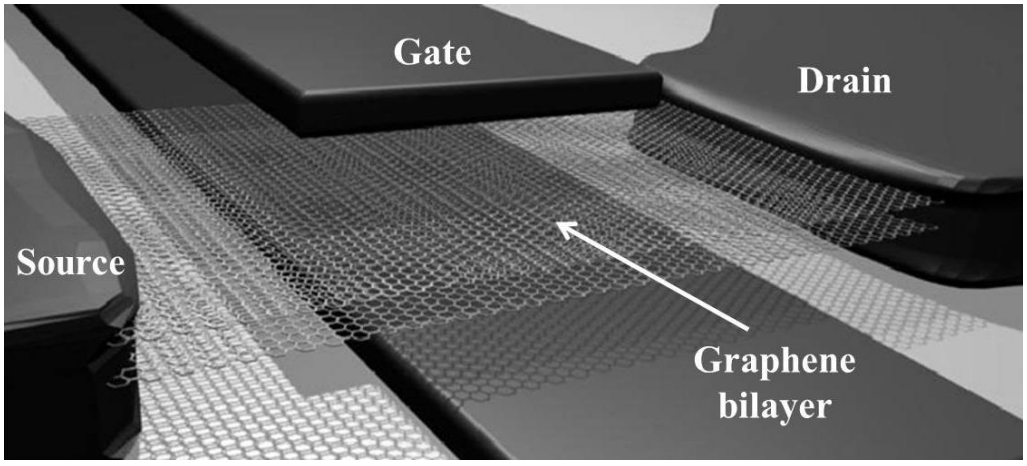

Figure 5 - Example of transistor based on grapheme.

When the light hit a material part of it can simply pass through the sample by transmission while the remaining part of energy, in the form of photons, interact with the system through light absorption, reflection, photoluminescence or light

scattering. Is the electronic and vibronic structure of a given material that determines the amount of light that will be transmitted, reflected or scattered. Single layer graphene, with its particular structure, is transparent at room temperature and it absorbs only 2-3% of the visible light that interact with it. As mentioned, the structure of the material influences its behavior, therefore, switching from single layer to multilayer graphene the interaction with light changes as well as the structure. As shown in the image in Figure 6 it can be immediately seen that single layer graphene is transparent, while flakes of two-layers graphene are clearly visible as a darker areas on the substrate. This means that only the structure of single layer graphene gives a completely transparent material, while increasing the number of graphene layers its reflectance will increase.

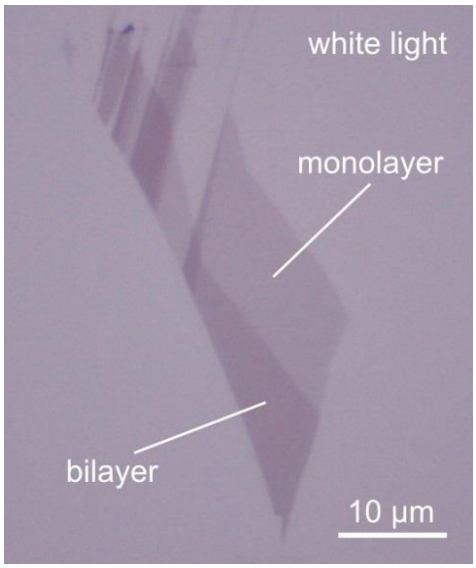

Figure 6 - Image of single and bilayer graphene flakes, respectively.

In the optoelectronic field, research is then focused on developing a reliable, cheap and highly reproducible fabrication technique which allows to obtain pure single layer graphene. The requirements for a material to be suitable in this field, are indeed the capability to transmit more than 90% of the incident light and a high electrical conductivity or small electrical resistance. Graphene owns these two crucial characteristic and consequently, touchscreens, liquid crystal displays (LCD) and organic light emitting diode (OLEDs) as well as LCD smart windows will be all soon based on graphene technology. Furthermore, the possibility of

replacing indium tin oxide (ITO) with graphene as transparent conductive oxide is under investigation. Recent developments have shown that graphene is potentially able to match the properties of ITO and thanks to its additional properties like flexibility, it can inspire more clever technology in optoelectronic field.

The strong, anisotropic bonding and the low mass of the carbon atoms make graphene a good material not only in terms of optical and electronic properties, but also for its thermal characteristics, since specific heat and thermal conductivity proved to be of great interest. The specific heat of a material C, represents the change in energy when the temperature changes by 1 K and determines not only the thermal energy stored within a body but also how quickly the body cools or heats. Recent measurements have evaluated the specific heat of the electron gas in graphene on the order of $2{,}6\ \mu Jg^{-1}K^{-1}$ at 5 K [13], lower than other two-dimensional electron gases and opening up interesting opportunities for graphene as a fast and sensitive bolometric detector, a device for measuring the power of incident electromagnetic radiation via the heating of a material.

As for the thermal conductivity (k), graphene shows a much higher value than the other carbon allotropes like graphite, diamond, carbon nanotubes or every other known material. Recently it has been measured a thermal conductivity greater than $5000 Wm^{-1}K^{-1}$ for suspended graphene at room temperature, being twice the one of diamond and five times greater than the value of graphite. Thermal conductivity simply relates the heat flux per unit area to the temperature gradient by means of $\boldsymbol{Q^n = -k\nabla T}$, where the negative sign indicates that the heat flows from high to low temperature. As in the case of optical properties a high quality of the graphene sample is required in order to reduce impurities, intrinsic disorder or even residues from sample fabrication that could lead to a decrease in thermal conductivity. It has also been noted [13] that k tends to decrease when graphene is in contact with a substrate, this behavior is due to the high sensitivity to surface or edge perturbations of phonon propagation. Hence, the study of thermal conductivity as well as the optimization of the fabrication processes is of crucial importance given the potential application of graphene in the field of thermoelectric. Indeed, the devices' size continues to shrink while the circuit density increases, thus, a high thermal conductivity is essential in order to

efficiently dissipate heat and to keep the components at a suitable working temperature. Despite graphene thickness of just one atomic layer, it shows exceptional mechanical properties. Using an atomic force microscope (AFM), scientists pressed graphene that was lying on the top of a circular wells and measured how far graphene could be pushed with a small tip without breaking it and it revealed to be stronger than diamond, graphite and three hundred times stronger than steel. It has been measured that the tensile strength of graphene could exceeds even 1 TPa and at the same time, graphene is also very stretchable and flexible. Measurements have shown that is possible to elongate graphene up to 20% of its initial length. With these peculiar mechanical properties, applications in high resistance new generation composite material, flexible displays, but also in pressure sensors are possible.

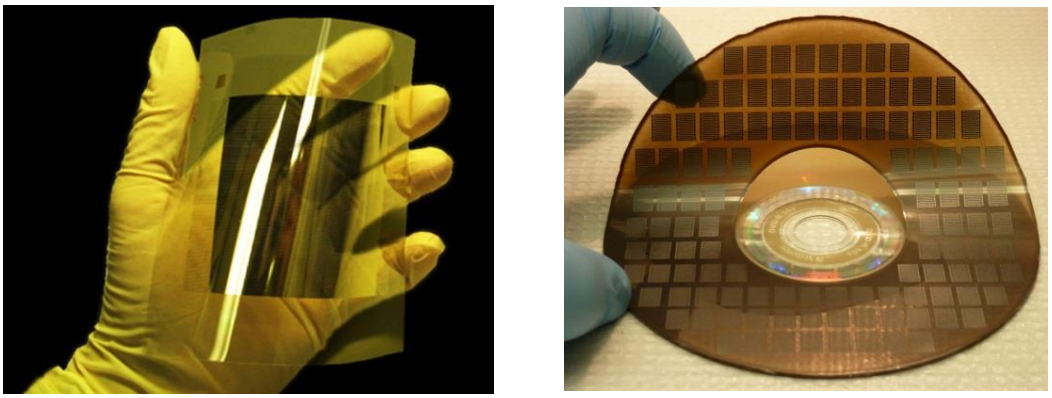

Figure 7 - On the left is shown the flexibility properties of a graphene device and to the right a sheet of laser-scribed graphene micro-supercapacitors.

Furthermore, like other carbon allotropes, graphene can also adsorb and desorb various atoms and molecules, like NO_2, NH_3, KOH and As. These weakly attached molecules often act as donors or acceptors and they lead to changes in the charge carriers concentration even though graphene can still remain highly conductive. It is even possible for graphene to be functionalized by several chemicals (OH^-, F^-), forming graphene oxide and fluorinated graphene. In the latter case, carbon atoms switch from sp^2 to sp^3 hybridization, with each carbon atom bound to one fluorine $(CF)_n$. This material is called fluorographene and it shows insulating behavior and it is relatively inert. Applications are mainly in biological field, thanks also to its hydrophilic nature that enhance biocompatibility. It has been also reported an application as magnetically

responsive drug carrier that can serve both as a magnetic resonance imaging and photoacoustic contrast agent. However, following these last considerations and aside the potential applications based on its functionalization, graphene will surely be the technology base for new generation of gas and chemical sensors. Graphene finds another application in the field of energy storage. Among the main difficulties in this field of application, the principal has always been energy storing in batteries and capacitors while not being used. Batteries can potentially store a lot of energy, but they cannot be charged quickly, while capacitors can be quickly charged, but they cannot hold as much energy as batteries. The goal, in the past years, it has been obviously to associate the positive characteristics of both batteries and capacitors without compromises. Lately, the focus it has been to enhance the capabilities of lithium ion batteries by incorporating graphene as an anode in order to offer higher storage capacities with much better longevity and charge rate. Furthermore, graphene is being studied and developed to be used in the manufacture of supercapacitors, devices able to be charged very fast and to store a great amount of energy. The applications for this kind of devices will probably be in the field of smart phones and portable computing, while graphene-enhanced lithium ion batteries might be used in electrical vehicles.

1.2 Methods of synthesis of graphene

1.2.1 Mechanical exfoliation

This method consists to impress on a graphite sample the energy required to break the cohesion forces between the planes and exfoliate it down to a single graphene sheet in the matrices. Graphene tends to form irreversible agglomerates or even restack to form graphite through Van der Waals interactions. Therefore preventing aggregation is essential for graphene sheets because most of their properties are strictly associated with individual sheets. The energy of Van der Waals interaction between the planes is $2eV/nm^2$ and the force required for exfoliation is approximately 300 $nN/\mu m^2$ [14].

1.2.1.1 Exfoliation with physical methods

Using a highly oriented pyrolytic graphite (HOPG) sample, the extremely weak force needed for exfoliation can be easily achieved with normal adhesive tape and then transferred onto Si/SiO2 molds. Previously the detachment of graphene sheets was achieved exploiting the forces developed at the tip of an AFM or STM during their use. The remarkably simple yet efficient method developed by Novoselov and Geim consists in using common adhesive tape to repeat the stick and peel process a dozen times which statistically brings a 1 μm thick graphite flake to reach a monolayer s. After checking for smooth and thin fragments on the tape with optical microscopy (which can reveal monolayers because of the peculiar optical characteristics of graphene), graphene and graphite pieces are then transferred onto cleaned substrate (usually Si or SiO2) gently pressing the tape on it. An example of this process is represented in Figure 8*:*

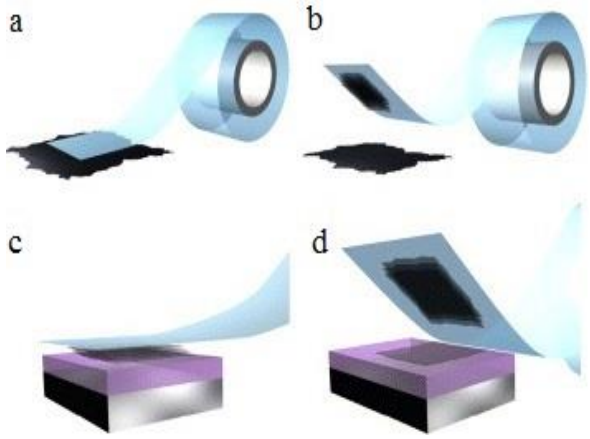

Figure 8 - Micromechanical exfoliation of graphene. (a) Adhesive tape is pressed against graphite so that the top few layers are attached to the tape (b). (c) The tape with flakes of layered material is pressed against a surface of choice. (d) Upon peeling off, the bottom layer is left on the substrate.

The main drawback of the physical mechanical exfoliation technique is that the process can leave glue residues on the sample, which is proven to have the tendency to limit the carrier mobility. A post-deposition heat treatment in reducing atmosphere is thus required to remove residual traces of glue. Characteristics of the produced samples:

- Good mechanical, electrical, thermal and structural properties
- High carrier mobility (1000 ÷ 3000 $cm^2V^{-1}s^{-1}$)

- Difficulties in controlling the size of the obtained flakes (approximately 5 μm)
- Method not suitable for industrial processing (appropriate only for research purposes)

1.2.1.2 Mechanical exfoliation in solution

This method uses solvents that allow the weakening of the cohesive strength of Van der Waals forces through the insertion of reagents in the space between graphite's planes. Dispersions containing graphite powder in a suitable solvent enables its intercalation through the planes and annealing at 1000°C followed by sonication complete the separation process as shown in Figure 9. Is therefore obtained a solution containing a dispersion of monolayers and multilayers graphene flakes, which subsequently undergoes to separation allowed by the differences in densities (Density Gradient Ultracentrifugation (DGU)) which will insulate the desired monolayers.

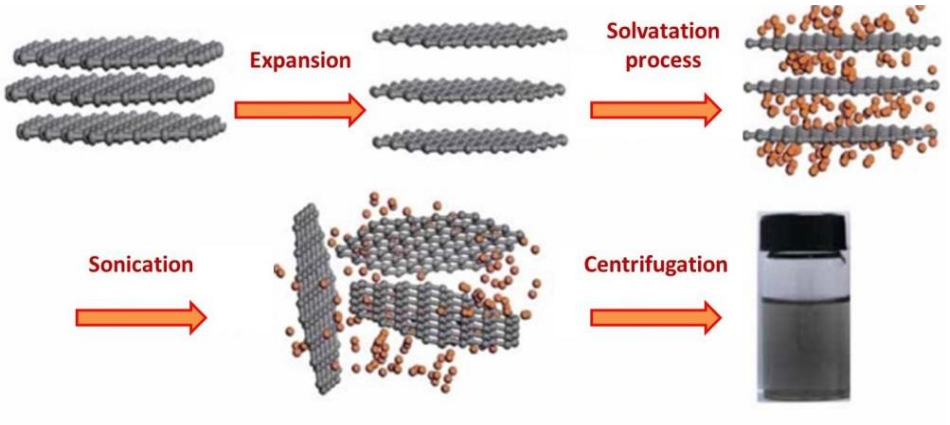

Figure 9 - Mechanical exfoliation performed in solution.

The utilized solutions are different, in particular Blake et al. and Hernandez et al. have shown that graphite can be exfoliated with N-methyl-pyrrolidone to produce monolayer graphene [15], [16]. Using this method the produced planes are almost defectless, however the process is very expensive due to the cost of the solution and because of the high boiling point of the solvent, the subsequent graphene deposition can be difficult. Lotya et al. [17] used instead a stable surfactant (sodium dodecylbenzenesulfonate) in aqueous solution to repel the otherwise

entangled monolayers exploiting the Coulomb repulsion among the surfactant covered sheets.

1.2.1.3 Exfoliation via intercalated graphite

This method was developed by Li et al. [18] and consists in using intercalated graphite with an organic solvent solution.

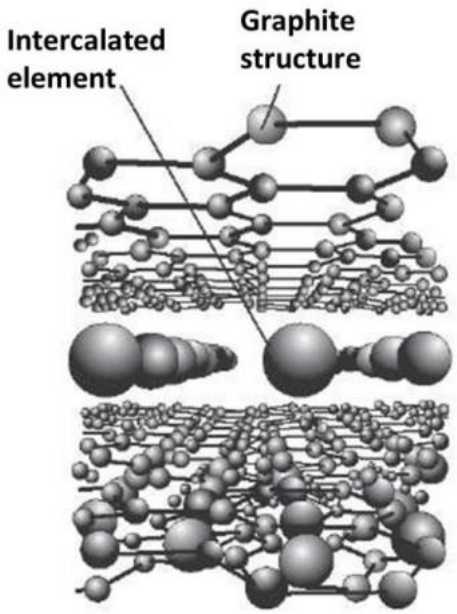

Figure 10 - Structure of intercalated graphite.

Graphite intercalation compounds are complex materials having formula XCy where the element or molecule X is inserted (intercalated) between the graphite layers which remain largely intact. The first step of the process is heating the intercalated graphite at 1000°C of temperature promoting the formation of gas and the subsequent production of multilayer graphene. To obtain monolayers, graphite is again intercalated with oil and the production of high quality individual layers is favored by sonication. The presence of elements between graphite layer leads to an increase in the interplanar distance (generally from 0.34 nm to approximately 1 nm) allowing an easier exfoliation.

Characteristics of the produced samples:

- Chemical treatments can cause the presence of defects and might lead to unintentional production of oxidized or functionalized sheets;

- The presence of functional groups generally promotes insulating effects to the graphene, while the presence of defects leads to the development of semiconductor characteristics;
- The oxide can be removed with thermal or chemical reduction processes.

Graphene obtained with this procedure has a large prevalence of multilayer flakes with approximate size of 400 nm and the presence of defects cannot be eliminated (the obtained product can be used for sensing devices).

1.2.2 Chemically obtained graphene from synthesis of graphene oxide

At present, chemical conversion of graphite into graphene oxide has emerged to be a practicable way to achieve graphene based monolayers in considerable quantities. Graphite oxide is usually synthesized through graphite oxidation using oxidants such as concentrated sulfuric acid, nitric acid and potassium permanganate as shown by Hummers experiences [19]. Compared to pristine graphite, graphene oxide is heavily oxygenated, bearing hydroxyl (-OH) and epoxy groups on sp^3 hybridized carbons on the basal plane and carbonyl or carboxyl groups (-COOH) located at the sheet edges on sp^2 hybridized carbons. Hence, graphene oxide is highly hydrophilic and can be easily exfoliated in water, creating a stable dispersion mostly consisting of single layered graphene oxide flakes. Chemical reduction of graphene oxide sheets has been performed with several reducing agents including hydrazine, and sodium borohydrate. Hydrazine hydrate, unlike other strong reductants, does not react with water and was found to be the best choice to produce very thin and fine graphite sheets. During the reduction process, the brown colored dispersion of graphene oxide in water, turns black and the reduced layers tend to aggregate and precipitate [20], [21]. This happens because of the tendency of the reduced graphene oxide to become less hydrophilic due to the removal of oxygen atoms and thus becoming easier to exfoliate in water and polar solvents as represented in Figure 11.

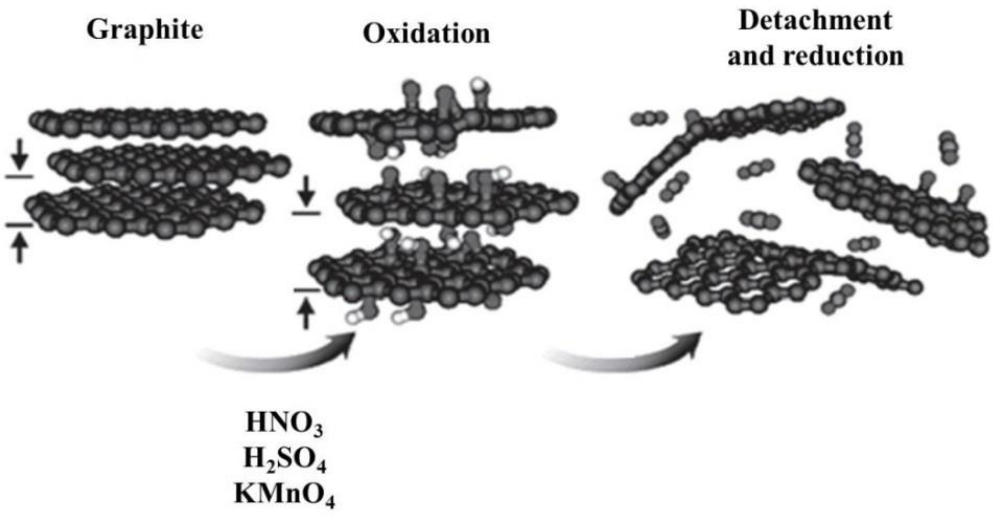

Figure 11 - Representation of the process with oxidation followed by reduction reaction.

Characteristics of the outcome:

- Production of both multilayer and monolayer
- Sonication method can be used to obtain individual planes
- Layers are thicker as a result of the presence of functional groups
- Oxidized graphene has insulating properties, however part of the oxide can be removed by thermal or chemical reduction

1.2.3 Growth supported by substrates

Three different types of deposition techniques are used for graphene growth:

- Thermal CVD
- PECVD: Plasma-enhanced chemical vapor deposition
- Thermal decomposition of substrates

1.2.3.1 Thermal CVD

Consists in the diffusive and convective transport of depositing species to a substrate and subsequent deposition enhanced by thermal energy, this process will be better described in chapter 3 since is the chosen process for the deposition of graphene in this thesis work.

1.2.3.2 Plasma Enhanced Chemical Vapor Deposition (PECVD)

The first report of the production of monolayers or few layers of graphene by PECVD involved a radio frequency PECVD system to synthesize graphene on various substrates in which grapheme sheets were produced from a gas mixture with 5% to 100% of CH_4 in H_2 (total pressure 12 Pa), with 900 W of provided power and substrate at 680°C of temperature [22]. Since then, much effort have been devoted to understand the graphene growth mechanism and to optimize experimental conditions to control the thickness of graphene films. Plasma enhanced chemical vapor deposition allow very short deposition time (less than 5 minutes) and a relatively low growth temperature of 650°C compared to the thermal CVD approach (approximately 1000°C). Growth mechanism is based on an equilibrium mechanism in which is present both graphene deposition through surface diffusion of carbon-bearing growth species provided from precursor gas and etching caused by atomic hydrogen.

1.2.3.3 Thermal decomposition of SiC

For large scale FLG (Few Layer Graphene) production, methods of growing graphene epitaxially on silicon carbide by thermal decomposition are showing promising results. After SiC substrates annealing at high temperatures, silicon atoms selectively desorb from the surface and carbon atoms are left on the substrate, naturally forming FLG (Figure 12). Because SiC is a wide band-gap semiconductor, FLG on silicon carbide can be useful as graphene substrate for electronics applications. SiC wafer technology is rapidly improving in terms of production cost and scale, and thermal decomposition method can be considered suitable for large-scale Few Layer Graphene fabrication.

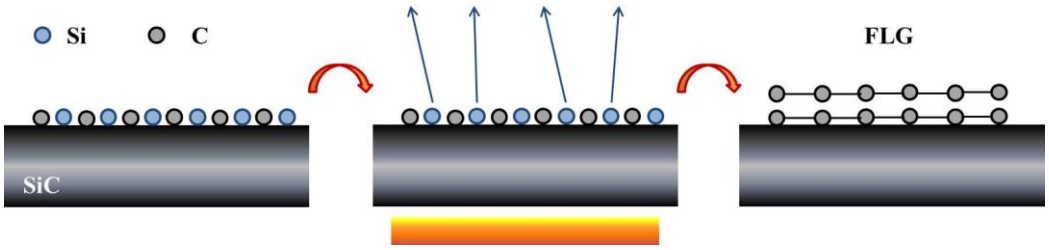

Figure 12 - Schematic illustration of thermal decomposition process.

Characteristics of the product using thermal decomposition:

- The thickness of the produced layer depends on the heating time and temperature;
- Presence of defects and inhomogeneities in the thickness;
- Lower mobility, approximately 100 times less than that exfoliated, also due to the presence of the substrate.

Therefore, two fundamental complications must be resolved before thermal decomposition method can have an industrial breakthrough. As said before, the FLG obtained so far present a relatively wide distribution of thicknesses and because the electronic properties of Few Layer Graphene also depend on its thickness, a reproducible way of growing wide, uniform FLG with the desired thickness must be developed. Moreover, it is still not fully understood how the SiC substrate affects FLG's physical properties and lacking a practical evaluation of the substrate's effects, it is difficult to choose the most appropriate applications of FLG [23], [24].

1.2.4 Production of graphene ribbons

1.2.4.1 Un-zipping of carbon nanotubes (CNTs)

In order to obtain graphene nanoribbons [25], [26] two possible procedures can be considered. In both cases nanotubes are 'unzipped' and rolled open to produce nanoribbons. The first method was developed by Jiao et al. [27] in which multiwall nanotubes are dispersed in a polymeric layer and then deposited on a Si substrate. The produced film is then removed using a KOH solution and at this stage the nanotube is subjected to argon plasma decomposition to obtain

nanoribbons. After removal of polymer residue with acetone and heating at 300°C for 10 min, is possible to obtain mono or multilayer nanoribbons (up to 10-20 nm wide), mainly used for the production of graphene transistors. The unzipping process of a carbon nanotube to produce a graphene ribbon is shown in Figure 13.

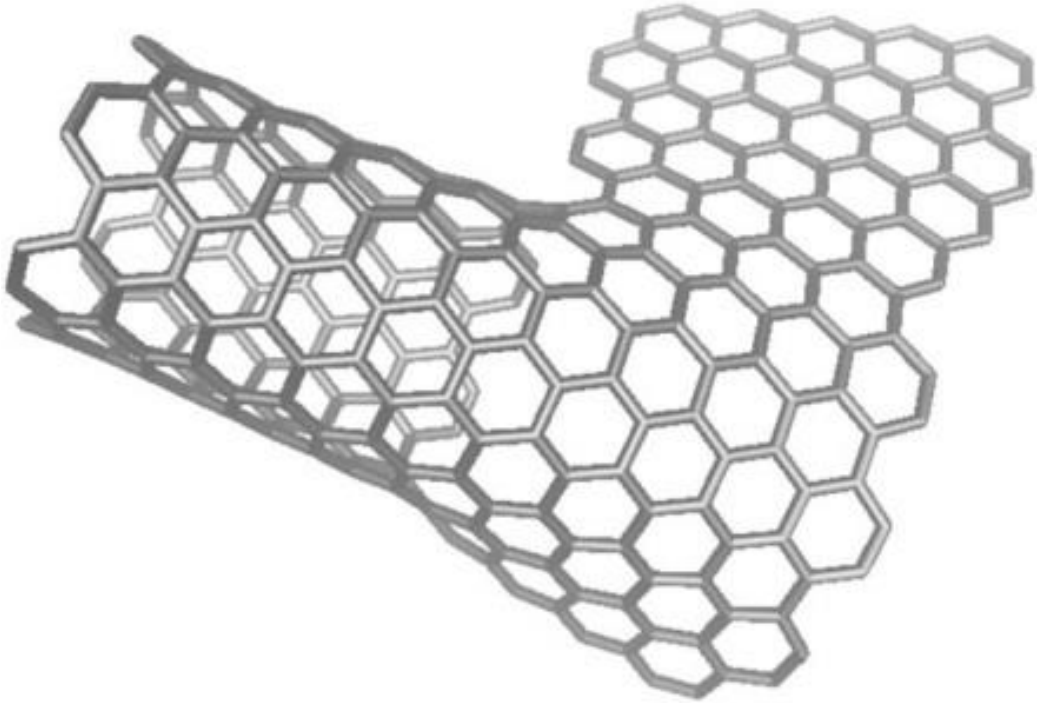

Figure 13 - Unzipping of a carbon nanotube to produce a graphene layer.

Another method has been developed by Kosynkin et al. [28] and it use multiwall carbon nanotubes (MWCNT) consisting of 15-20 concentric cylinders, with diameters of approximately 40-80 nanometers. This method consists in treating the nanotubes with concentrated sulphuric acid followed by potassium permanganate as oxidizing agent at room temperature and finally heating the system at 55-70 °C. This process chemically unzips the nanotubes, forming nanoribbons up to 4 micrometers long and 100-500 nanometers wide with thicknesses from 1 to 30 graphene layers. It is probable that the chemical mechanism of the unzipping process involves the oxidation of carbon-carbon double bonds in the nanotubes, therefore negatively influencing the nanoribbons conduction properties. By means of a reducing agent it is possible to improve the conductivity obtaining multilayer ribbons with improved characteristic for electronic applications.

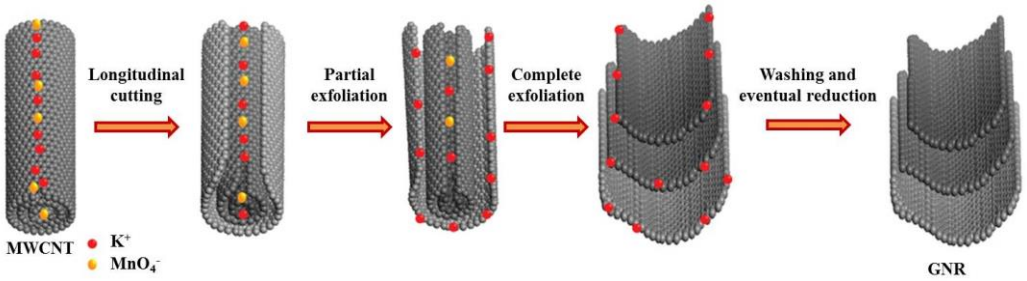

Figure 14 - Schematic representation of Kosynkin et al. method.

The main characteristics of Kosynkin procedure are the ability to produce mono, bi and multilayer graphene ribbons according to the size and number of concentric cylinders in the used nanotubes and the production of a good quality outcome.

1.2.4.2 Chemical method

This method from Mullen et al. [29] is a bottom-up process to fabricate graphene nanoribbons (GNR) onto gold surfaces from 10,10-dibromo-9,9-bianthryl precursor monomer. In the fabrication procedure, thermal deposition of monomer onto a gold surface removes the halogen substituents from the precursors and provides the molecular building blocks for the desired graphene ribbons in the form of surface-stabilized biradical species. During a first thermal activated step, the biradical reactants diffuse across the substrate and undergo radical addition reaction to form linear polymer chains with formation of CC bonds at 200°C forced by the specific chemical functionality pattern of the monomer. In a further thermal activation step a surface-assisted cyclodehydrogenation establishes an extended fully aromatic system creating the typical graphenic network which is pursued. The described process is shown in Figure 15.

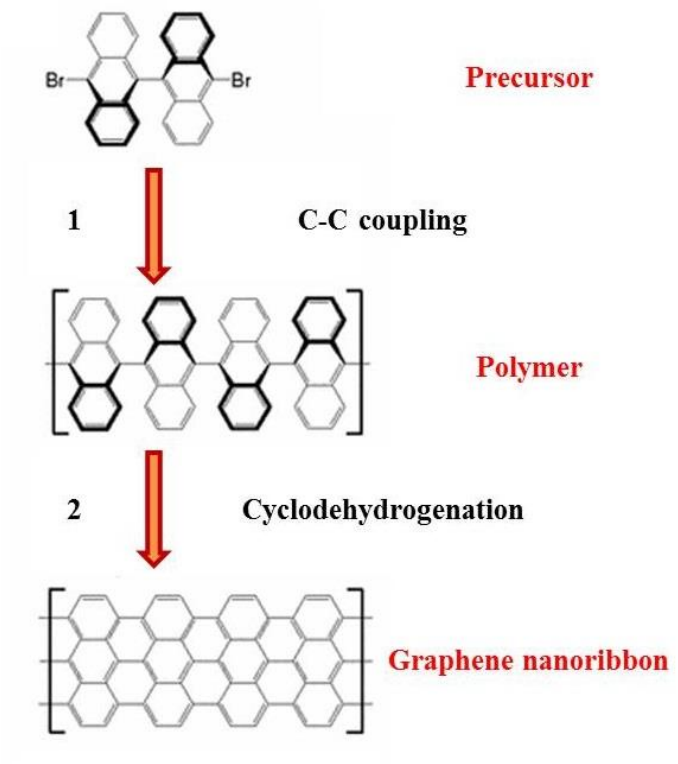

Figure 15 - Scheme of the surface-supported fabrication of graphene nanoribbons (GNR) via two-step process: (1) dehalogenation of precursor molecule 10,10'-dibromo-9,9'-bianthryl followed by a C–C coupling and (2) cyclodehydrogenation.

1.3 Graphene on polycrystalline metals

Graphene, as previously exposed, has been typically produced from graphite using several methods, these techniques are suitable for producing large-area graphene films and during the years, researchers have tried to further develop them in order to grow high quality graphene sheets onto extended surfaces. Particularly in the past few years, a great interest risen on the graphene growth over polycrystalline metals and a brief overview on the fabrication techniques and the ways to control the graphene growth on polycrystalline metals will be illustrated. Using a specific range of experimental conditions, graphene growth is possible on different metal substrates such as group 8 (iron and ruthenium), group 9 (cobalt, rhodium, iridium), group 10 (nickel, platinum) and group 11 metals (copper and gold) as well as on stainless steel and commercial alloys like Si-Cu, which are suitable substrates for supporting thin films graphene growth. Generally, the use of Ni and

especially Cu is predominant because their availability and processability reduce costs, moreover, it has always been possible to grow large-area graphene films on these substrates and to transfer graphene sheet into electronic devices for testing. The ability of a metal to produce high quality graphene films is affected by several factors, the main one being, like in any other field, production and fabrication cost, since usually the metal substrate is etched away during the transfer process. Differences between metals are also a key factor, since they may promote graphene formation by segregation(carbon is absorbed into the substrate at high temperatures and then segregates to the surface forming the honeycomb lattice of graphene during cooling), or the metal substrate acts as a catalyzer for the decomposition of the carbon source promoting carbon fragmentation; this method of graphene growth is called surface growth mechanism. The choice to use polycrystalline metals arises from the difficulty to produce and grow single crystal metals and as a consequence, to grow large-area single layer graphene on this kind of substrates. The characteristic of polycrystalline metal films, usually obtained from sputtering or evaporation techniques, is that the structure presents multiple grains. An annealing process is then usually required to improve surface roughness or to promote a specific metal facet. However, grain boundaries influence the quality of the graphene films, since it has been demonstrated that they are the source for graphene defects and nucleation of multilayer graphene. Obviously, the thickness of the metal film determines the size of the metal grains [30], resulting in larger grains for thicker samples. Graphene growth, is less effective on thicker samples, therefore, an appropriate range of parameters has to be chosen. Since defects lead to nucleation sites, reducing their number is crucial in order to obtain high quality graphene. For the surface catalyzed reactions, the number of graphene nucleation sites can be controlled by reducing the surface defects of the metal, but also adjusting the rate of carbon exposure, since slower rates result in fewer nucleation sites and hence larger graphene domains. However, slower rate means a longer exposure time at high temperature and the effect of these operative conditions on the substrate structure and on the graphene quality has to be taken into account. A good selection of a range of operative

parameters and good substrate quality are therefore fundamental requirements in order to grow high-quality graphene.

1.3.1.1 Iron and Ruthenium

Graphene growth on polycrystalline iron is usually attained via chemical vapor deposition (CVD) at low pressures and relatively low temperatures (600-800°C). The carbon source is generally acetylene and reduced surface coverage as well as reduced graphene thickness is observed lowering source exposure times. The number of graphene layers can also be controlled varying the metal film thickness, resulting in thinner graphene with thicker iron films, is also reported that for Fe films thinner than 5nm only carbon nanotubes were formed [30].Temperature plays similarly a key role, leading to thicker graphene films for higher growth T, but it also reduces the number of defects, therefore a balance of operative conditions has to be achieved. As for Ruthenium, reports have shown the possibility to grow graphene on different substrates based on this material. Indeed, Ru sputter-coated on SiO_2 (analogue to that in this work), fused silica and sapphire (Al_2O_3) revealed to be suitable substrates for graphene growth. Generally, ethylene is used as carbon source at temperatures around 800-950°C, then a cooling process in UHV is carried out in order to obtain single layer graphene continuous across grain boundaries. This thesis work shows that is also possible to grow graphene via chemical vapor deposition, on electrodeposited Ru over electrodeposited copper, using a mixture of methane and hydrogen gases.

1.3.1.2 Group 9 metals

Cobalt, as single crystalline metal deposited on sapphire, gives the chance to grow uniform single layer graphene through CVD of methane at high temperature, instead, with a polycrystalline structure (with grain size < 3 μm) and deposited on SiO_2 or Si, it leads to an inhomogeneous film containing both single layer graphene and multilayer graphene flakes due to its high density of grain boundaries. Acetylene is the carbon source and, together with low pressures and high temperatures (from 800 to 1000°C) gives the possibility to grow non uniform graphene of varying thickness which can be reduced raising the temperature or decreasing the exposure time. It has been studied that decreasing the thickness of cobalt films lead to an increase in the percentage of monolayer graphene on the

metal substrate (Figure 16). Furthermore, the etching of the Co substrate is possible using aqueous solutions of $FeCl_3$ or HCl. As for Rhodium, graphene growth is allowed when Rh foils are repeatedly annealed under ultra-high vacuum conditions in order to promote the emergence of the Rh(111) face [30]. Graphene growth is obtained after exposure of the metal surface to benzene (C_6H_6) vapor and thanks to segregation of carbon at grain boundaries. Graphene islands begin to grow when the threshold solubility of carbon in rhodium is reached and subsequently it covers the entire substrate surface by coalescence. Possibility of forming multilayer graphene is due to further segregation of carbon from the bulk during cooling, therefore setting the right growth temperature is crucial.

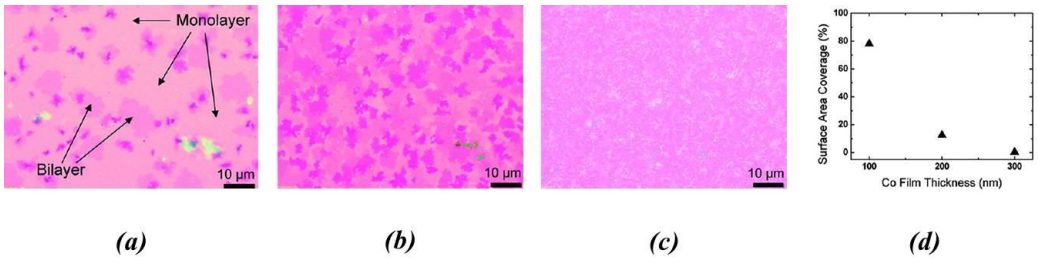

Figure 16 - Optical micrographs of graphene grown on (a) 100 (b) 200 (c) 300 nm Co films. (d) Percentage of surface area covered by graphene as a function of substrate thickness. Data retrieved from [30]

By pulsed laser deposition and electron beam evaporation it is possible to deposit single crystal Iridium films on sapphire or YSZ (yttria-stabilized zirconium oxide) on which graphene growth proved to be possible. CVD of ethylene at 677°C under ultra-high vacuum conditions with 10 minutes of carbon exposure were performed in order to obtain monolayer graphene on Ir/sapphire, with a surface covering greater than 95% of the total surface. As for Ir/YSZ, carbon source is acetone and graphene growth starts at approximately 327°C and proceeds to a well-ordered graphene monolayer upon heating to 727°C.

1.3.1.3 Nickel and Platinum

Nickel with copper has been one of the most used substrate to be used to grow graphene. It is possible to use a large variety of carbon sources, as methane, benzene, acetylene, ethylene or even PMMA [30], [31]. CVD growth of graphene has been primarily performed at atmospheric pressure, allowing graphene to extend across the grain boundaries of nickel to form continuous films. A slow

anneal of the Ni substrate has to be done in order to obtain larger grain sizes and therefore better graphene quality. Reports [30], [32] have studied the effect of growth temperature, gas mixing ratio and growth time in chemical vapor deposition process, showing that high temperatures, high hydrogen concentration and short growth time are fundamental for synthesizing few layer graphene with low number of defects. Cooling rate also plays a crucial role in graphene deposition, since thinner graphene is obtained with fast cooling rate and short growth time. Methods have been developed for graphene growth using CVD on Ni substrate with a mixture of methane, argon and hydrogen gases in order to obtain the desired outcome. The use of Ni for industrial applications is due to the ease for graphene to grow on it, but also to its propensity to be quite easily etched away using HCl solutions or $FeCl_3$ aqueous solutions. Graphene growth on nickel surfaces has also been demonstrated through diffusion and segregation of carbon from underlying amorphous carbon or nanodiamond films [30]. On platinum, growth of uniform graphene monolayer has been achieved through chemical vapor deposition using methane as carbon source. Low pressure coupled with high temperatures of about 1000°C have been used during the process, with particular attention on the temperature range, since it controls the thickness of graphene layers. On the contrary to nickel or copper, increasing the temperature leads to a rise of number of graphene layers. Exposure time and the flow rate also play an important role, since increasing these two parameters leads to irregularity in the shape of bi or multilayer graphene [30].

In Figure 17 are shown some SEM images of graphene grown on platinum foils with particular attention on the effect of Pt grain boundaries (Figure 17(c),(d)).

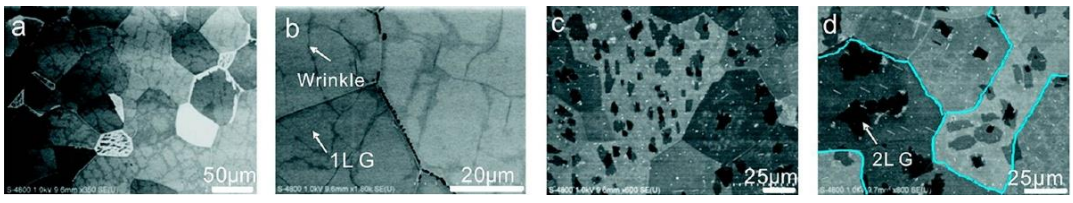

*Figure 17 - **(a,b)** SEM images of single layer graphene grown on platinum foils. (**c,d**) SEM images of sequential growth of bilayer flakes with irregular boundaries on Pt domains. Data retrieved from*[30]

1.3.1.4 Copper and Gold

Copper has been one of the first and most widely used metallic substrate for graphene growth and both ambient or low pressure conditions are suitable for its deposition. The interest in Cu is due to the peculiar characteristic of copper to yield to a self-limiting graphene growth process. First studies demonstrated centimeter scale graphene film in copper foils through high temperature CVD of methane under ultra-high vacuum conditions. This film was characterized by the presence of approximately 95% of single layer graphene, while the remaining was bi and multilayer graphene. The particularity is that graphene thickness was independent from methane exposure time and from copper thickness. Cu purity instead, influences the number of graphene layer, starting from single layer graphene for 99.999% Cu foil going to bilayer graphene for 99.8%. Moreover, sonication in acetone prior annealing and reduction of annealing pressure were found to be beneficial to graphene uniformity, as well as hydrocarbon concentration which impact graphene homogeneity due to its effect on the number of nucleation sites, producing fewer sites for lower concentrations.

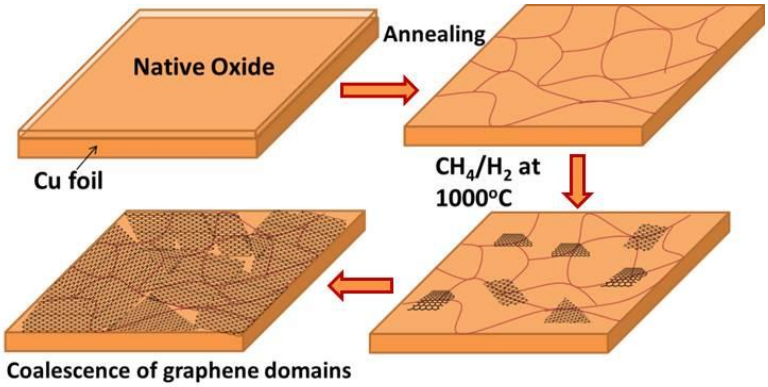

Figure 18 - Stages of graphene growth on a copper polycrystalline substrate.

The choice of operative pressure can also influence the carbon source concentration that has to be managed during the process, because with low pressure conditions, is preferable to keep as low as possible the methane concentration at the beginning of the deposition in order to reduce the number of nucleation sites and then increasing it during the reaction to promote continuous graphene coverage. In atmospheric pressure instead, graphene easily grow on polycrystalline copper across its grain boundaries. With low CH_4 concentrations,

graphene growth on electrodeposited copper is possible, with a surface covering always greater than 90%, while using high gas concentrations brings to graphitic domains. Furthermore, mechanical polishing of the copper surface leads to a higher quality of the graphene film due to the reduced number of sites that can nucleate on the smoother surface. Low and high temperature growth has also been demonstrated on copper foils [30], [31] using both liquid and solid carbon sources, as example is possible to directly place the carbon source on the top of the Cu substrate prior to heating. By this mechanism, monolayer graphene may grow through the annealing of the copper foils with an amorphous carbon coating at 1030°C under hydrogen flow. Hydrogen is also fundamental for low temperature growth using PMMA as carbon source operating at 800°C, since the right mix of argon and hydrogen can control graphene thickness, obtaining monolayers for high H_2 flow rate. Moreover copper etching leaves good quality graphene after its removal as has been shown using Cu etchant solutions such as ammonium salts or aqueous solution of iron chloride. Graphene growth is also possible on gold substrate, but obviously the problem with gold is its cost, especially because most of the time, in order to obtain the graphene layer and utilizing it, is needed the etching of the metal substrate that could lead to an expensive waste of precious material. Anyway, atmospheric pressure CVD using methane at 850-1050°C produce high monolayer graphene percentage on gold surfaces. Temperature has a weak influence on the thickness of graphene and on defect concentration, but using higher T means having a more defective graphene domains and multilayer graphene instead of single layer.

1.3.1.5 Graphene on alloys

It has also been investigated the possibility to grow graphene for several alloys. Stainless steel can act as a substrate for graphene growth using chemical vapor deposition at approximately 800°C and with these process conditions in both low and atmospheric pressure produces inhomogeneous growth. Cooling temperature plays again an important role in the process, since with high cooling rates (greater than 140°C/min) there is no detection of graphene, while with very slow cooling rate there is the chance to obtain graphite-like material. As for carbon source exposure time, it has been noted that it does not really influence the number of

graphene layers but increasing deposition times, higher graphene quality is obtained, while significantly shorter exposure leads to discontinuous graphene growth. Ni-Cu alloys can be used to grow graphene in sandwich structures with SiO_2/Si substrate. Carbon impurities in the nickel film, almost 3 atom %, act as carbon source, diffusing along with the Ni atoms during the high temperature annealing , resulting in graphene formation on the surface of the alloy. The number of graphene layers depend on the nickel layer thickness, while in alloys with a higher atom percentage of nickel, the growth of graphene becomes inhomogeneous, with regions of multilayer deposit on the top of the surface. CVD at high temperature (1000°C) using methane, argon and hydrogen is also possible in order to grow monolayer graphene, along with very short exposure time and very fast cooling rates. Furthermore, low temperature CVD with benzene as carbon source is another way to obtain multilayer graphene. Other substrates such as alloys of gold and nickel, can be obtained evaporating Au films (0-10 nm) onto polycrystalline Ni films (approximately 550 nm) on SiO_2/Si slides. Acetylene is the most common carbon source to grow graphene and almost 75% of the alloy surface is covered with monolayer graphene if the temperature is kept at 450°C under low pressure conditions. Is important to remember that, not only in this case, preannealing at 600°Cwith hydrogen gas is crucial for graphene growth. The etching of the alloy is then achieved performing a two-step process involving aqueous solutions of $FeCl_3$ and KI/I_2. It has also been investigated the use of nickel-molybdenum alloys which processing with chemical vapor deposition of methane at 1000°C allows a total surface coverage with monolayer graphene. Its formation is achieved through a surface catalyzed process rather than from carbon segregation due to the fact that carbon dissolved in the bulk is no more available as it bond with Mo to form molybdenum carbide.

1.4 Chemical vapor deposition

1.4.1 Types of CVD process

Chemical vapor deposition (CVD) is a widely used technology to process various materials. Its most common applications involve applying solid thin film coatings

to surfaces, but it is also used to produce high purity bulk materials and powders, as well as fabricating composite materials via infiltration techniques. It can be used to deposit a very wide range of materials, the majority of the elements in the periodic table have indeed been deposited by CVD techniques, both in the form of pure elements and more often combined to form compounds. Chemical vapor deposition involves flowing a precursor gas or gases into a chamber containing one or more heated objects to be coated. Chemical reactions occur onto the hot surface or in its vicinities, resulting in the deposition of a thin film on the target substrate (figure 19). This is process is complementary to the formation of chemical byproducts that are expelled from the reaction chamber along with unreacted precursor gases.

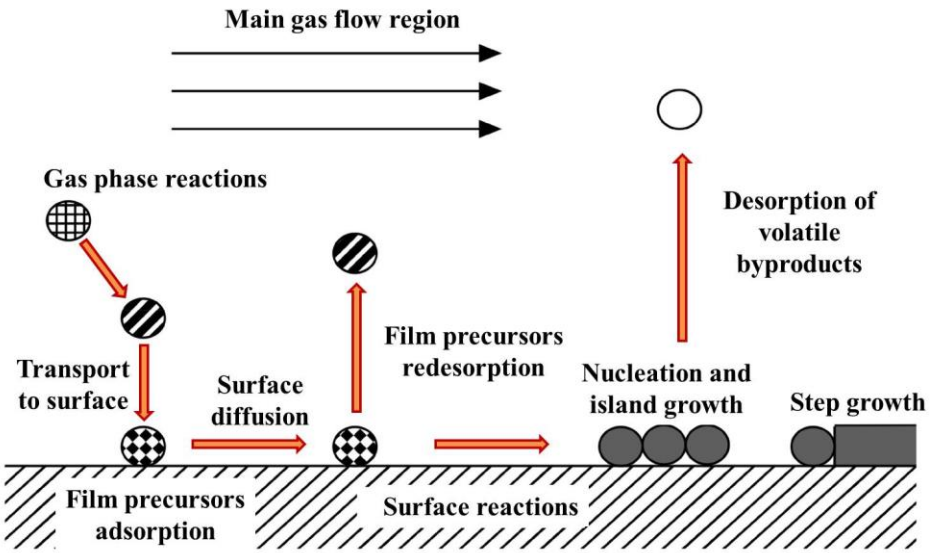

Figure 19 - Schematic representation of the CVD process.

Since the large variety of deposited materials and the wide range of applications, CVD is performed under a wide range of conditions and using various experimental settings. These processes generally differ from each other by the methodology used to initiate the chemical reactions and the working conditions.

Classified by operating pressure:

- ***Atmospheric pressure CVD (APCVD)*** Chemical vapor deposition performed at atmospheric pressure;

- ***Low-pressure CVD (LPCVD)*** Chemical vapor deposition at sub-atmospheric pressures. Reduced pressures tend to reduce unwanted reactions in the gas phase and improve film uniformity across the substrate;
- ***Ultrahigh vacuum CVD (UHVCVD)*** CVD executed at very low pressure, typically below 10−6 Pa (≈10-8 torr).

Chemical vapor deposition classified by physical characteristics of the gaseous phase:

- ***Aerosol assisted CVD (AACVD)*** In which the precursors are transported to the substrate by means of a liquid/gas aerosol, which can be ultrasonically generated. This technique is suitable for use with non-volatile precursors;
- ***Direct liquid injection CVD (DLICVD)*** CVD in which the precursors are in liquid form or dissolved in a convenient solvent. Liquid solutions are injected in a vaporization chamber through injectors and the precursor vapors are then transported to the substrate as in classical chemical vapor deposition. This technique is suitable for use with liquid or solid precursors. An advantage of this process is that high growth rates can be achieved during the deposition.

Chemical vapor deposition using plasma:

- ***Plasma-Enhanced CVD (PECVD)***Chemical vapor deposition that utilizes plasma to enhance chemical reaction rates of the precursors. PECVD processing allows deposition at lower temperatures, which is often critical in the manufacture of semiconductors. The lower temperatures also allow the deposition of organic coatings, such as plasma polymers, that have been used for nanoparticle surface functionalization;
- ***Remote plasma-enhanced CVD (RPECVD)*** Is similar to PECVD with the difference that the wafer substrate is not directly in the plasma discharge region. Removing the wafer from the plasma region allows processing temperatures to decrease even to room temperature;

- ***Microwave plasma-assisted CVD (MPCVD)*** In which plasma has a high frequency electromagnetic radiation in the range of GHz;
- There are also a variety of enhanced CVD processes which involve the use of, ions, photons, lasers, hot filaments, or combustion reactions with the aim of increase deposition rates lower deposition temperatures. There are also many derivatives of the CVD terminology, such as ***metal-organic chemical vapor deposition (MOCVD)*** which are sometimes used to identify the class of molecules used during the deposition process.

1.4.2 Characteristic of CVD process

Chemical vapor deposition process has arisen as principal method for depositing thin films because of its great number of favorable characteristics . One of the primary advantages is that CVD films are generally quite conformal, the film thickness on the sidewalls of deposited features is indeed comparable to the thickness on the top side. This means that films can be applied to complicatedly shaped topographies, including open insides and undercuts of the piece, and that high aspect ratio holes (wide radius) and other features can be completely filled without shadowing effects. Another advantage of CVD is that the deposited materials can be chosen among a wide variety of elements and compounds and can besides be deposited with very high level of purity. This is a consequence of the relative ease with which impurities are removed from gaseous precursors using distillation techniques. Is also an effect, in case of vacuum chamber deposition, of intrinsic turnover at which undergoes the environment inside the reactor which leads to faster removal of possibly unwanted byproducts. Other advantages include relatively high deposition rates in particular cases even of some millimeters per hour, and the fact that CVD often doesn't require as high a vacuum as PVD processes (which for example can reach a deposition rate of some micrometers per hour). Chemical vapor deposition also has some disadvantages such as the fact that precursors need to be volatile around room temperature. This is non-trivial for a number of elements in the periodic table, although the use of metal-organic precursors has improved this negative aspect. CVD precursors can also be highly toxic ($Ni(CO)_4$), explosive(B_2H_6), or corrosive ($SiCl_4$) and the

byproducts of can also be dangerous (CO, H_2, or HF) or difficult di dispose. Some of these reactants, especially the metal-organic precursors, can also be quite expensive. Another disadvantage is that the films are usually deposited at elevated temperatures, creating some restrictions to the kind of substrates that can be coated and moreover it negatively affects the energy consumption. This aspect can also lead to stresses in deposited films derived from a possible difference in thermal expansion coefficients, which can cause mechanical instabilities in the deposited layer.

1.4.3 Thermal CVD

The CVD growth appears to be the most promising technique for large scale production of mono or few-layer graphene films. Although the formation of so called monolayer graphite was mentioned in early CVD studies on single crystal metals the first successful synthesis of few-layer graphene films using CVD was reported in 2006 by Somani and coworkers using camphor as precursor on nickel foils [33]. This study started a new route in graphene synthesis posing several issues like the control of layers number and the minimization of graphene folding. Since then much work has been made to obtain graphene layers on several types of metallic substrates trying to achieve control on graphene thickness. After chemical etching of the metallic foil, the graphene layers can be detached and then transferred to another substrate, providing high quality graphene layers without complex mechanical or chemical treatments. The growth mechanism of graphene on substrates with average to high carbon solubility (over 0,1 of atomic percentage) such as Co and Ni proceed through the diffusion of the carbon through the metallic thin film at the growth temperature and the subsequent carbon precipitation, out of the bulk metal to the surface upon cooling. In contrast, the graphene growth on low carbon solubility substrate (less than 0,001 of atomic percentage) like Cu mainly happens on the surface through the four-step process described by Li and co-workers [34].

1) Catalytic decomposition of hydrocarbon precursor on Cu to form C_xH_y
2) Formation of first nuclei as a result of local supersaturation of C_xH_y

3) Nuclei growth and formation of graphene islands on C_xH_y species which saturate or supersaturate Cu surface.

4) Full coverage of Cu surface by graphene under certain temperature, hydrocarbon flow rate and precursors partial pressure.

If the amount of available C_xH_y on the exposed Cu surface is insufficient to expand the C at the island edges, Cu surface will be only partially covered in graphene. Understanding the graphene growth mechanism, led to application of various approaches to control graphene growth rate in order to obtain monolayer graphene. Thermal CVD process outcome is then influenced by the use of multiple polycrystalline substrates (Ni, Cu, Ir, Pt, Ru, Co) which play the role of catalysts for graphene growth and the growth mechanism itself which varies from metal to metal and depends on the structure and deposition conditions. Wet-etching of the target metallic foil, subsequently allows the transfer of graphene on other substrates. Obtained samples generally have good electrical properties and the relatively low deposition time can lead to a large scale production of monolayer or layer of a few atomic planes of graphene.

1.4.4 Industrial applications of CVD

Chemical vapor deposition applications can range across a wide variety of industrial sectors and some of these uses are listed below:

- coatings for several applications such as wear resistance, corrosion resistance, high temperature protection and erosion protection
- production of semiconductors and related devices such as integrated circuits, sensors and optoelectronic devices
- dense structural parts: CVD can indeed be used to produce components that are difficult or expensive to produce using conventional fabrication techniques. Dense parts produced via chemical vapor deposition are generally thin and could be deposited onto a mandrel
- optical fibers for telecommunications

- in composites field preforms can be infiltrated using CVD techniques to produce ceramic matrix composites such as carbon-carbon, carbon-silicon carbide and silicon carbide-silicon carbide composites. This process is sometimes called chemical vapor infiltration or CVI.

2 ELECTRODEPOSITION

2.1 Brief history of electroplating

Modern electrochemistry was established by Italian chemist Luigi V. Brugnatelli in 1805. Brugnatelli used the work of his colleague Alessandro Volta, when he invented five years earlier the voltaic pile, to facilitate the first electrodeposition. Brugnatelli's inventions were suppressed by the French Academy of Sciences and did not become used in general industry for the following thirty years. By 1839, scientists in Britain and Russia had independently developed metal deposition processes similar to Brugnatelli's, for copper electroplating of printing press plates. Russian scientist Boris Jacobi, not only rediscovered galvanoplastics, but developed electrotyping and galvanoplastic sculpture which quickly became a fashion trend in Russia, also due to people like inventor Peter Bagration, scientist Heinrich Lenz and science fiction author Vladimir Odoyevsky who all contributed to further development of the technology. Among the most notorious cases of

electroplating in the mid-19th century Russia, there are gigantic galvanoplastic sculptures in St. Isaac's Cathedral of Saint Petersburg and the gold-electroplated dome of the Cathedral of Christ the Savior in Moscow, the tallest Orthodox church in the world.

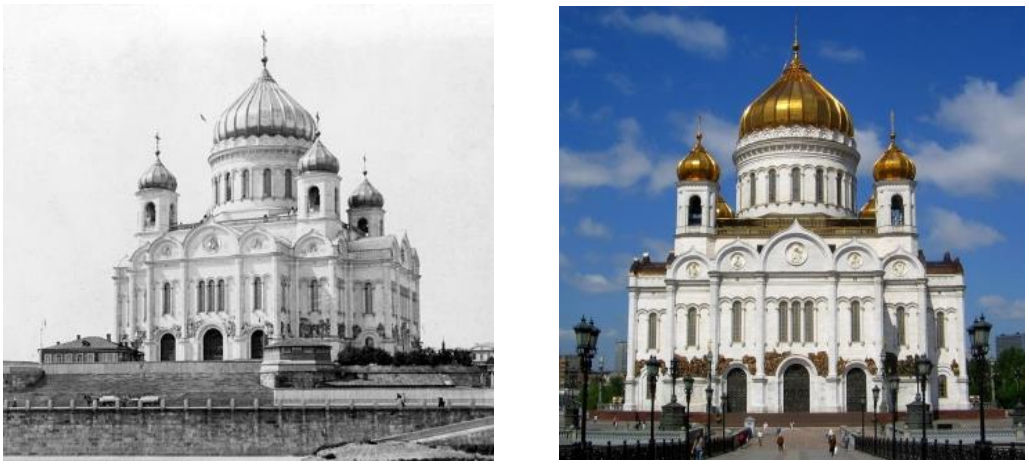

Figure 20 - Cathedral of Christ the Savior in Moscow (on the right the 1990s rebuilt version), was the first church in which the dome has been gilded using electroplating.

Soon after John Wright of Birmingham from England discovered that potassium cyanide was a suitable electrolyte for gold and silver electroplating and Wright's associates, George and Henry Elkington were awarded of the first patents for electroplating in 1840, they later founded the electroplating industry in Birmingham from where it spread around the world. The Norddeutsche Affinerie in Hamburg was the first modern electroplating plant starting its production in 1876 [35].

As the science of electrochemistry grew, its relationship to the electroplating process became evident and other types of non-decorative metal electroplating processes were designed. Commercial electroplating of nickel, brass, tin, and zinc were developed by the 1850s and electroplating baths and equipment based on Elkingtons' patents were scaled up to accommodate the plating of numerous, large objects and for specific manufacturing or engineering applications. Plating industry received a big boost with the advent of the electric generators in the late 19th century, with higher currents available, metal machine components, hardware, and automotive parts requiring corrosion protection and enhanced wear properties, along with better appearance, the processed could become industrially

competitive. The two World Wars and the growing aviation industry gave an high incentive to further developments and refinements including such process as hard chromium plating, bronze alloy plating, sulfammate nickel plating, along with numerous other plating processes. Deposition settings evolved from manually operated wooden tanks to automated equipment, capable of processing parts at a rate of thousands of kilograms per hour.

2.2 Characteristics of electroplating

Electrodeposition is the application of metallic coatings to metals or other conductive surfaces by electrochemical processes. The work piece to be plated is the cathode (negative terminal) and the anode (positive terminal), can be differentiate in two types: sacrificial anode (dissolvable) and permanent anode (inert). Sacrificial anodes are formed by the metal that is going to be deposited, while permanent anodes is designed to only complete the electrical circuit, but cannot provide a source of fresh metal to replace what has been removed from the solution by deposition at the cathode. Titanium activated, platinum and sometime lead are usually used as materials for inert anodes. The electrolyte is the electrical conductor in which current is carried by ions rather than by free electrons as in metal and it completes a circuit between the two electrodes. Upon application of current, the positive ions in the electrolyte will move toward the cathode and the negatively charged ions toward the anode. This migration of ions through the electrolyte constitute the current flux in the fluid part of the circuit, while the migration of electrons from the anode through the wiring, the electric generator and then back to the cathode constitutes the current in the external circuit. The metallic ions of the salt in the electrolytic solution carry a positive charge and are thus attracted to the cathode. Since the cathodic work piece is attached to the negative pole of the electric source, it supplies electrons to the solution, and when cations reach the negatively charged mold, it provides electrons to reduce those positively charged ions to metallic form. Metal atoms will thus be deposited onto the surface of the negatively charged cathode. On the contrary, the anode is connected to the positive pole of the electric source and therefore it attracts anions accepting electrons from the deposition bath. The rate at which the anode is

consumed is equal to the rate at which the cathode is plated, unless parasitic reactions take place at the surfaces of the two electrodes. The most common of these reactions is hydrogen reduction from water, a process that competes with the metal deposition. The process is schematized in Figure 21 for the deposition of copper from a soluble anode on a generic metal, a procedure used for this thesis work.

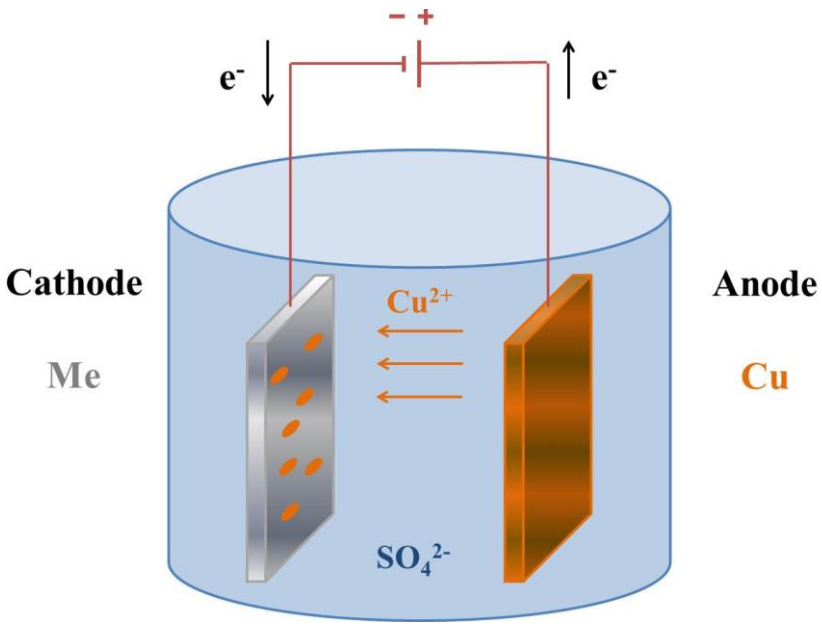

Figure 21 - Schematized deposition process of copper on generic metal via soluble anode method using copper sulfate as electrolytic solution.

2.3 Applications of electroplating

Electrodeposition is used industrially to produce a dense, uniform, and adherent coating of pure metal or alloy upon a surface exploiting the effect of an electric current. The produced coating is usually suitable for decorative or protective purposes, or enhancing specific surface's properties. Electroplating products are widely used in many industrial fields such as automotive, naval, airspace, machinery, electronics, jewelry, defense and toy industries. Electroplating finds numerous applications as thin films and as three dimensional, thick structures in microdevices, other uses include the development of materials for printed-wiring boards, contacts, connectors, and magnetic recording devices. The interesting properties for both thick and thin films cover a broad range, including thermal,

magnetic and optical and shielding effects suitable to improve corrosion and wear resistance. High-resolution lithographic techniques have enabled electronic device integration, with electrodeposited layers reaching several hundred microns of thickness therefore the importance of electrodeposition as a production technology in the microelectronics industry is growing. For some of the previously listed fabrication processes, electrodeposition offers advantages over competing technologies such as physical and chemical vapor deposition, because it requires simpler instrumentation and operating conditions. With the growing miniaturization trend, electrodeposition has established itself as the preferable manufacturing technology and it is also promising in the deposit of metals and alloys for microelectronic fabrication and HARMs (High Aspect Ratio Microdevices). Fabrication of high aspect ratio microstructures by electrodeposition is also creating an increasing interest for a multitude of applications in microelectromechanical systems (MEMS).

Lithography is also comprised as step of the LIGA process. LIGA is the German abbreviation for the three major process steps of creation of high-aspect ratio microstructures, lithography (*Li*thographie), electroplating (*G*alvanoformung) and molding (*A*bformung). The use of the LIGA process overcomes many drawbacks of other traditional production methods and pattern transfer techniques such as chemical etching, sputter etching, reactive ion etching. Electrodeposition is an integral part of the LIGA process, it is employed after exposure and development of the resist and is used to create a complementary pattern onto a metal substrate by filling the spaces left uncovered by the non-conductive resist growing from the electrically conductive substrate. The metal pattern produced in such way can then be used as microdevice itself or as mold for plastic replication. Electrodeposited alloys and composites are particularly interesting because of their unique and often superior properties compared with their pure metal counterparts and are therefore exploited in various occasions. In alloy electroplating the deposition rate of the more noble metal is often diffusion controlled, consequently the control of the growing material's composition becomes a transient problem and complicates the electrodeposition behavior. Particles in the nanometric range can extend the use of electrodeposited composites to microdevices fabrication, since are

intrinsically in the order of micrometers, the composite material that constitute these devices must contain particles that are at least an order of magnitude smaller, hence nanometrically sized.

2.4 Electrical relations

2.4.1 Faraday's Laws of electrolysis

In 1833 the English scientist Michael Faraday developed its laws about electrolysis. Faraday's first and second law of electrolysis state that the quantity of material deposited on an electrode is proportional to the amount of electricity used through the process.

- Faraday's first law of electrolysis: the mass of a substance altered at an electrode during electrolysis is directly proportional to the quantity of electricity transferred at that electrode.

Quantity of electricity refers to the quantity of electrical charge, typically measured in coulomb.

- Faraday's 2nd law of electrolysis: for a given quantity electric charge, the mass of an elemental material transferred at an electrode is directly proportional to the element's equivalent weight (which is the mass of a given substance that will supply or react with one mole of electrons in a redox reaction).

The equation representing the second law is:

$$m = \frac{Q\ M}{F\ z}$$

which will be used and analyzed again in a following chapter.

2.4.2 Current efficiency

It is stated in Faraday's laws that the amount of chemical charge at an electrode is exactly proportional to the total quantity of passing electricity. However, if several reactions take place simultaneously at the electrode, the product may

decrease due to side reactions such as hydrogen evolution developing in aqueous baths as result of the electrolysis of water

$$2H_3O^+ + 2e^- \rightarrow H_2 + 2H_2O$$

partial reduction of metal ions in solution or co-deposition of the second metal during the electrodeposition of a binary alloy. Therefore, inefficiencies may arise from these unwanted or competing processes which take place at the electrodes instead or beside the intended reaction. Current efficiency is therefore a fraction, usually expressed as a percentage, that indicates the ratio between the desired chemical process and the total chemical change:

$$CE = \frac{W_{real}}{W_{th}} 100$$

where $\boldsymbol{CE}$ is the current efficiency in percentage, $\boldsymbol{W_{real}}$ is the weight of deposited or dissolved metal and $\boldsymbol{W_{th}}$ is the theoretical weight expected from Faraday's laws. Cathode efficiency is the current efficiency applied to the cathodic reaction, and anode efficiency is that applied to the anodic reaction.

2.4.3 Current distribution

Except for simple cell's geometries, such in case of concentric anode and cathode, the current is not uniform over the surface of an electrode. In fact, the manner in which the current distributes itself over an electrode surface in any practical case is quite complicated, usually far too much so to be simply calculated from geometry. Current will tend to concentrate at edges and points and unless the resistance of the solution is extremely low (lower than in any practical case), it will flow more readily to parts in vicinity to the opposite electrode than to more distant areas. Except for simple pieces subject to electroplating, the thickness of deposit which depends on the current density will therefore not be uniform over the deposited surface.

2.4.4 Potential relationships

Since the whole process of electroplating is caused as a consequence of the application of a voltage or a current, understanding the relation between these two quantities is fundamental. The applied potential difference guarantees the current

flow through a conductive medium and this relationship is represented by Ohm's law as follows:

$$E = RI$$

where ***E*** is the voltage in Volt (V) and ***R*** is the resistance of the medium in Ohm (Ω). The electrode potential is the electrical potential difference between an electrode and a reference electrode. The absolute potential of an electrode is not directly measurable, hence it has to be referred to an arbitrary zero point defined by the potential of a reference electrode. Typically, in various applications is used as reference a Standard Hydrogen Electrode (SHE) which has a potential, at any temperature, defined equal to zero. SHE exploit the equilibrium between H^+ and hydrogen gas to generate this reference potential, despite its not practical use in laboratory. Therefore, other reference electrodes are used, such as Ag/AgCl or Hg_2/Hg_2Cl_2 saturated calomel. Even though, at steady state conditions, electrode potential and current density are related with direct correspondence, the growth process is a non-stationary reaction. Potentiostatic processes develop with changes in current density during time with constant E, while galvanostatic processes at constant current occur with potential variations. Surface state evolution (variation of roughness and morphology through the process) and changes in the solution composition at the electrode surface (pH or chemical species concentration can change as well), are the reasons for this current-potential behavior [36], [37]. However, is particularly interesting when the current density is equal to zero. If the potential at which $i = 0$ corresponds to the thermodynamic equilibrium of an electrode process, it is defined as equilibrium potential of that process (***Eeq***). Thus, considering the equilibrium between a metal and a solution containing its ions, the equilibrium potential is given by the Nernst equation as follows

$$E_{eq} = E_0 + \frac{RT}{nF} \cdot \ ln(aM_{z+})$$

where ***a*** is the thermodynamic activity of the electroactive species, ***R*** is the gas constant equal to 8,314 J $k^{-1}mol^{-1}$, ***T*** is the absolute temperature in K and E_0 is the standard electrode potential, which is a constant characteristic of the material constituting the electrode and it is always referred to the SHE. Substituting in this

equation the values for $\boldsymbol{F}$, $\boldsymbol{R}$ and $\boldsymbol{T}$ (considered at room temperature 298 K) is obtained another widely used expression for Nernst equation, given by

$$E_{eq} = E_0 + \frac{0{,}059}{n} \cdot \log a$$

Thermodynamic equilibrium means that a dynamic equilibrium between metal ions being discharged and ionization of metal atom exists, so that the net rate of the process is zero. Therefore in order to have the deposition of a metal at the cathode surface, the system has to move away from its equilibrium. This is obtained by shifting the electrode potential in the cathodic (negative) direction from its equilibrium value. Therefore, a negative potential increases the rate of the reduction process, while a positive potential shift increases the rate of anodic reaction (oxidation) [36], [37]. The value of this shift is called overpotential and is given by

$$\eta = E - Eeq$$

This overpotential can have values from few mV up to some V and it is strictly related to process rate and deposit morphology. Since the whole electrodeposition process is made by two partial reactions occurring in opposite directions, their rate, at the equilibrium, is quantified by the exchange current density $\boldsymbol{i_0}$ which is related to the overpotential. Hence if a metal has high values of $\boldsymbol{i_0}$, its overpotential is low, and vice-versa. This relation is valid only if the metal ions in the solution are not part of complexes, otherwise is possible to vary the value of $\boldsymbol{\eta}$ at a given current density in order to change the film morphology which changes forming smaller grains for increasing values of overpotential. Furthermore, electrode reactions always occur in more than one step, as a result there is an overpotential associated with each of these stages. Can be highlighted four possible partial reactions, thus, depending on the respective speeds of every process can be found four types of rate control on the overall deposition:

- Charge transfer
- Diffusion
- Chemical reaction

- Crystallization

Thus, four different kinds of overvoltage are distinguished and the total overvoltage η can be considered to be composed of four components:

$$\eta = \eta_{ct} + \eta_{d} + \eta_{r} + \eta_{c}$$

Overvoltage is instead the difference between the cell voltage, when a current is flowing, and the OCV (open circuit voltage), it then represents the extra energy required to induce the cell reaction.

2.5 Electrolytic baths

Morphology, composition, quality and properties of electrodeposited metal coatings strictly depend on the electrolyte used during the process and different metals may need different types of electrolyte in order to be deposited. Thus, several solvents can be used to dissolve the metal ions precursors and the most common electrolytic baths are based on aqueous solvents, but also organic or ionic liquids. In aqueous solutions, as discussed before, the side reaction at the cathode surface is hydrogen evolution involving a local increase in pH values. At the anodic side instead, metal dissolution (in the case of sacrificial anode) or oxygen evolution represent the two main processes:

$$M^0 \rightarrow ze^- + M^{z+} \qquad \text{anode dissolution;}$$

$$4OH^- \rightarrow 4e^- + O_2 + 2H_2O \qquad \text{oxygen reduction;}$$

As for hydrogen evolution, the oxygen can bring to an acidification of the solution, leading to a variation of the pH. In practical applications, salts and other soluble compound containing metal ions are not used alone in the actual electrolytic bath, since other additives may be used in order to produce better metal coating, influencing the properties of the electrolytic bath. Alkali or inorganic acids increase the bath electrical conductivity and an increased electrolyte conductivity means lower applied voltage resulting in better thickness uniformity of the deposit. Alkali and acids are also used to control the pH in the solution, which is a crucial parameter to produce high quality coatings and the use of buffering agents provide also the acidity stability across the entire solution

preventing the acidification due to hydrogen evolution at the electrode surface (the pH increases due to H^+ consumption). Other additives have the purpose of activating the surface, making easier the detachment of hydrogen bubbles by decreasing the surface energy of the electrode. These hydrogen bubbles may create a phenomenon known as pitting in which macroscopic point defects are present at the plated surface. These additives take the name of surfactants and they are mainly divided in brighteners, that permit no post deposition polishing giving bright deposits, and levelers, which allow a smoother surface of the metal film. Anyway disadvantages occur, coming from the application of these substances, since their concentration must not be too high, because of the inhibition of the deposition process due to the increase of η . Another problem is that additives concentration decreases during the electrodeposition process due to their adsorption at the electrode surface, so that small adds have to be done in order to maintain as constant as possible their concentration. To overcome these disadvantages has been developed new classes of non-aqueous electrolytes such as molten salts like LiCl-KCl, NaCl-KCl, ionic liquids and organic solvents which are not discussed since not used in this thesis work.

2.6 Surface preparation

Substrates for electrodeposition may need pretreating processes like surface cleaning, surface modification and rinsing in order to enhance the outcome quality and to remove contaminants. This contamination can be extrinsic, like organic debris and mineral dust coming from the external environment, or intrinsic coming from the native oxide layer [37]. Poor adhesion or even deposition inhibition may arise from the interaction between contaminants and the depositing material, is therefore fundamental to remove them from the surface in order to achieve plating. Cleaning procedure has the obligation to minimize substrate damages while removing contaminants or debris. Exist both chemical and mechanical cleaning the former includes the application of solvent degreasing, alkaline cleaning or acid cleaning, while the latter is basically divided in polishing and buffing. Oils and grease of various types may exist on the bare surface and they are removed through organic solvents, either by dipping the substrate in the

solvent or by vapor degreasing. Hot alkaline cleaning solutions are used instead to clean the surface from dirt and solid soil. Hydrochloric, sulfuric or nitric acids are quite useful to remove oxides that can be present on the metal substrate. Taking into consideration mechanical techniques, during polishing abrasives are applied in order to remove small amounts of metal, in order to free the surface from macroscopic imperfections left by grinding processes. Subsequently, buffing via smaller abrasives is used and a smaller amount of metal is removed from the surface, resulting in a smoother surface. Rinsing in water, differently from processes listed above, can be applied after the electrodeposition process, since when workpieces are transferred from one electrolytic bath to another, or when they leave the final treating solution, they carry some residual from the solution in which they were dipped.

2.7 Nucleation and growth

Another aspect to discuss is the actual nucleation and growth of a material coming in contact with a substrate (in this case deposited metal on the substrate); in formation and growth of adion clusters, two processes are fundamental:

1) The arrival and adsorption of ions or atoms at the surface
2) The motion of these adsorbed ions (adions, adatoms) on the surface

An ion deposited on the surface of a perfect crystal is not a stable entity but it can increase its stability by the formation of clusters. The free energy of formation of a cluster of ***N*** ions, ***G(N)***, has two components (terms):

$$\Delta G(N) = -Nze|\eta| + \phi(N)$$

The first term is related to the transfer of N ions from the solution to the crystal phase (favorable) and the second term is related to the increase of the surface energy due to creation of the surface of a cluster. This increase in surface energy is equal to the difference of the binding energies of ***N*** bulk ions and ***N*** ions as arranged on the surface of the crystal. Both terms are functions of the size of the cluster ***N*** and the dependence of the energy of formation of a cluster ***G(N)*** on the number of adions ***N*** in a two-dimensional cluster is shown in Figure 22:

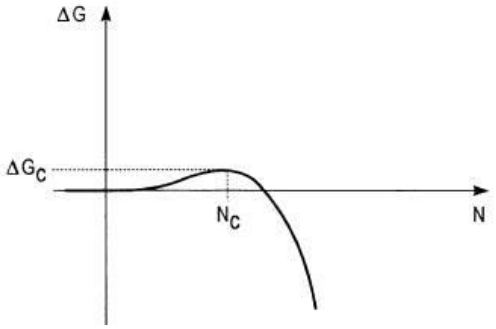

Figure 22 - Free energy formation of a cluster as a function of size N (a cluster of N atoms); Nc is the size of the critical cluster (nucleus).

The free energy initially increases, reaches a maximum, and then decreases increasing ***N***. At its maximum, the cluster size is ***Nc*** (critical nucleus) and the spontaneous growth of clusters is possible after the maximum in ***ΔG*** is reached. This critical cluster is the nucleus of the new deposited phase and is characterized by equal probability for growth and dissolution. The growth of clusters before a maximum is reached, and when average ***ΔG*** is increasing, is due to statistical energy fluctuations that allow local high values of ***ΔG***.

For the determination of the growth mode the surface free energies of the substrate and the coating, as well as the relative lattice parameters are important. Considering Figure 23:

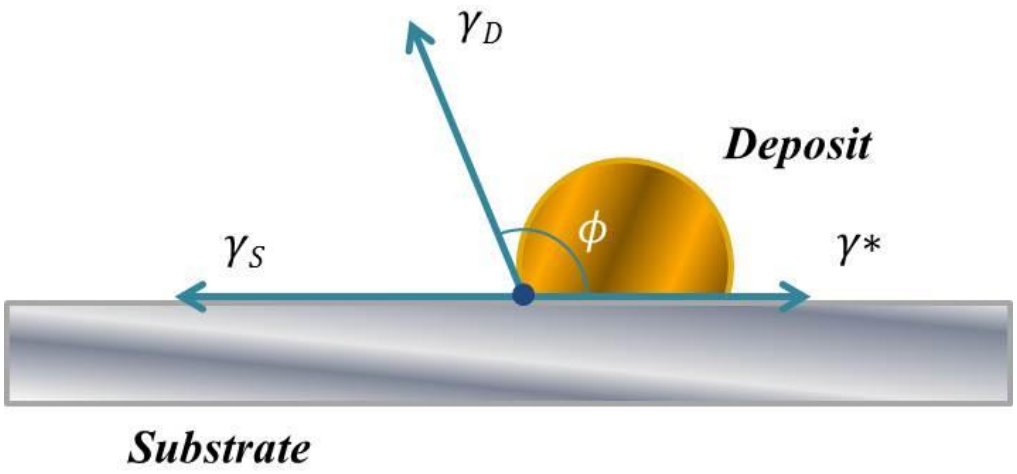

Figure 23 - Representation of surface free energies.

If the substrate is approximated as a flat rigid surface and the growing cluster as a drop on top of it, the equilibrium among the surface energies is represented by Young's equation:

$$\gamma_S = \gamma_D \cos \phi + \gamma*$$

Bauer described three growth modes close to thermal equilibrium, which depend on the relationship between these three contributions of the total surface free energy and the lattice misfits between the two phases:

a) In ***Volmer–Weber (VW) growth***, adatom-adatom interactions are stronger than those between adatom and the surface, leading to formation of three-dimensional clusters or islands. It can be also seen that this process is enhanced by large misfits in lattice parameters between the substrate and the deposited material. Growth of these clusters, along with coarsening, will cause rough multi-layer films to grow on the substrate surface. Analytically this condition is developed if:

$$\gamma_S > \gamma_D + \gamma*$$

b) In ***Frank–van der Merwe (FvdM) growth***, adatoms attach preferentially to surface sites resulting in atomically smooth, fully formed layers. This layer-by-layer growth is two dimensional, indicating that there is no misfit

between the two phases and complete films form prior to growth of subsequent layers. Hence this condition is verified for:

$$\gamma_S = \gamma_D + \gamma^*$$

c) ***Stranski–Krastanov (SK) growth*** follows a two steps process: initially, complete films of deposited materials, up to several monolayers thick, grow in a layer-by-layer fashion on the crystal substrate. Beyond a critical layer thickness, if either positive or negative lattice misfit develops, three-dimensional islands of the deposited metal form on top of the first layers. As a result growth continues through the nucleation and coalescence of adsorbate islands.

In Figure 24 are represented the three different growth processes:

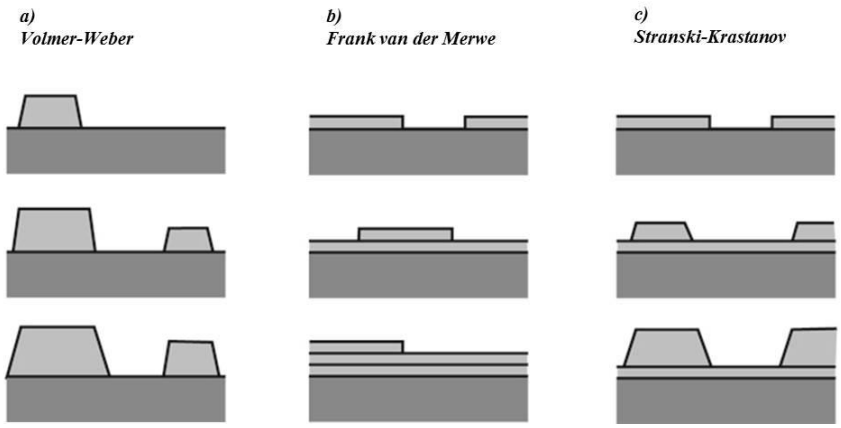

Figure 24 - Schematization of the three primary modes of thin-film growth, (a) VW mode(island growth), (b) FvdM mode (layer by layer growth), (c) SK mode (layer by layer and island growth).

Metal electrodeposition from aqueous solutions typically occurs by the Stranski-Krastanov and Volmer-Weber modes.

2.8 Related processes

Processes related to metal deposition principally include electroless deposition, immersion plating and electroforming and they all follow the basic principles of electrochemistry.

Electroless deposition, also known as autocatalytic plating, is a special type of electrodeposition. The peculiarity of this process is that it comes without an

external power source. Indeed, a chemical reducing agent is used to reduce the metal to deposit from its ionic state in solution. Hence, the electrons needed for the following reaction are supplied by this reducing agent, as follows:

$$M^{n+} + ne^- \rightarrow M$$

However, a catalytic surface is needed to guarantee this reaction, once deposition starts, the deposited metal has to be catalytic itself. It follows that not all metals have an autocatalytic behavior (nickel is an example of metal that can be plated through this technique). The main advantage in electroless deposition is that deposition on non-conductive surfaces as plastics or glass, is possible thanks to a surface activation pre-treatment.

Immersion plating is a technique that involves the deposition of a metallic coating on a substrate by chemical replacement from a solution containing salts of the depositing metal. As the electroless process, it does not require the application of a power source, but it also does not need a reducing agent. The deposition process stops when all the metallic surface is covered by a deposited layer [37].

Electroforming occurs instead in a plating bath where the desired final metal is plated typically on a base form, a mold, or on a mandrel. Subsequently the deposited metal is detached from the mold. The advantage lies in the exact reproducibility of the base material on which the electrodeposition process occurs. This technique has been used in this thesis work to produce the samples which will act as substrate for graphene growth and will be furthermore discussed.

3 EXPERIMENTAL PROCEDURE

3.1 General description of the samples

The main advantage of electrodeposition processes respect to the usual ways of producing substrate for graphene growth, is that this technique is much less expensive than for example physical depositions techniques, which are briefly explained in the next paragraph.

3.1.1 Physical deposition techniques

To perform graphene chemical vapor deposition on metallic substrates, it is common to prepare the samples via vaporization of the metal, typically through processes like Electron Beam Evaporation and other physical methods of deposition, which ensure a high quality of the substrate. Physical vapor deposition (PVD) consists of three fundamental steps

- Vaporization of the material from a solid source assisted by high temperature vacuum or gaseous plasma.
- Transportation of the vapor in vacuum or partial vacuum to the substrate surface.

- Condensation onto the substrate to generate thin films.

Several typologies of physical deposition techniques are used to create a suitable catalytic surface in order to deposit graphene, which differ in the methods used to generate and deposit material. The most common are:

- ***Cathodic arc deposition*** In which a high-power electric arc is discharged at the target (the source of the material that will form the substrate) and subsequently the substance is blasted away in form of highly ionized vapor and then deposited onto the mold that will generate the final substrate.
- ***Evaporative deposition*** The material to be deposited is heated to a high vapor pressure using electrical resistances in a relatively low vacuum environment.
- ***Pulsed laser deposition*** In which high energy pulsed laser ablates material from the target creating a vapor that will deposit onto the mold.
- ***Sputter deposition*** A glow plasma discharge that can be localized around the target material by a magnet, bombards the material sputtering it away as a vapor for subsequent deposition and formation of the substrate.
- ***Electron beam physical vapor deposition*** In which the material to be deposited is heated by electron bombardment in a high vacuum environment and is deposited by condensation on the cooled mold.

Sputtering and Electron Beam deposition are among the most common used techniques to produce substrate for graphene chemical vapor deposition as they create high quality surfaces in terms of purity, defectiveness and roughness. Despite these advantages the main problem with these physical techniques is the high cost of the deposition setting (i.e. the price for the evaporator itself). In addition to that there are maintenance and operating costs of the machines, the relatively complexity of utilization and the waste of catalytic substrate material inherent to the nature of the process. This last aspect can be explained taking into account the high cost of the typical metals used for these kind of substrates and with a basic knowledge of the deposition methods. In these physical deposition processes, the workpiece to cover using the target material is usually placed in a

chamber kept under a variable degree of vacuum (depending from the considered method) which will be entirely covered itself at the end of the process, exploiting only a partial amount of material to create the substrate.

3.1.2 Electrodeposition techniques

To overcome these disadvantages is proposed as alternative method for substrates production, the electrodeposition technique that consists in an electrolytic process (also called electroplating) in which a current is used to reduce cations of the desired metal which are subsequently deposited at the cathode. These cations can come from a solution of ions or from an anode made of the metal to be deposited. In this process all the metal is used to cover only the desired areas onto the sample without material wasting and high costs. The setting used to perform electrodeposition is also considerably cheaper than the physical deposition settings and much easier to use.

Copper and ruthenium are used as materials to build the substrates because of their complete immiscibility, this is been exploited to use copper as supporting media for the ruthenium layer, but during the development of the work the substrates evolved to face various aspects arisen after graphene deposition. The four main experimental sample settings are: an electroformed copper layer covered on one side by an electrodeposited ruthenium layer (*Type A*), a simple electroformed copper substrate (*Type B*), an electrodeposited ruthenium substrate on silicon dioxide (*Type C*) and an electroformed copper substrate covered on both sides by electrodeposited ruthenium (*Type D*).

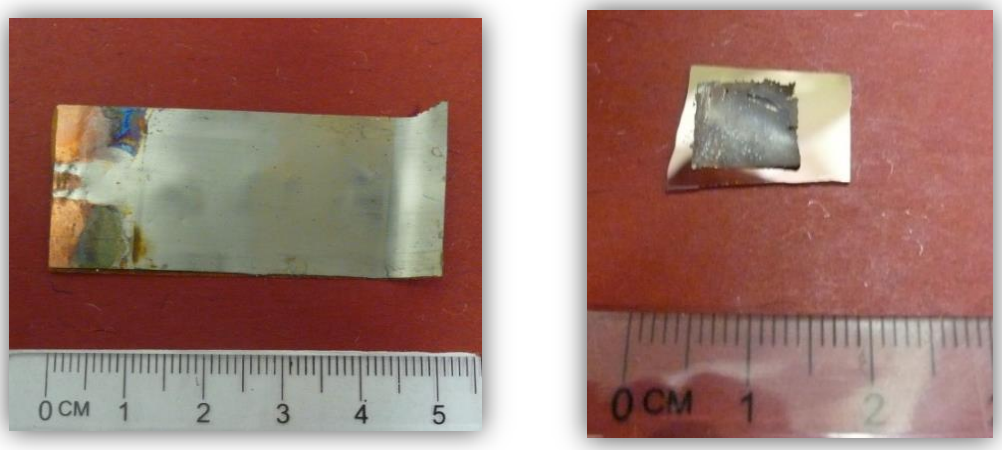

Figure 25 - On the left side a picture of a Type A sample before cutting, on the right a Type C sample (ruthenium foil supported by a silicon slice with native oxide on it.

Type A samples were produced electroforming a copper layer on a polished steel plate until a thickness of about 40 µm is reached in order to obtain a self-standing substrate, is then used on one side for ruthenium electrodeposition with an approximate thickness of 500 nm. The only reason behind the choice of 40 µm as copper thickness is just the possible optimization of the production process, in order to reach sufficient structural properties (comfortable handling) and minimize copper deposition time, since as previously explained the thickness of the copper substrate does not affect the thickness of the eventually deposited graphene.

Type B samples are merely the electroformed copper foil (40 µm thick), produced with the same process, without the subsequent ruthenium electroplating.

Type C samples are produced starting from *type A*, the copper foil is then etched away and the remaining ruthenium layer is placed on top of an oxidized silicon wafer.

Type D samples are still based on *type A*, but they are subjected to a double side ruthenium deposition, in which the back side of the copper layer is also covered with a ruthenium layer.

3.2 Ru-Cu SYSTEMS

The combination of metallic elements ruthenium and copper form a system which shows complete immiscibility in the bulk (as shown in the Ru-Cu phase diagram in figure 26) , but they produce bimetallic entities in which copper is present on the surface of ruthenium [38], [39].

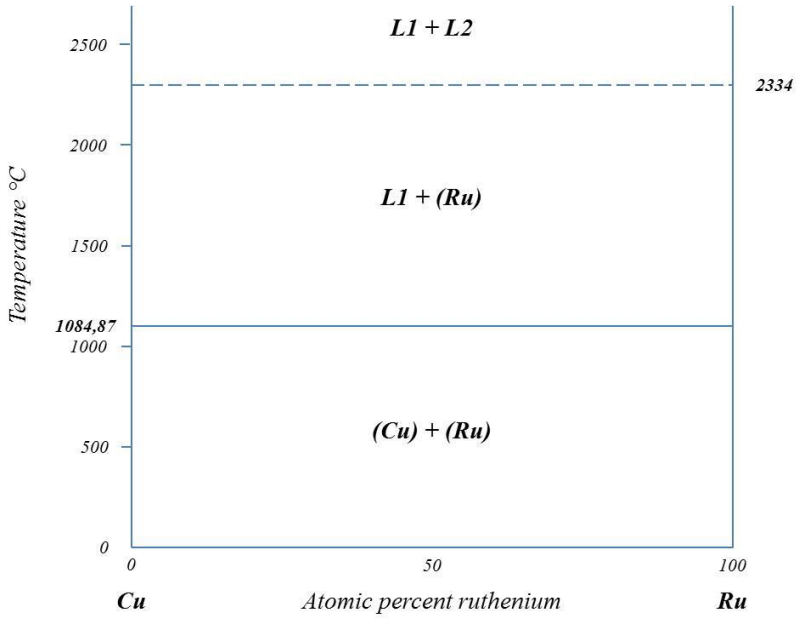

Figure 26 - Phase diagram of a copper-ruthenium system showing the complete immiscibility of the elements at any composition and temperature.

This behavior of the two elements led to the use of copper as substrate for ruthenium growth, despite the low melting temperature of copper (Tm of 1084,87°C) could be seen as a problem during high temperature graphene deposition, usually performed approximately at 1000°C, while for ruthenium such problem is not present since it melts at 2334°C. This particularity had profound effect during the development of this work and during the design of the samples. Hence their behavior will be further and better analyzed during the exposure of the work done in the next chapter.

3.3 Electroplating solutions

To deposit copper onto the polished steel plate, has been used an aqueous solution consisting of 200 g/l of $CuSO_4 \cdot 5\ H_2O$ and 2,7% volume of H_2SO_4. This solution is designed to be used concurrently to a copper soluble anode which provided the Cu^{2+} ions. In acid solution, copper is indeed oxidized at the anode to Cu^{2+} then associated with the anion SO_4^{2-} in the solution to form copper sulfate. After diffusion to the cathode, the copper cation is reduced to metallic copper by gaining electrons provided by an external source of current. In this case the electrodeposited metal comes from the dissolution of the copper anode which provide cations, without practical consume of the solution. Ruthenium deposition is however carried out performing another plating method which uses insoluble anodes, therefore the electroplated metal cations are provided by the solution. The bath used to the deposit ruthenium is composed of hydrate $RuCl_3$ (8 g/l) and sulfamic acid NH_2SO_3H (15 g/l), in this case the solution is designed to work with a platinum insoluble anode. As previously stated ruthenium ions are entirely provided by the solution itself, which has to be restored after a certain number of depositions.

3.4 Preparation of the substrates

The step-by-step preparation of the four samples setting is described in details, including possible difficulties and disadvantages of the various production processes.

Type A samples were produced depositing a copper substrate on a polished and flexible steel plate using kapton tape to mask the cathode surface. In this way unwanted copper deposition is avoided and sample size is controlled (typical dimensions about 2 cm wide and 5 cm long) while providing sharper edges to enhance the subsequent detachment. As previously described has been used a water solution consisting of 200 g/l of $CuSO_4 \cdot 5\ H_2O$ and 2,7% volume of H_2SO_4 and a copper anode. The deposition was performed at room temperature, mild agitation, with a current intensity of 20 mA/cm^2 for approximately 90 minutes, to reach a thickness of about 40 µm, in order to obtain a self-standing copper layer.

The low current intensity is preferable to avoid stress deformation effects after detachment from the steel plate or during graphene deposition at high temperature. Distortion during chemical vapor deposition is still slightly perceptible despite the low current density and can be furthermore enhanced by the linear thermal expansion coefficients differential between copper and ruthenium ($\alpha Cu=16,6 \times 10^{-6} K^{-1}$ $\alpha Ru= 6,4 \times 10^{-6} K^{-1}$). After the deposition the copper foil is easily detachable from the steel plate bending the flexible mandrel. The surface in contact with the steel will be used as substrate for ruthenium deposition and graphene growth because of the lower roughness. After the detachment the surface is mechanically polished with velvet spinning plates sprayed with alumina powder. The back face of the copper foil is then covered with tape to prevent the formation of ruthenium in the subsequent phase, the electrodeposition of Ru. This is performed at 50°C with current intensity of 5 mA/cm^2 for about 30 minutes. The solution is prepared with hydrate $RuCl_3$ (8 g/l) and NH_2SO_3H (15 g/l), a platinum anode was used and the ruthenium substrate reach an approximate thickness of 500 nm. Since the CVD reactor has limited space to locate the substrates in the reaction chamber and to improve the efficiency and the number of samples, the 10 cm^2 piece has been cut to form 1 cm^2 square samples.

Type B conformation is similar to the previous setting, in which an electroformed copper substrate has been produced from the same $CuSO_4$ and H_2SO_4 solution with the same process shown before and the same characteristics. The size of the samples is the same both in surface area (approximately 2 cm wide and 5 cm long) and thickness (40 µm thick). The main difference is the absence of the subsequent ruthenium electroplating onto the copper layer, which has been polished in the same fashion of the previous samples with comparable roughness. The intact samples are then divided in to various independent substrates with dimension of approximately 1 cm^2.

Type C samples are designed to neglect the hypothetical influence of copper presence during the graphene deposition. To do so was chosen silicon oxide as substrate because of its high melting temperature and low interactions with ruthenium, however an electroless deposition with hydrofluoric acid has been

excluded due to the etching power of HF on SiO_2 that would have exposed the ruthenium layer into direct contact with Si. Studies on Si-Ru phase diagram (in Figure 27) has shown miscibility between those two elements at high temperature typical of that of graphene deposition range.

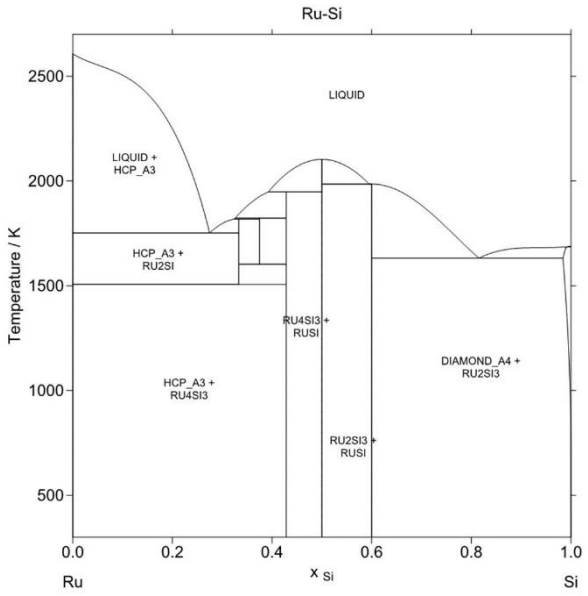

Figure 27 - Phase diagram of a ruthenium-silicon system.

Type C samples are therefore produced starting from *type A* conformations, which are etched in nitric acid to dissolve the copper foil. The main problem with this process is the intrinsic fragility and handling difficulties related to the 500 nm thin ruthenium layer. Once the original *type A* sample is carefully lay onto the nitric acid solution surface, if the amount of HNO_3 into the aqueous solution is properly tuned (35 % volume), it floats on top of the solution and when the copper is completely etched, the remaining ruthenium layer remain unaltered. A too high concentration of nitric acid can lead to excessive bubbling and subsequent disintegration or damaging of the ruthenium layer. After the bubbling is ceased the floating foil is carefully fished with a glass slide and after water rinsing it is transferred onto a silicon wafer with native oxide on top of it. This phase is followed by drying at room temperature.

Type D samples are similar to *type A* and *type B* substrates, but are subject to a double side ruthenium deposition. The copper layer is produced as in the first two

cases with the same process and has the same surface characteristic and dimensions. In this case the back side is not covered with kapton tape, to allow covering of both sides of the copper foil. During ruthenium deposition (performed under the same conditions and using the same solution as in *type A*) the polished face is directed towards the platinum anode. This to ensure good current distribution and optimal plating of the substrate, since the back face is not relevant for the deposition of the graphene layer. Despite non-ideal current distribution, the secondary face of the sample presents an high quality ruthenium plating but a rougher surface, that anyway does not play a significant role in the subsequent deposition. As in the first two cases the main sample is divided into different 1 cm^2 secondary substrates.

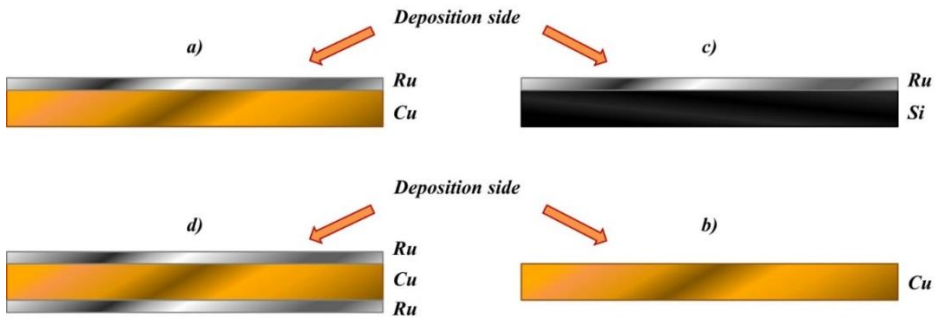

Figure 28 - Scheme of the four different sample's setting indicating the side undergoing graphene deposition being a) Type A, b) Type B, c) Type C and d) Type D.

3.5 Sample characterization

To characterize the fundamental aspects of the different substrates, various techniques had been taken in consideration in order to collect data during and after the development of the samples. One of the first steps has been to verify and to ensure a constant ruthenium thickness through all the samples, of about 500 nm, since ruthenium growth becomes difficult and slow after such threshold thickness. A functional deposition time to guarantee a suitable thickness was set at 30 minutes but the Faraday law has proven to have a low reliability in terms of predicting the thickness of a deposit in case of ruthenium, especially with long deposition times and not ideal conditions. The Faraday law states that the mass of

a metal deposited at the cathode is proportional to its molar mass divided by the change in oxidation state upon electrolysis process.

$$m = \frac{Q\ M}{F\ z}$$

Where ***m*** is the mass of the metal deposited at the electrode, ***Q*** is the total electric charge (intensity of current times period of application), ***F*** is the Faraday constant (96485 C mol^{-1}), ***M*** is the molar mass of the metal and ***z*** is the number of electrons transferred per ion. For Faraday's first law, ***M***, ***F***, and ***z*** are constants, so that the larger the value of ***Q*** the larger ***m*** will be. For Faraday's second law, ***Q*** (selected by the operator), ***F***, and ***z*** are constants, so that the larger the value of ***M/z*** (equivalent weight), again the larger ***m*** will be. Once the deposited metal mass is obtained, is almost immediate to get the thickness of the deposit using the area of the substrate and the density of the metal. A more reliable method is to characterize the sample using X-ray fluorescence (XRF) which make use of X-rays, a type of electromagnetic wave comparable to visible light rays but with a substantially shorter wavelength. These waves can easily pass through substances and become stronger as the atomic number of a substance through which it passes decreases. XRF analysis is a method that uses characteristic X-rays (fluorescent X-rays) generated when a substance is irradiated. These fluorescent emissions are electromagnetic waves created when irradiated X-rays ***hv*** force inner-shell electrons of the target atoms to an outer-shell and outer-shell electrons promptly move to inner-shells to fill the vacancies (as shown in Figure 29). These emitted X-rays ***hv'*** possess energies that are characteristic to each type of element, enabling both qualitative and quantitative analysis, although only the quantitative aspect was required in this work, since the nature of the composing elements of the samples is already known.

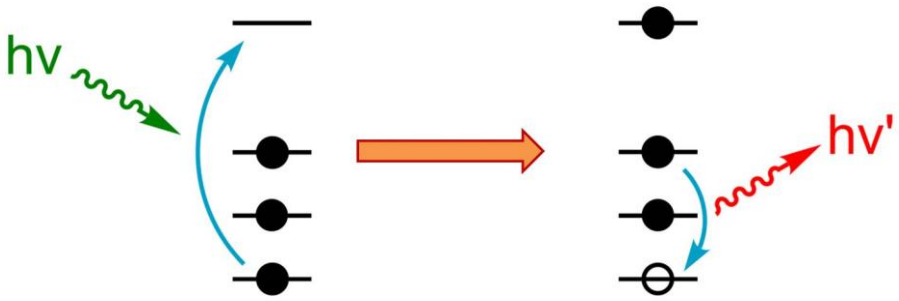

Figure 29 - Schematic representation of the principle governing X-ray fluorescence.

X-rays are generated when the X-ray tube accelerates electrons at a high voltage and bombards them against a metal anode and the fluorescence reemitted from the sample is then detected to quantify its intensity and energy level. The aim of the characterization of the sample is just to measure the thickness of the ruthenium layer on top of the copper foil. Both coating and the substrate materials produce X-ray fluorescence radiation, but the ruthenium coating attenuates the copper layer's radiation. The degree of attenuation depends on the characteristics of the coating, particularly its thickness that can be derived exploiting this effect. After ruthenium deposition, samples undergo to this kind of characterization to roughly determine if the 30 minutes deposition time is sufficient to ensure a thickness approximately of 500 nm. These measures always gave values of thickness above 400 nm, reassuring about the effectiveness of the process parameters, in particular deposition time and current density.

XRF characterization is still not completely accurate to determine ruthenium thickness but it can be helpful during the development of the samples. To precisely know the thickness of the coating, can be useful to rely on microscopy methods like scanning electron microscopy (SEM). In a typical SEM, an electron beam is emitted from an electron gun in which the cathode is a tungsten filament, since it has a high melting point and low vapor pressure it can be heated until electron emission. The emitted electron beam, which typically has an energy ranging from 0,2 keV to 40 keV, is focused through one or two condenser lenses to reach approximately a diameter from 0,4 nm to 5 nm. The beam passes then through pairs of deflector plates in the electron column, typically in the final lens, which deflect the beam in the *x* and *y* axes making possible the scanning of the

sample surface over a rectangular area. When the electron beam interacts with the sample, the electrons lose energy by repeated random scattering and absorption within the interaction volume inside the sample. The energy exchanged between the specimen and the electron beam results in several effect such as reflection of high-energy electrons by elastic scattering, emission of secondary electrons by inelastic scattering and the emission of electromagnetic radiation. Each of these phenomena can be sensed by specialized detectors. The beam current absorbed by the specimen can be detected and used to create images of the distribution of specimen current. The signals are then amplified and displayed as variations in brightness on an image that relates every pixel to the position of the beam on the specimen in the microscope. The resulting image is therefore a map of the distribution of the signal intensity being emitted from the area of the specimen that undergoes to scanning. To make this possible the sample has to be placed in a high vacuum chamber, otherwise the electron beam will interact with the atmosphere and will not reach the target substrate. In order to see and evaluate the thickness of the ruthenium deposit, the samples has been cut and their sections has been investigate through scanning electron microscopy. Since the cut was performed using a common pair of scissors, the sectioning is not sharp, consequently the ruthenium coating tends to crack and bend at the edge of the investigated cross section. Instead of having an ideal sectioning with two distinguishable exposed areas composed by the two different materials, the copper substrate is only visible through the cracked ruthenium that has been bent by the cutting action and smeared over the sectioned copper foil. As shown in Figure 30, after various trials has been found a suitable area to examine, in which a ruthenium scale is partially detached and its section is properly oriented for a realistic estimation of its thickness. A close up of the ruthenium scale is shown in Figure 31 and it presents, as expected, a thickness in the order of 500 nm.

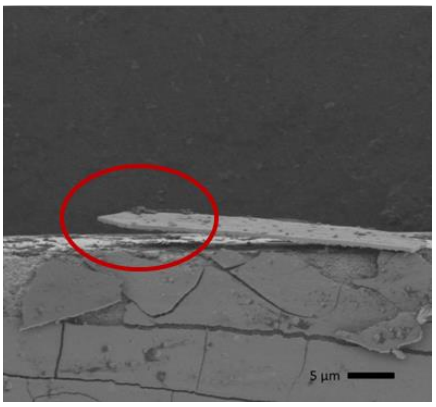

Figure 30 - On the left a scale of ruthenium seen via scanning electron microscopy (in the red circle).

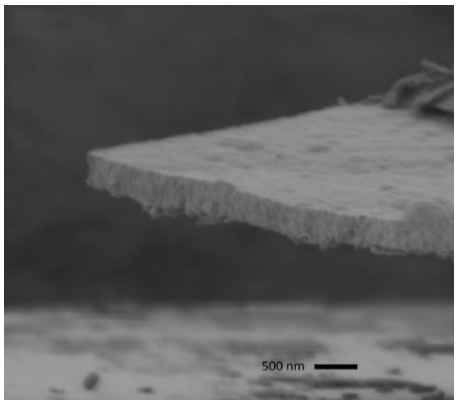

Figure 31 - On the right a close up of the same scale.

Another simple and immediate method that can be used to characterize the substrate, in order to have a reasonable degree of certainty of having copper on the back side and ruthenium on the main side, is to perform a resistivity measurement. To achieve this result was used a four-terminal sensing or four point probes method**.** This characterization method consists in a simple apparatus for measuring the resistivity of conductor samples by passing a current through two outer probes and measuring the voltage through the inner probes in contact with the substrate. The resistivity is then obtained using the equation:

$$R_s = C\,\frac{V}{I}$$

Where $\boldsymbol{R_s}$ is the superficial resistivity of the substrate, $\boldsymbol{V}$ is the measured potential at the inner probes, $\boldsymbol{I}$ is the imposed current at the outer probes and $\boldsymbol{C}$ is a constant equal to 4,53. This number is related to the fact that has been performed a measure of surface and not bulk resistivity and it takes into account various corrections associated to edge effects. To reveal the presence of copper or ruthenium respectively on the back and front side of the sample, the theoretical and the measured values of resistivity has been compared. The obtained values are:

- Measured back side resistivity: 2,45 10^{-08} mΩ cm
- Theoretical copper resistivity: 1,72 10^{-08} mΩ cm
- Measured front side resistivity: 6,31 10^{-08} mΩ cm

- Theoretical ruthenium resistivity: $7{,}10\ 10^{-08}$ mΩ cm

Both measured resistivity are comparable to the theoretical values of the element that should be found on the respective side, slight deviations could be ascribed to the lack of suitable corrections taking into account the depth of the material or possible presence of impurities coming from handling or production aspects. On the front side, a lower value of resistivity can be also explained by the presence of copper traces which could increase the superficial conductivity, probably due to slight grain boundaries diffusion, which unlikely happen in the opposite direction due to the much larger path the ruthenium should travel to reach the back surface.

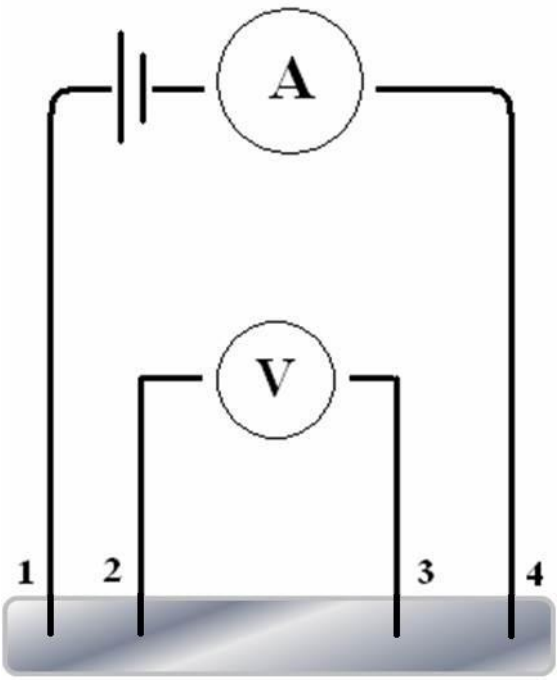

Figure 32 - Four-point probe in which measurement of resistance occurs between connections 2 and 3 while current is supplied through probes 1 and 4.

Another aspect to consider is the roughness of the various substrates and to do that has been used an atomic force microscope (AFM). The AFM setting consists of a cantilever used as probe with a sharp tip at its end that is used to scan the sample surface. When the tip is dropped into proximity of a sample surface, forces between the tip of the probe and the specimen lead to a deflection of the cantilever. The kind of forces that can be measured in an AFM characterization include mechanical contact force, van der Waals forces, capillary forces, chemical bonding or electrostatic forces. Those depend on the typology of characterization

needed or on the sample which is sensed. Typically, the deflection is measured using a laser beam reflected from the polished top surface of the cantilever into an array of photodiodes. Other methods that can be used include for example the utilization of piezoelectric sensing devices. The amount of deflection of the cantilever is related to the z direction displacement of the surface being investigated and moving the tip or the sample in the other two directions, can be build a three dimensional map of the sample surface.

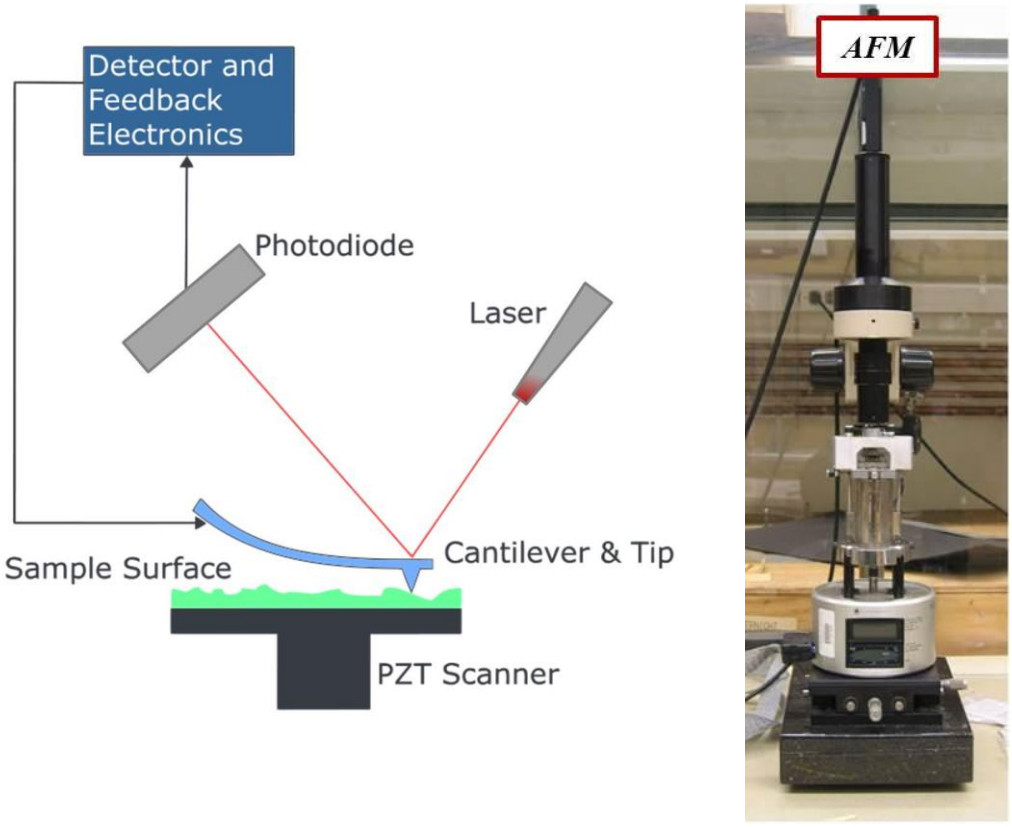

Figure 33 - On the left side a scheme showing the general functioning of an atomic force microscope and on the right the Berkeley's AFM used to characterize the substrates.

The AFM can be operated in several modalities, depending on the application. These various modes are divided into contact, non-contact or tapping mode. In **contact mode** the tip is dragged across the surface of the sample and the mapping is performed either using the degree of deflection of the cantilever or using the feedback signal required to keep the cantilever at a constant distance from the surface. In **non-contact mode**, the tip of the cantilever does not touch the sample surface. The probe is instead oscillated and the van der Waals forces decrease the resonance frequency of the cantilever. Adjusting the average tip-to-sample

distance, a constant frequency can be maintained, and measuring this distance in every point of the surface, allows the scanning software to construct a topographic image of the sample surface. In **tapping mode**, the cantilever oscillates up and down at its resonance frequency through a small piezoelectric element mounted in the AFM tip holder. The interaction of forces acting on the cantilever cause the amplitude of its oscillation to decrease as the tip gets closer to the sample. A tapping AFM representation is therefore produced by imaging the force of the intermittent contacts of the tip with the sample surface while the cantilever is scanned over the specimen. The main advantage of this technique is to decrease the damage done to the surface (and also to the tip) compared to that done in contact mode. This last method has been used to obtain the roughness values of the back and front side of the various samples. While the characterization of the back side is secondary, was important to achieve the same roughness throughout the various samples main side and verify that.

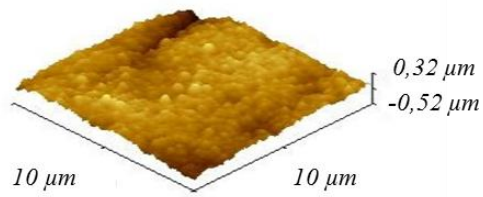

Sample 1 front side
R_a=65,8 nm
R_{rms}=88,6 nm

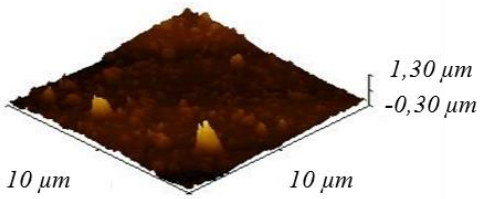

Sample 2 front side
R_a=65,8 nm
R_{rms}=94,8 nm

Figure 34 - Comparison via AFM between two different Type A samples obtained from two distinct electrodeposition and polishing processes.

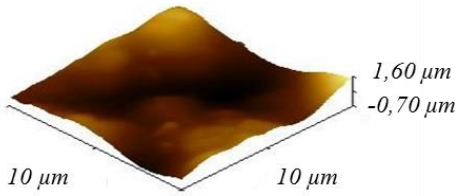

Sample 1 back side
Ra=311 nm
Rrms=389 nm

Figure 35 - AFM of the back side of a generic Type A sample showing higher roughness respect to the polished main side.

Where Ra is the arithmetic average roughness and Rrms is the root mean squared roughness, both necessary for a complete study of the surface. The back side shows a higher roughness than the main one because during the electroplating process the side in contact with the smooth mold was the other one, in addiction the secondary surface has not been polished. The front side in both samples has instead a much lower roughness because of the nature of the electroplating process itself and the polishing procedure which has been performed. Comparing the two samples' front side are obtained really close values of surface roughness both in Ra (in this case the identical value is a lucky coincidence) and in Rrms.

3.6 Thermal chemical vapor deposition

As previously indicated, graphene was growth through chemical vapor deposition because of reproducibility, reliability and the fact that can produce, with suitable machinery, large area coverage and high-quality graphene.

CVD, specifically thermal chemical vapor deposition, is a technique able to produce thin solid film, developed on substrates from vapor species through chemical reactions, which play a crucial role in the process and are the distinctive characteristic of CVD processes compared to other deposition techniques as for example physical vapor deposition. A basic representation of a typical thermal CVD reactor is shown in Figure 36 [40].

The system of gas delivery is always present and it is composed by as many gas channels of gaseous precursors are needed for the deposition to be achieved. Reactive gas species are introduced into the reactor chamber to a tubing system and mass flow controllers (MFC) that provide the possibility to control the flow

rates of each fed gas, while a mixing unit guarantees the homogeneous and uniform blending of gases before they can reach the deposition area.

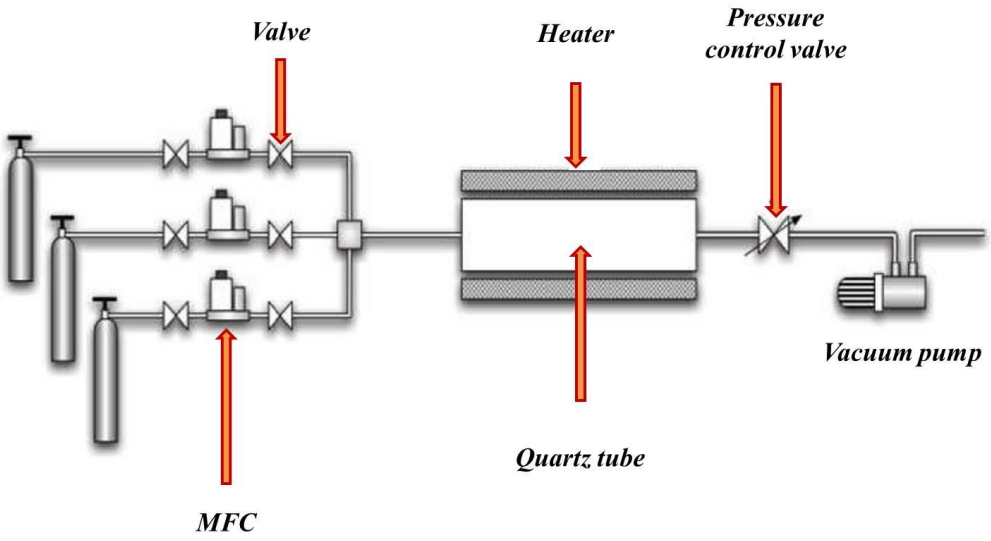

Figure 36 - Scheme of a basic tube-furnace CVD system, the tanks may contain CH_4, H_2 and Ar.

The reactor is where the substrates are initially placed and heated in order to activate their surfaces, and where the chemical reaction for the production of the graphene takes place. Downstream of the plant a pump is present to both create the vacuum inside the reactor and to dispose the by-products possibly formed during the deposition process. Despite the ease with which is possible to control the operative parameters as temperature, pressure, flow rates and deposition time, chemical vapor deposition is a long way off to be an easy process to control. Transport kinetics of gas species tend to be quite complicated indeed, because convection and diffusion dominate in different regions of the quartz tube inside the reactor. Furthermore, the deposition reaction takes place in different steps and the identification of these stages is not always immediate.

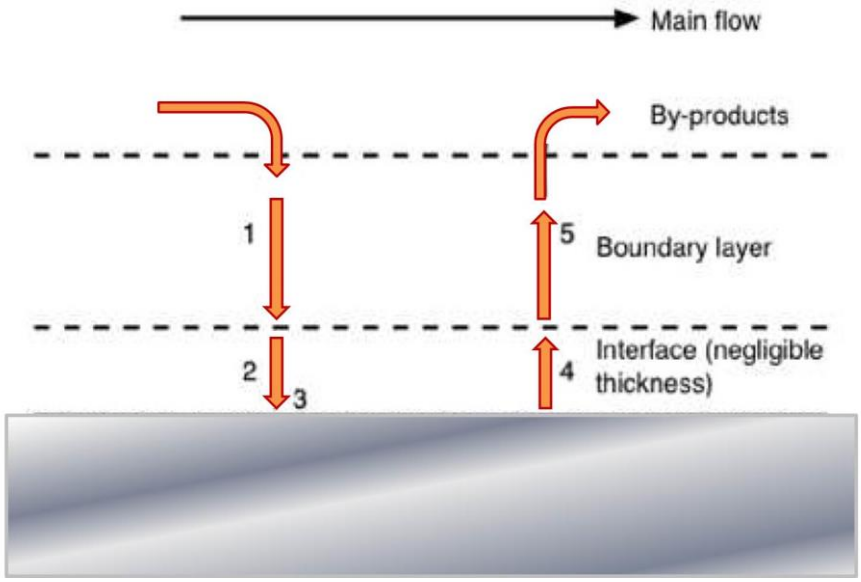

Figure 37 - Stages of the reaction developing into the deposition chamber.

As shown in the scheme above (Figure 37), initially the reactants diffuse through the boundary layer (1) and they are transported and then adsorbed onto the substrate surface (2). Subsequently surface diffusion due to high temperatures followed by chemical reaction on the surface takes place (3) and finally, the by-products are desorbed from the surface and diffuse away along the boundary layer due to differential of pressure created by the pump at the end of the chamber [40]. Is interesting to point out that one of the reasons making thermal CVD so practical is the fact that allows better coverage thanks to surface diffusion (step 3) enhanced by the high temperatures intrinsic in this particular process. The boundary layer can affect the uniformity of the thin film deposited, because as shown in Figure 38, it assumes a parabolic shape along the direction of the gas flow, resulting in a differential diffusion rate with slower amounts of diffusion at the thick boundary layer region. As a consequence there is the possibility to deposit thin films with different thickness values depending on the position taken in consideration on the substrate respect to the direction of gas flow, or even the sample position inside the chamber.

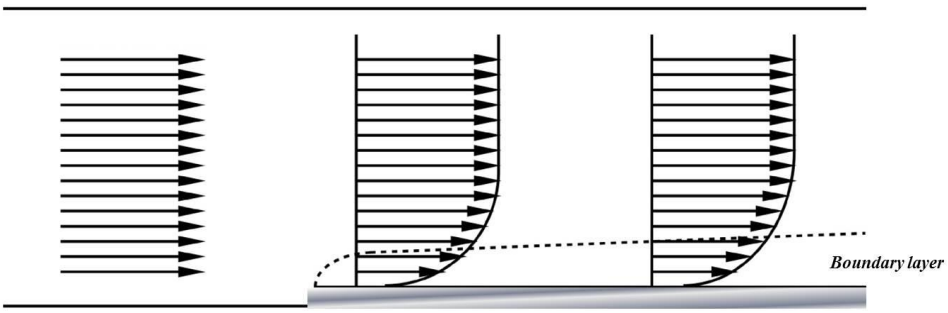

Figure 38 - Shape of the boundary layer region at the substrate surface.

As for the influence of the operative conditions, pressure has influence on tuning the diffusion rate by acting on the thickness of the boundary layer. Working with low pressures during the process means to minimize the diffusion rate by lowering the boundary layer above the substrate, this is due indeed to the inverse relation between the layer's thickness and the pressure in the chamber. Temperature, instead, has a dual function and it affects both the kinetic of the process and the microstructure of the deposited film. Higher temperatures mean greater diffusion rates and faster reactions, while low temperature can lead to structures with smaller grains in the deposited film by decreasing the diffusion length of the adsorbed atoms onto the substrate surface. This can be desirable for a great variety of deposited thin films, but, specifically, not for high-quality graphene that requires a large grained structure. In the case of this work was also to be taken into account the relative low melting temperature of copper, but this issue will be better discussed in following paragraphs. In a chemical vapor deposition process the substrate also plays a key role in the whole procedure since chemical reactions usually need a certain amount of energy to occur, metal catalysts are used as substrates for the deposition. The reason is that they have the characteristic of lowering the energetic barrier of the reaction making possible the deposition at lower temperature compared to processes carried out without catalysts.

Thermal chemical vapor deposition is then a very complex mechanism and will be exposed in the next chapter that the influence of all these factors involved in the process, is rather significant on the final outcome. The situation is even more complicated in the case of graphene, since is composed of a layer of just one atom

in thickness and every change in the operative conditions have profound consequences and can compromise the success and quality of the deposition.

3.7 Graphene deposition

The procedure used to perform graphene deposition went through a slow development and refining during the thesis work carried out at the University of California Berkeley. Since copper has a relatively low melting temperature of approximately 1083°C, there is an issue involving the possibility of melting the copper while working at high temperatures typical of high temperature chemical vapor deposition technique. To quantify this problem and provide a possible solution, were almost simultaneously tested two different methods to deposit graphene: low and high temperature CVD, which will be discussed in the next paragraphs.

Since it was previously discussed the general aspect of a CVD reactor, can be useful now to briefly introduce the actual device that was used to produce all the samples described in this thesis work. Graphene deposition was carried out in a Lindberg MTS Reactor, shown in Figure 39. Samples are loaded from the left side in a quartz tube in which the chemical reactions take place.

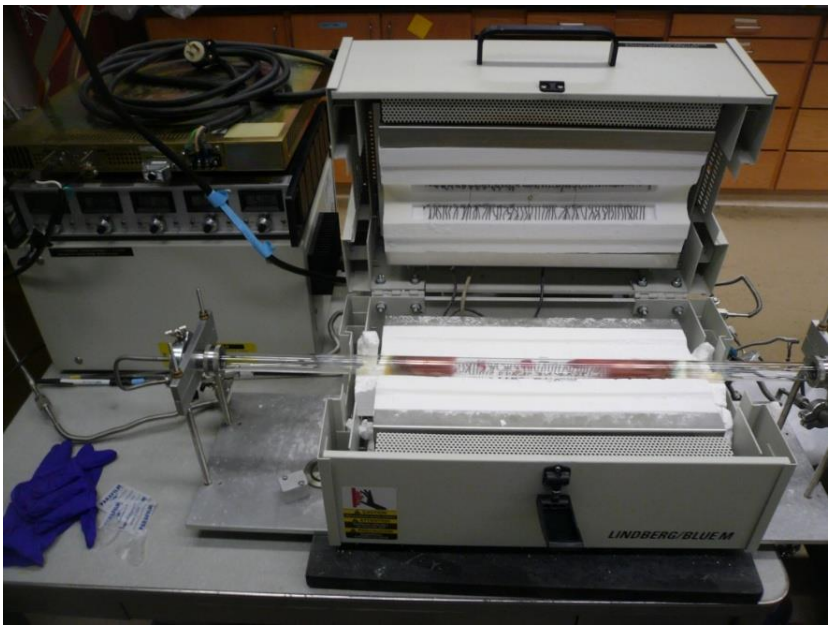

Figure 39 - CVD reactor used for graphene synthesis.

The reaction chamber (quartz tube) is surrounded by a refractory material containing heating coils and thermocouples. A vacuum pump is connected with the right side of the quartz tube and controlled by a valve, while on the left side a gas inlet allows to govern the flow of the gas mixture inside the tube. A device allowing gas mixture manipulation is linked by means of electrovalves to the gas channels (Figure 40), and with a thermostat it is possible to set the desired temperature.

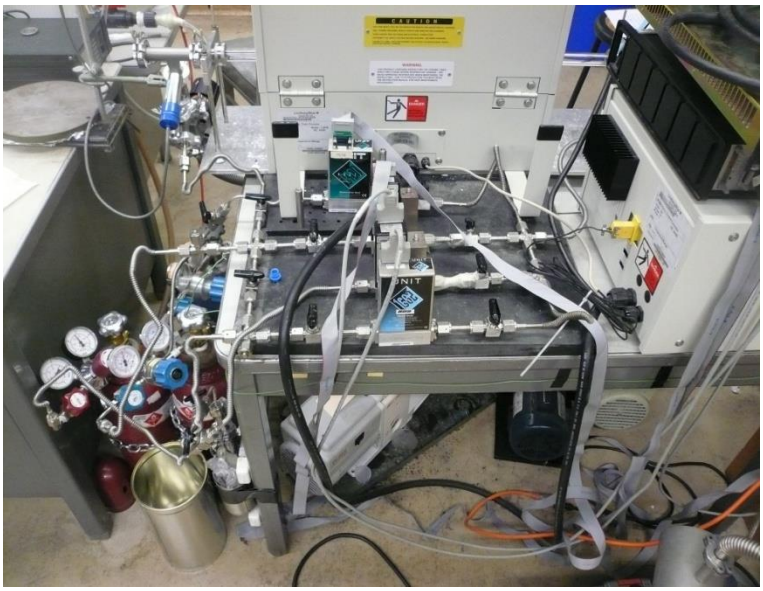

Figure 40 - Particular of the electrovalves controlling the flow of the various gases.

In order to minimize waste of material and to simplify the loading and unloading of the samples inside the quartz tube, the sample are cut in pieces of approximately 10 mm x 10 mm, except for *Type C* samples which are developed using 1 cm^2 sized ruthenium substrate onto a larger silicon slice. Before undergoing every deposition, all the samples undergo to a cleaning procedure, consisting in a two-step sonication first with acetone and then with isopropyl alcohol. Sonication is maintained five minutes for both the steps. The loading and unloading phases are performed carefully pushing or pulling the various samples inside the tube using a suitable hook. At the beginning of the deposition procedure the CVD quartz tube chamber is heated at 800°C in order to clean the chamber from impurities and to evaporate possible traces of humidity, then the furnace is cooled down and as soon as the inner temperature reaches a safe value (usually 200°C) it is possible to load the sample and start the graphene deposition.

3.6.1 Low temperature CVD

Low temperature chemical vapor deposition was carried out testing two different carbon sources: liquid benzene (C_6H_6) and liquid toluene (C_7H_8) since being both ring-structured molecules, resembled the basic unit of graphene and the molecules just needed to dehydrogenate and connect to each other to form graphene structure, making easier its growth compared with high temperature CVD which exploit the use of gaseous methane (CH_4).

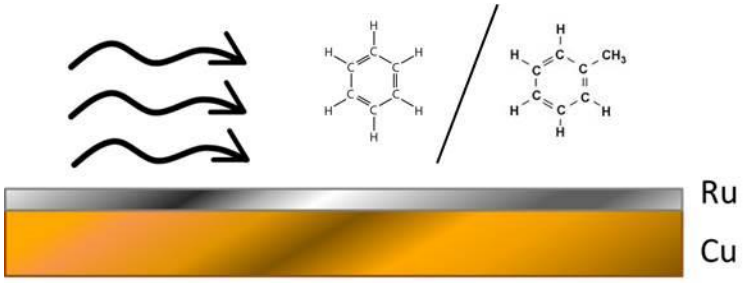

Figure 41 - Scheme of deposition with toluene or benzene as precursors on Type A sample.

To feed the liquid precursors into the chamber, a small amount of benzene or toluene were poured in a ceramic container with cylindrical shape and placed at the beginning of the quartz tube as far as possible from the reactor furnace, as shown in Figure 42 and then covered with aluminum foil which was punctured in order to open 5 holes of approximately 1 mm of diameter to let the liquid precursor pass. The temperature in that section of the quartz tube was almost the same as the one in the external environment, so there was no danger of contamination from the container or the aluminum foil. Since benzene and toluene are volatile chemical species under atmospheric pressure and room temperature conditions, the vacuum pump was turned off in order to reach a safe atmospheric pressure. Subsequently, evaporated precursors together with a flow of H_2 were let flow in order to saturate the quartz tube with benzene or toluene molecules.

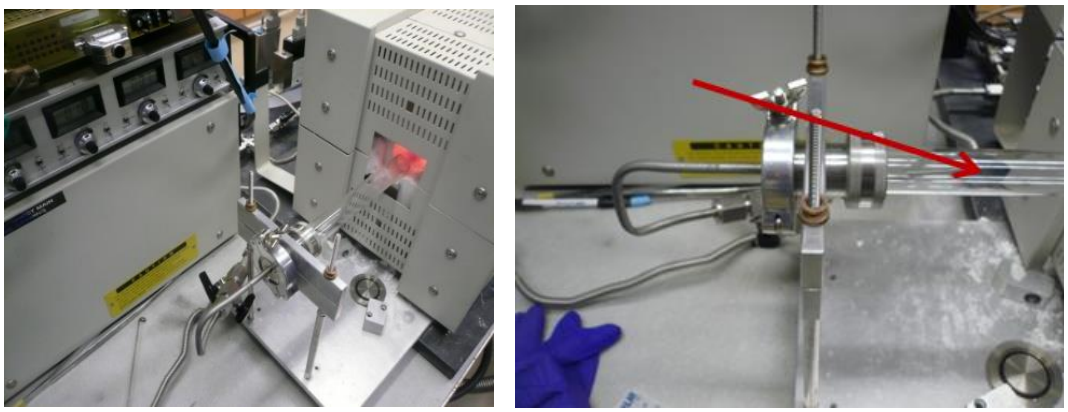

Figure 42 - On the left is shown the inlet of the gases in the quartz tube, on the right a close up on the same area indicating where the cylindrical container can be located. This whole manifold can be dismounted to allow sample loading and unloading.

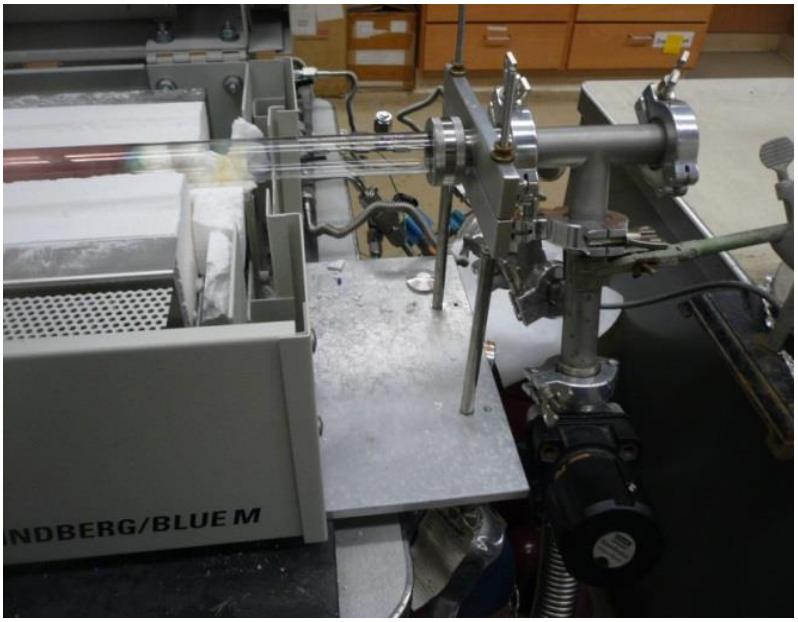

Figure 42: (b) Particular on the right side of the deposition chamber showing the valve (in black) connected to the vacuum pump

Subsequently the reactor was brought to the desired temperature for the chosen time of deposition. The final step was the cooling process, performed with a cooling rate of 20°C/min. Deposition time, temperature and pressure were varied during numerous tests for both toluene and benzene without promising results. The outcome of this part of the work is better exposed and discussed in the next chapter.

3.6.2 High temperature CVD

In parallel with the tests concerning low temperature chemical vapor deposition was developed a method to perform graphene growth with high temperature CVD. First of all to avoid sample oxidation, the tube is under vacuum with Hydrogen flow since the beginning of the deposition, this also helps to clean the sample from native oxidation and keep the surface clean and active for the deposition process [41]. Under this conditions ($2 \cdot 10^{-3}$torr of pressure and 10 standard cubic centimeters per minute of hydrogen) the temperature is set at 1000°C to anneal and clean the sample. At least 25 minutes are needed to reach 1000°C since the loading of the sample, but the next step of the deposition process is performed at a total of 30 minutes from the loading and the simultaneous beginning of the heating curve. After the annealing of the duration of overall 30 minutes, 20 sccm of methane are inflated in the tube for 10 minutes while the temperature still at 1000°C. This step is the actual graphene deposition and it uses methane as carbon precursor and after this deposition stage the temperature is set to 0°C and the cooling curve begins. When the temperature in the chamber reaches 600°C the methane flux is stopped, while the hydrogen flow is maintained till the temperature inside the furnace reaches a safe value to allow the unloading of the sample (typically 200°C) without danger for the operator and excessive thermal shock for the sample. This described is the experimental setting which gave the best results in terms of reliability and quality of the deposited graphene but various parameters had to be tuned to reach this routine. In the next chapter will be illustrated the passages that lead to this specific procedure.

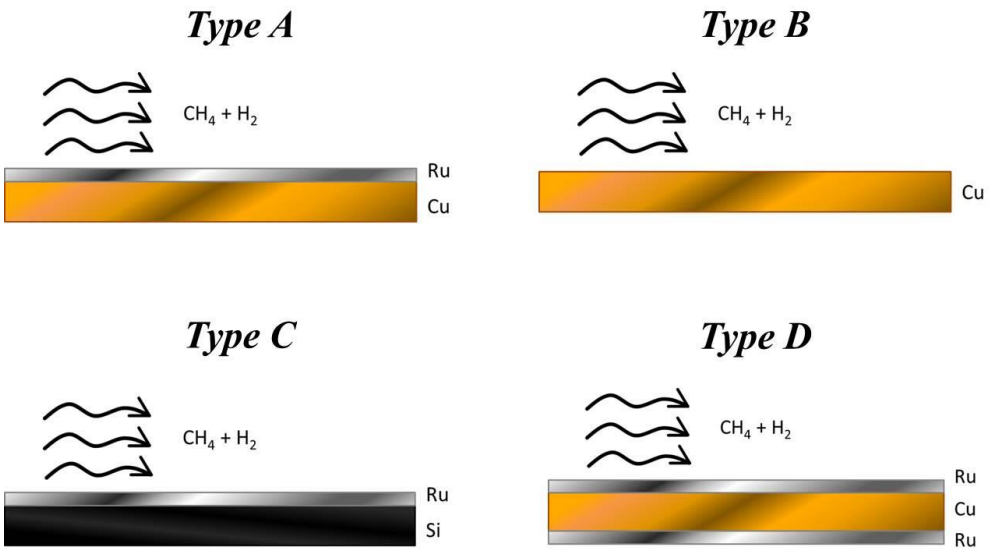

Figure 43 - Scheme of a high temperature CVD process occurring on the various substrates.

Since high temperature chemical vapor deposition gave much better results than the low temperature CVD, this last one was abandoned and the issue coming from the low melting temperature of copper has been faced changing the sample's features, specifically developing *Type D* samples. The results obtained with this new sample setting are discussed in chapter 4.

4 EXPERIMENTAL RESULTS AND DISCUSSION

4.1 Characterization methods

4.1.1 Raman spectroscopy

Raman spectroscopy provides an incredibly sensitive tool for detection and characterization of graphene. Raman spectroscopy is a light scattering technique, useful to study the fundamental excitations in solids and molecules.To briefly explain this concept, has to be said that at molecular level photons can interact with matter by absorption or scattering processes. Scattering may occur either elastically, or inelastically. The elastic process is termed Rayleigh scattering, while the inelastic process is called Raman scattering. The electric field component of the scattering photon perturbs the electron cloud of the molecule and it therefore excite the system. Raman scattering occurs when the sensed molecule exchanges energy with the photon and subsequently decays to vibrational energy levels above or below that of the initial state. The frequency shift corresponding to the energy difference between the incident and the scattered

photon is the Raman shift. A plot of detected number of photons versus Raman shift from the incident laser energy gives a Raman spectrum (obviously the number of photons will depend on the energy of the light source, therefore Raman signal is usually measured in arbitrary units). Different materials have different vibrational modes, and therefore characteristic Raman spectra. Most Raman spectrometers for material characterisation (Berkeley's Labram microRaman spectroscope with its optics is shown in Figure 44) use a microscope to focus the laser beam, light from the sample passes then back through the microscope optics into the spectrometer where is subsequently detected.

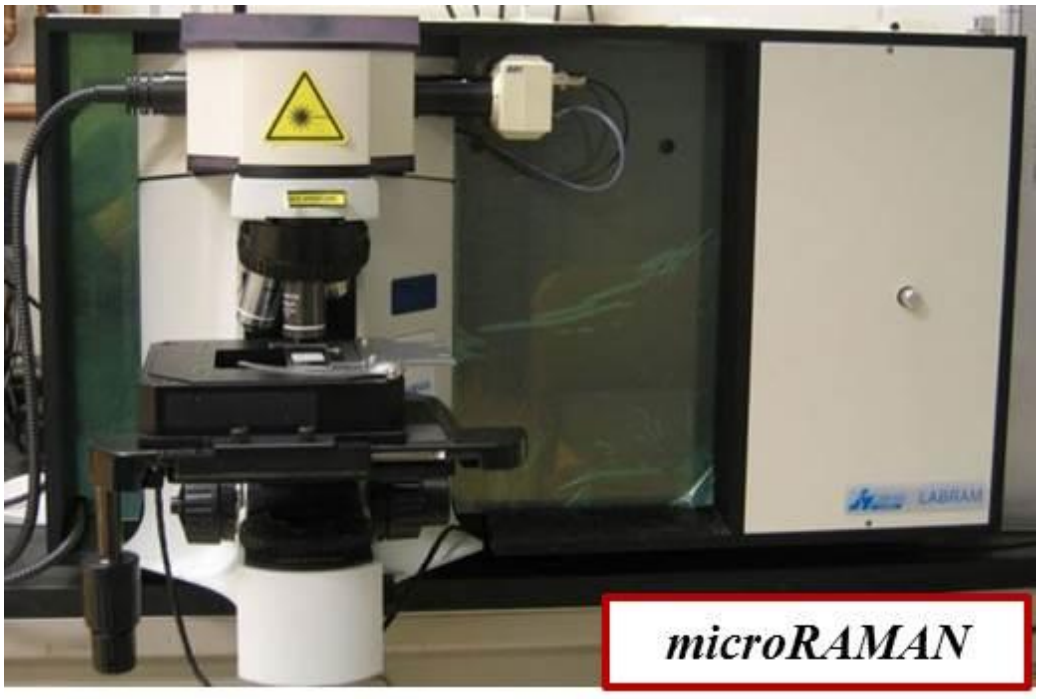

Figure 44 - Picture of the UCB Labram microRaman used to perform all the measurement in this thesis work.

4.1.2 Graphene Raman spectra

A typical Raman spectrum for a graphene layer presents a peak around 1580 cm^{-1} on the Raman shift called G peak, typically corresponding to the main graphite peak. In the case of graphene though, its G peak must be considerably less intense (approximately four times smaller) with respect to another peak, called 2D peak, placed roughly at 2700 cm^{-1}. With an increase in the number of graphene layers a gradual change in the 2D peak is expected (Figure 45), tending to evolve in the

graphitic peak and therefore showing a different shape and position. The 2D peak shows a composite nature due to the overlapping of two different peaks as the graphene layers increase in number [42–44]. With respect to the single layer graphene, in a few-layer graphene the second of these peaks (approximately 2697 cm^{-1}) tends to outweigh the first (about 2655 cm^{-1}) consistently altering the shape of the 2D peak. Another interesting information for the goal of this work which can be obtained from Raman Spectroscopy, is the possible appearance of a third peak in the spectrum, called D peak and placed around 1350 cm^{-1}. It is related to the presence of various degree of defects in the graphene pattern. The more intense is the D peak, the more defective will be the deposited graphene.

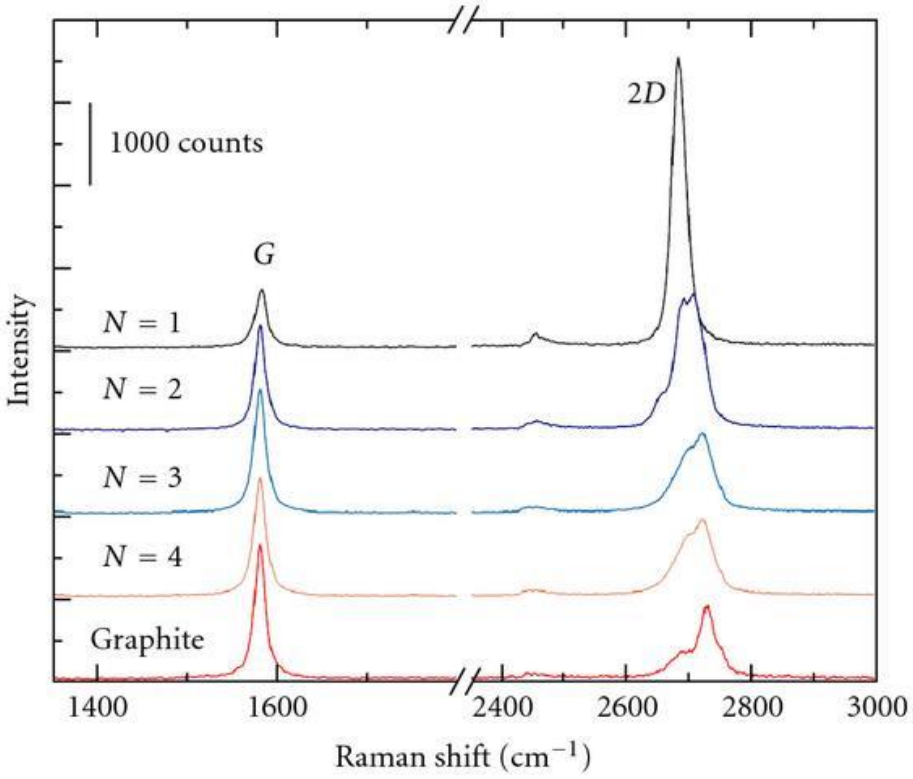

Figure 45 - Layer dependence of graphene Raman spectrum.

The following image (Figure 46) shows a superposition of two different graphene's Raman spectra performed during this thesis work, its again intended to highlight the change occurring in the shape and position of the peaks depending from the number of layers composing the deposition outcome. It can be noticed that increasing the amount of layers there is a shrinkage in the 2D peak placed at approximately 2700 cm-1. These particular spectra shows an almost negligible D

peak (meaning a low defect density), and in the case of the black spectra also a less intense G peak (located at 1580 cm-1) which indicate the presence of a graphene composed by very few layers. The grey one can be expected to have an higher number of layers.

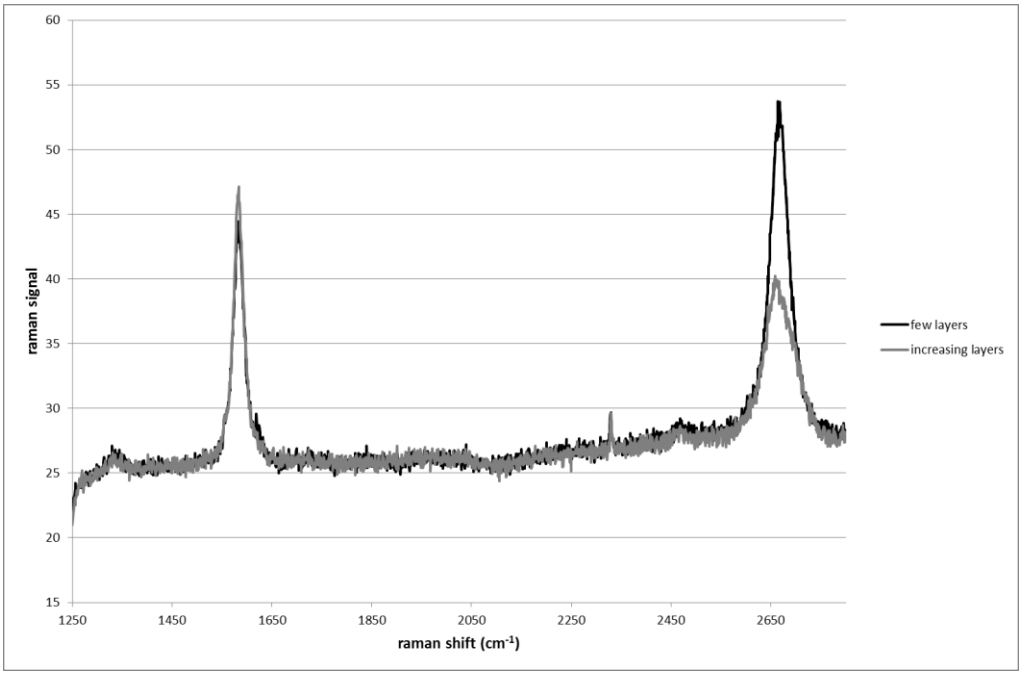

Figure 46 - Plot comparing two Raman spectra of graphene's deposits with a different number of layers.

4.1.3 X-ray photoelectron spectroscopy

X-ray photoelectron spectroscopy (XPS) is a surface-sensitive quantitative spectroscopic technique that measures the elemental composition, chemical state and electronic state of the elements that exist within a material. XPS spectra are obtained by irradiating a material with a beam of X-rays, while simultaneously measuring the kinetic energy and number of electrons that escape from the top of the material analyzed. Since the energy of an X-ray with particular wavelength is known and because the electron's kinetic energies are measured, the electron binding energy of each of the emitted electrons can be determined using the following equation

$$E_{bind} = E_{ph} - (E_k + \phi)$$

where $\boldsymbol{E_{bind}}$ is the binding energy of the electron, $\boldsymbol{E_{ph}}$ is the energy of the X-ray photons used, $\boldsymbol{E_k}$ is the kinetic energy of the detected electron and $\boldsymbol{\phi}$ is the work

function of the spectrometer. A typical XPS spectrum is a plot of the number of electrons detected and their binding energy. Since each element has a characteristic electronic configuration, is produced a particular set of XPS peaks at characteristic binding energy values that univocally identify them. An important aspect for this thesis work is that the number of detected electrons in each of the characteristic peaks is directly related to the amount of element within the XPS sampling volume. Ultra-high vacuum conditions are indeed needed for counting the number of electrons, because generally the detector in XPS instrument is usually several tens of centimeters far from the irradiated substrate, therefore, since the distance is considerable, UHV conditions are essential. XPS (Figure 47) generally consists of a source of X-rays, an UHV stainless steel chamber with UHV pumps, an electron collection lens, an electron energy analyzer, an electron detector system, a moderate vacuum sample introduction chamber and a sample holder. As for the X-rays source, a monochromatic aluminum K-alpha X-rays are usually produced by diffracting and focusing a beam of non-monochromatic X-rays off of a thin disc of crystalline quartz, resulting in a photon energy of 1486,7 eV.

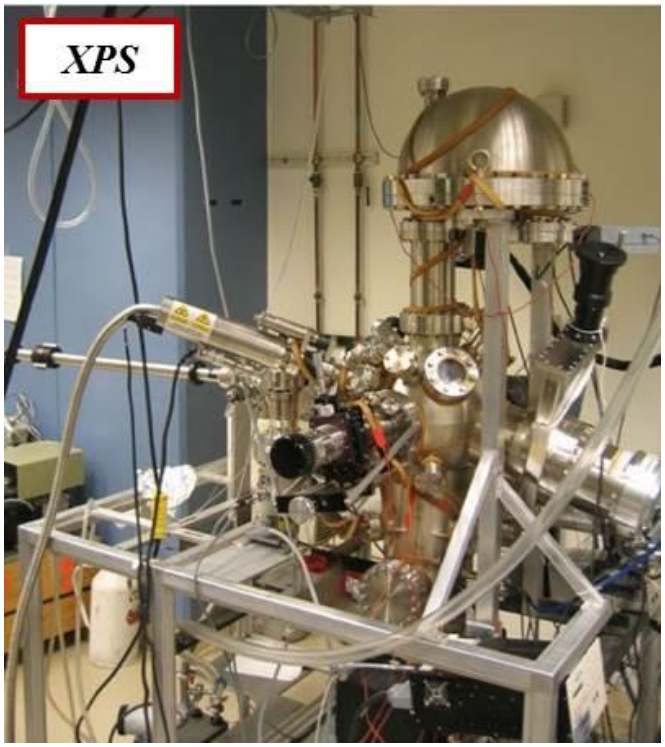

Figure 47 - Picture of the X-ray photoelectron spectroscope in University of California, Berkeley.

4.1.4 Scanning electron microscopy

As already introduced in the previous chapter, a scanning electron microscope (SEM) is a type of microscope that produces images of a sample by scanning it through a focused beam at high-energy electrons. These electrons interact with the sample atoms producing various signals containing information about the surface topography, its morphology and in some cases its chemical composition. In Figure 48 is shown a simple scheme of a typical scanning electron microscope. The types of signals produced by this microscope include secondary electrons (SE), back-scattered electrons (BSE), characteristic X-rays and cathodoluminescence (CL). Secondary electrons are commonly used for high resolution sample images, showing its morphology and topography allowing the vision of details less than 1 nm in size. Due to the nature of the electron beam (very narrow), SEM micrographs have a large depth of vision leading to an almost 3D appearance useful to understand the surface structure of the detected substrate. Obviously is possible to range through a wide range of magnifications, typically from 20X to almost 30000X. Back-scattered electrons, instead, are electrons reflected back

from the sample by elastic scattering and they are suitable to illustrate compositional contrast in case of multiphase samples. Characteristic X-rays are instead generated by inelastic collisions between the incident electrons and the negative charges present in the shells of the sample atoms. These last electrons become therefore excited and when they decay to lower energy states, they produce X-rays with a specific wavelength then used to identify the nature of the emitting material.

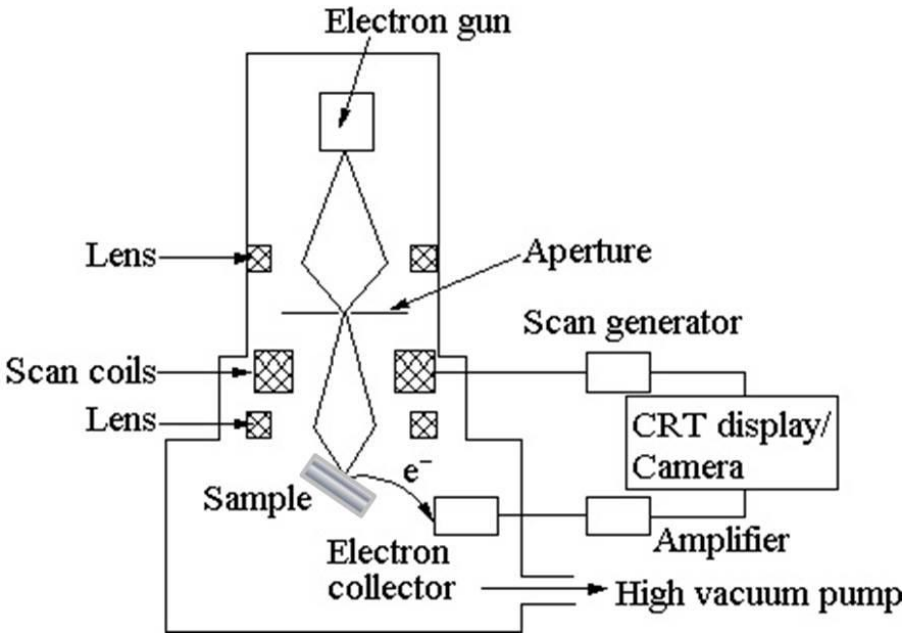

Figure 48 - Example of operating principle of a scanning electron microscopy.

The analyzed samples must also be properly prepared in order to fit in the specimen chamber and are generally rigidly mounted on a specimen holder called a specimen stub. SEM is also very practical since is a non-destructive analysis technique, does not indeed lead to a volume loss in the sample, and is therefore possible to analyze the same substrate multiple times. Taking again in consideration figure 48, the operating principle of a standard scanning electron microscope can be illustrated: the electron beam is emitted from an electron gun fitted with an electrically heated tungsten filament cathode which, as explained in chapter 3 can produce electron beam with an energy approximately between 0,2 keV and 40 keV and it is then focused by condenser lenses in a spot with diameter which can range between 0.4 nm and 5 nm. Subsequently the electron beam is

deflected inside the column in order to enhance scanning in the x and y axes in a raster fashion over a rectangular area of the sample surface. Thus, when the primary beam interacts with the sample, the electrons lose energy by repeated random scattering and absorption within the specimen interaction volume which will depend on the electrons energy and the kind of substrate. Every signal produced, is then detected by specialized sensors, and finally each pixel of computer videomemory is synchronized with the position of the beam on the specimen inside the microscope's vacuum chamber. The resulting image is therefore a distribution map of the intensity of the signal being emitted from the sensed area.

4.2 Low temperature chemical vapor deposition

As described in the previous chapter, since copper has a relatively low melting point, the first deposition trials were conducted exploiting a low temperature chemical deposition process. The precursors used to achieve graphene growth were benzene and toluene. Various attempt with both the reactants gave disappointing results despite changing various deposition parameters such as temperature, pressure, and deposition time.

The first trials were conducted on *Type A* samples using toluene as precursor at temperature of 600°C and atmospheric pressure (since liquid toluene would immediately evaporated under vacuum conditions) with an hydrogen flow of 10 sccm (standard cubic centimeter per minute) and a deposition time of 20 minutes. This deposition setting gave no results and produced a substantial damage to the ruthenium layer, therefore the parameters were changed in order to avoid possible oxidation and dissolution of Ru by increasing the H_2 flow and decreasing the deposition time. Despite working at 600°C, atmospheric pressure, 70 sccm of hydrogen and a deposition time of 15 minutes the outcome was similar to the previous attempts. Using the same parameters as the first trials was nonetheless deposited amorphous carbon on the surface of a *Type B* sample (Figure 49):

- Temperature 600°C

- Atmospheric pressure
- 10 sccm of hydrogen
- 20 minutes of deposition time

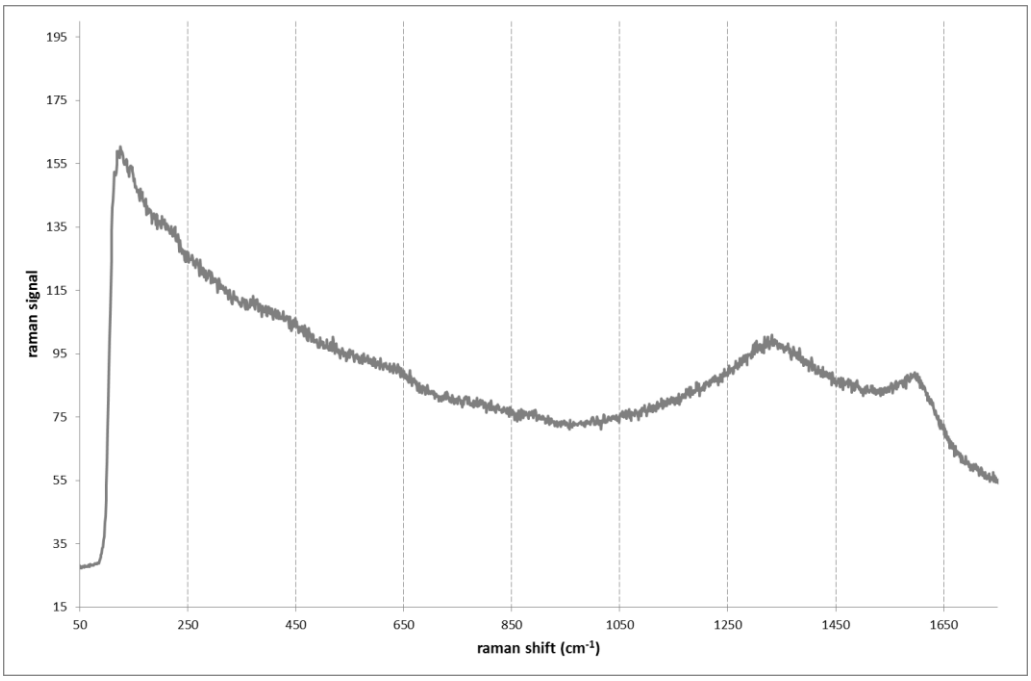

Figure 49 - Raman spectra of amorphous carbon from toluene on copper (peaks at approximately 1340 cm^{-1} and 1590 cm^{-1}).

As a consequence of these experiences were tested various depositions using benzene as precursors on *Type A* samples. The temperature was always set at 400°C and the depositions were performed at atmospheric pressure, but varying both deposition time and amount of flowing hydrogen. At low H_2 fluxes (20 sccm) was not recorded trace of graphene or amorphous carbon, but for higher hydrogen flows (50 sccm) was detected the presence of amorphous carbon as shown in Figure 50. Changing deposition time (3, 5, 10 and 20 minutes) had just a slight effect on the amount of carbon present on the substrate and no significant progresses were achieved using low temperature chemical vapor deposition as process to grow graphene.

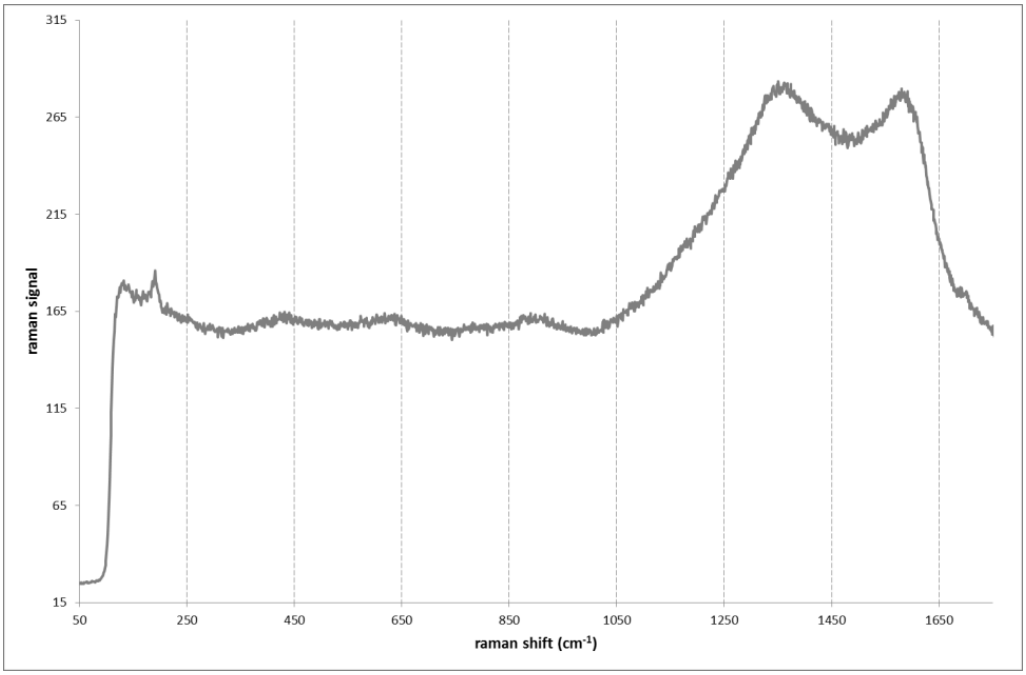

Figure 50 - Raman spectra of amorphous carbon from benzene on copper and ruthenium (peaks at approximately 1360 cm^{-1} and 1590 cm^{-1}).

4.3 High temperature chemical vapor deposition

Despite concerns about the possible disadvantages due to low copper melting temperature coupled with the relatively severe conditions of high temperature chemical vapor deposition, various attempts were carried out with these technique. Was immediately evident that this path is much more promising, since the first experience with methane as gaseous precursor was in fact found high quality graphene on *Type A* samples (ruthenium on copper) through Raman spectroscopy (will be highlighted in Figure 52). Therefore low temperature CVD was dropped in favor of high temperature depositions. All the samples then underwent graphene deposition at high temperatures.

The setting that is going to be shown represents optimal conditions which were found after several trials varying annealing time, deposition time, deposition temperature, hydrogen and methane flow. As explained in chapter 3, the deposition starts heating the CVD quartz tube at 800°C to clean the chamber from impurities, then the furnace is cooled down till the temperature reaches 200°C and it is then possible to load the sample in the reactor. Hydrogen flow since the

beginning of the deposition, in order to clean the sample from native oxides and keep the surface uncontaminated and active during the deposition process. Under this conditions ($2 \cdot 10^{-3}$torr of pressure and 10 standard cubic centimeters per minute of hydrogen) the temperature is set at 1000°C. At least 25 minutes are needed to reach 1000°C since the loading of the sample (the heating rate is fixed and not controllable), but for the next step of the deposition was waited a total of 30 minutes from the loading of the sample and the simultaneous start of the heating curve. After this 30 minutes annealing, 20 sccm of methane (the gaseous precursor) are inflated in the tube for 10 minutes (temperature still at 1000°C. Immediately after the deposition the temperature is set to 0°C and the cooling curve starts. When the temperature in the chamber reaches 600°C the methane flux is interrupted, while the hydrogen is maintained till the temperature of the furnace reaches a safe value to allow the unloading of the sample (typically 200°C). To summarize:

- Temperature at 1000°C
- Pressure at $2 \cdot 10^{-3}$torr
- 10 sccm of hydrogen
- 20 sccm of methane
- Annealing time 5 minutes
- Deposition time 10 minutes

Was obvious though (via optical investigation) that copper had reached the top of the substrate migrating both through ruthenium grain boundaries, since copper and ruthenium are immiscible and the high temperature may have promoted a change in the grain size and shape of ruthenium. Another aspect to take in consideration is the possibility of Cu evaporation and recondensation from the exposed back side of the *Type A* sample. An indication of this effect was the copper residue inside the quarts tube (Figure 51).

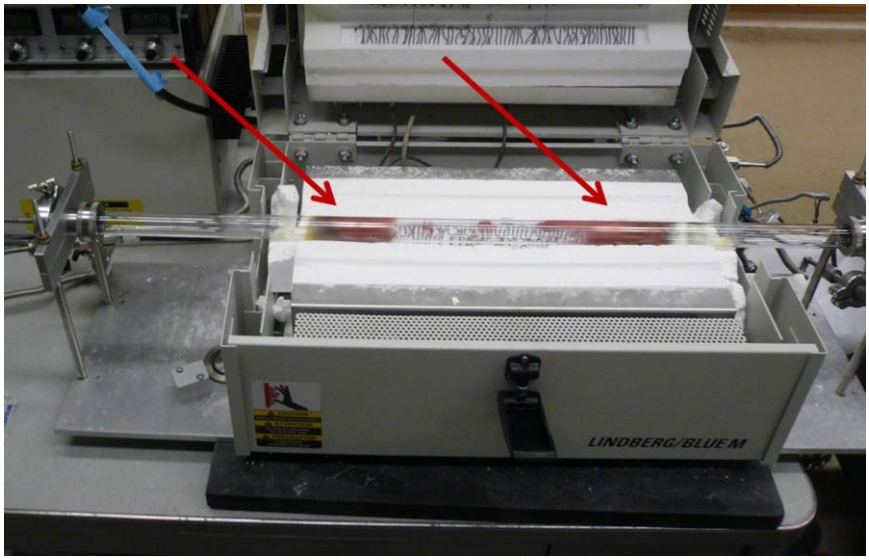

Figure 51 - Copper residue after various depositions on the inner side of the quartz tube.

Having both Cu and Ru on the substrate lead to the development of *Type B* (only copper) and *Type C* (only ruthenium) samples, in order to investigate the behavior of this polycrystalline electrodeposited elements as substrate for graphene growth.

This procedure was taken as standard for all subsequent deposition, including *Types B*, *C* and *D* samples.

4.3.1 Raman spectra of Type A graphene

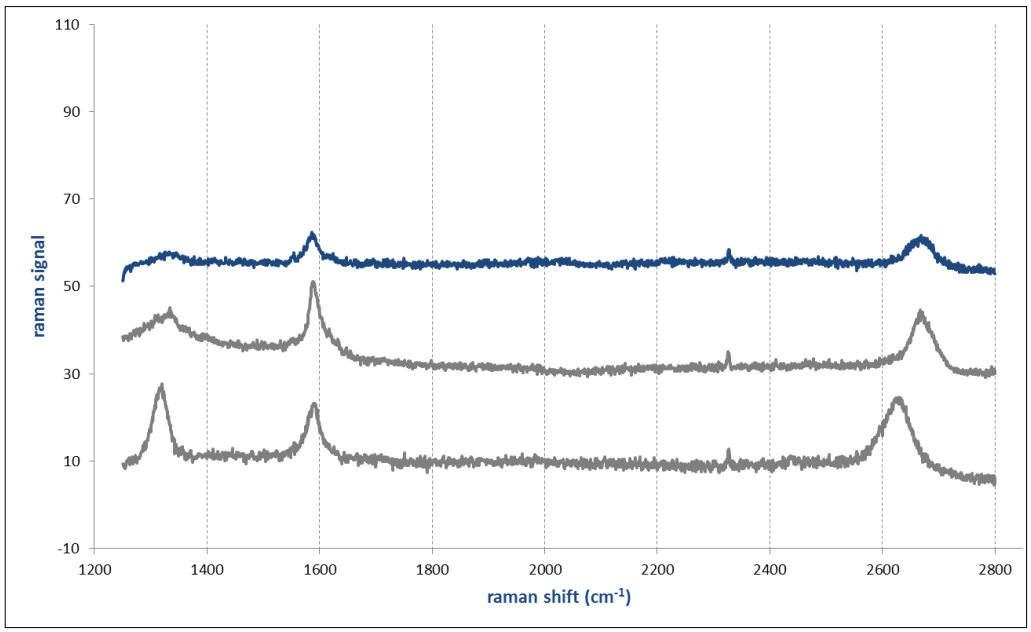

Figure 52 - In blue the Type A graphene's Raman spectrum from high temperature chemical vapor deposition with methane as precursor.

As shown in the plot above (Figure 52) the blue curve represent the Raman spectra of graphene growth on a *Type A* substrate, in which is noticeable a relatively good quality outcome. At approximately 1300 cm^{-1} is present a negligible D peak (representing the degree of defectiveness of the deposited graphene) and around 1600 cm^{-1} the G peak is comparable in size (slightly less intense) with the 2D peak at roughly 2700 cm^{-1}. This spectra can be related to graphene with a low defect density but a relatively high amount of layers. Anyway this number must be in the order of some unities, since the comparable intensities of the two peaks and the XRD considerations that will be exposed in paragraph 4.6.

4.3.2 Raman spectra of Type B graphene

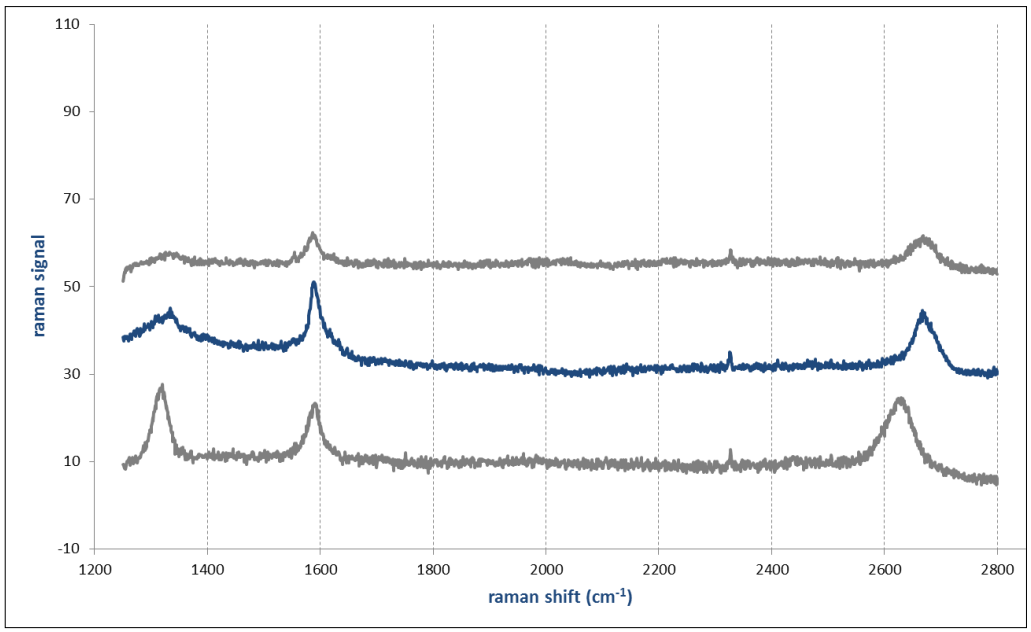

Figure 53 - In blue the Type B graphene's Raman spectrum from high temperature chemical vapor deposition with methane as precursor.

As displayed in the graph above (Figure 53), again the blue curve represent the Raman spectra of graphene growth on a Type B substrate, in this case can be seen a less good quality deposition. At about 1300 cm-1 is present a D peak which this time is not negligible anymore, having approximately half the intensity of the other peaks and therefore indicating an increase in graphene defectiveness. At 1600 cm-1 the G peak is slightly more intense than the 2D peak placed at around 2700 cm-1. Type B spectra can be associated to a graphene with a slightly higher defect density and rather high amount of layers, despite this number should not be much higher than some unities, given the comparable size between G and 2D peaks.

4.3.3 Raman spectra of Type C graphene

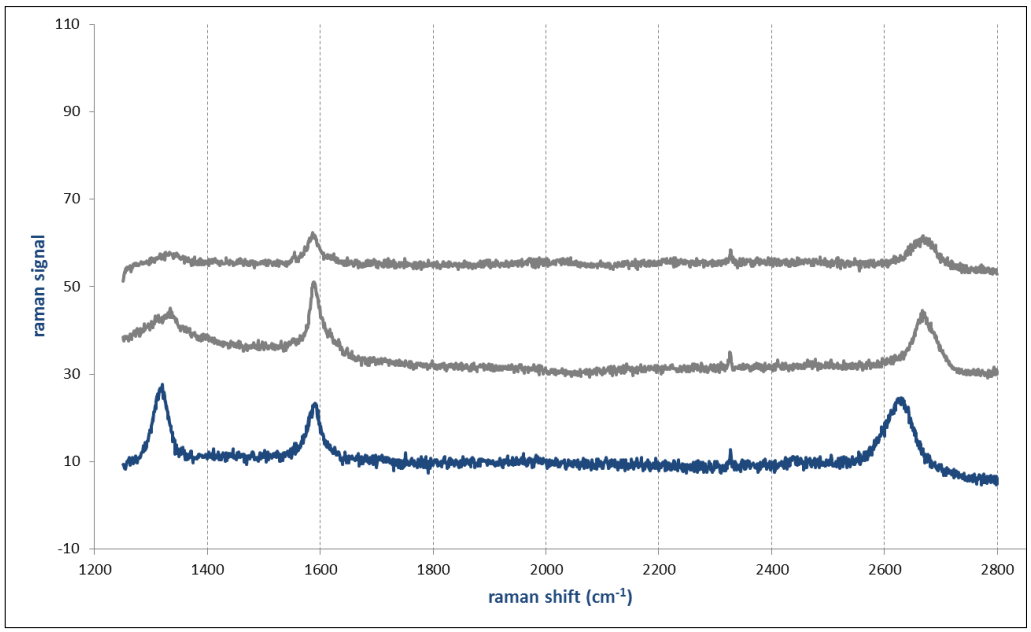

Figure 54 - In blue the Type C graphene's Raman spectrum from high temperature chemical vapor deposition and methane as carbon precursor.

The graph above (Figure 54) shows, in blue, a curve representing the Raman spectra of graphene deposited on a *Type C* substrate (ruthenium on silicon oxide). The first peak at about 1300 cm^{-1} represents the D peak (a higher D peak is related to a higher defect concentration) which is again not negligible and is instead much more intense than the *Type A* and *Type B* correspondent peaks. At a Raman shift of about 1600 cm^{-1} the G peak is though less intense than the 2D peak (last peak on the right at 2700 cm^{-1}). This lead to the conclusion that *Type C* spectrum is linked to a graphene with a high defect density but smaller amount of layers respect to the previous two samples. This can be related to the production process of the ruthenium substrate, being indeed rather severe and could somewhat compromise its properties. This was the only available process to avoid formation of secondary phases which could compromise the purity of the ruthenium substrate preserving the essential characteristic of being electrodeposited.

4.3.4 Raman spectra of Type D graphene

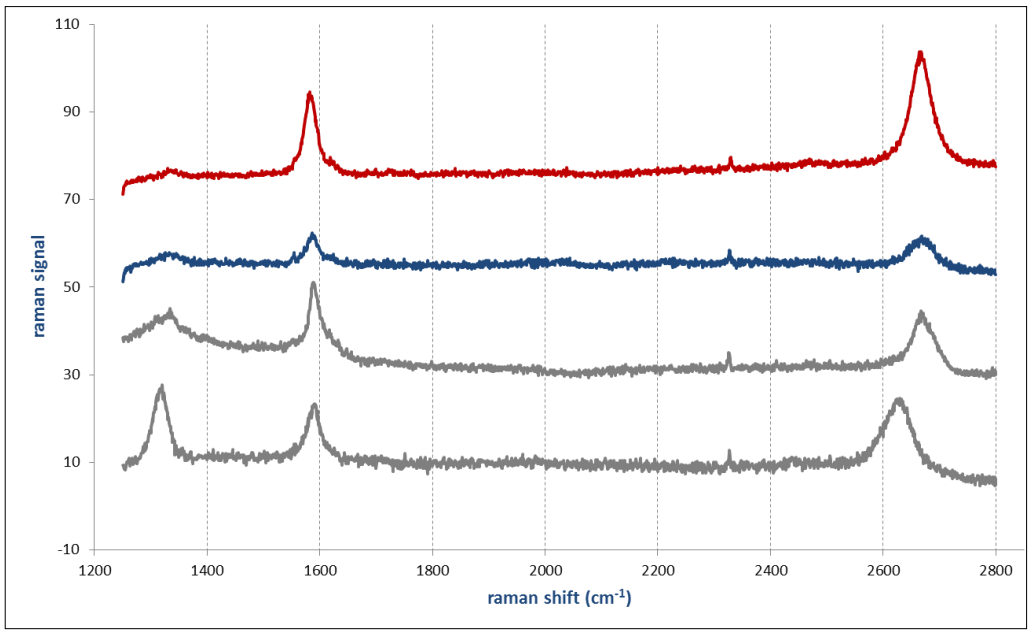

Figure 55 - In red the Type D graphene's Raman spectrum from high temperature chemical vapor deposition and methane as carbon precursor.

As previously explained, having noticed copper residues inside the quartz tube and on the surface of the deposited (or even just annealed) substrate, led to think about two possible occurring phenomena:

- Copper diffusion through ruthenium grain boundaries
- Evaporation and recondensation of copper from the exposed back side to the top side

The first phenomena can be possible since at high temperature ruthenium rearrange its grains, and diffusion inside them is not taken in consideration since the diffusion kinetic at grain boundaries is much higher than through the grain itself, and also because of the previously discussed immiscibility between the two elements. The second phenomenon is due to the fact that at temperature this close to copper Tm and at pressures this low, it can occur evaporation of the element. To exclude or somehow reduce this second effect were designed and developed Type D samples, which would prevented back side evaporation through a ruthenium diffusion barrier. The validation and quantification of this barrier effect is discussed in following paragraphs, here is just illustrated the deposition

outcome in terms of quality of graphene on Type D substrates. As can be seen in the graph above (Figure 55), the red curve represents the Raman spectra of graphene deposited on a Type D substrate (copper between two ruthenium layers). The first peak at 1300 cm-1 is the D peak relative to the defectiveness of graphene, which is almost irrelevant. At Raman shift of approximately 1600 cm-1 the G peak is considerably less intense than the 2D peak (last peak at around 2700 cm-1). This lead to the conclusion that Type D graphene spectrum is related to the best graphene yet deposited, with the lowest defect density and an amount of layers that can be reasonably said to be not more than two or even a high quality graphene monolayer.

It is noticeable in every Raman spectrum a small and sharp peak always located at about 2300 cm-1, which is not related with the graphene or the substrate, being recorded in every measurement with every sample even not related with this work, it can arise from a defect in the machinery or an external influence (probably artificial room illumination).

In the next paragraph Figure 56 shows that the resulting graphene quality varies with the location on the substrate and can even be improved.

4.3.5 Dependence of Raman spectra from position and strain

As stated above, the Raman spectra of all substrates taken in consideration for the previous graphs are somehow representative of the average graphene quality achieved for every sample, to show that, in Figure 56 is illustrated a comparison among three different *Type D* graphene's spectra. All three curves come from the same sample in three different areas, and is immediately noticeable that graphene can achieve high quality through the whole sample reaching a particularly high quality in the case of position 1 spectrum. Was not noticed particular tendencies about relations between position on the sample and quality of the graphene and this issue was not further investigated. What is worthy of attention is though the fact that while in Figure 55 there is not a precise alignment among the four spectra (particularly noticeable the positions of the various 2D peaks), there is instead an appreciable superposition among the three spectra obtained from the same substrate (Figure 56).

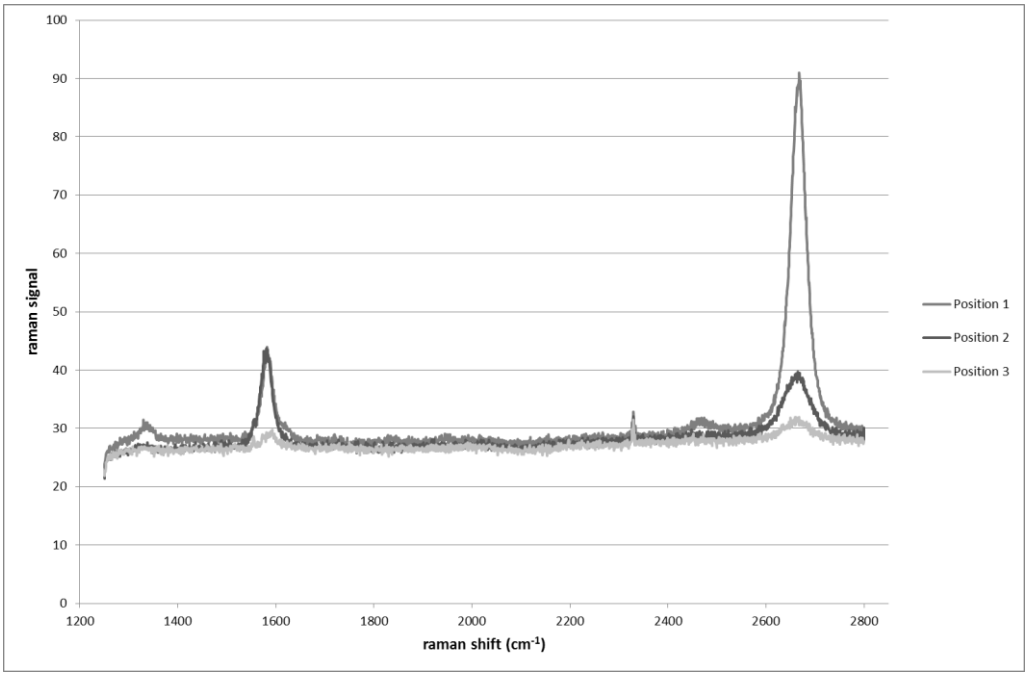

Figure 56 - Comparison among various graphene's Raman spectra from different position on the same Type D sample.

This particular effect has been already noticed [45] and is related to the fact that graphene can undergo to strain during its growth and remain in a stressed state. The carbon bond is therefore subject to elongation or shortening depending to the sign of the strain (tension or compression) and produce a shift in the position of the peak. It is not likely that (despite electroformed substrates are subject to relatively high levels of residual stresses) the shift is due to this phenomenon, since high annealing temperatures can easily cancel residual stresses. If graphene subjected to Raman spectroscopy comes from a unique sample, the strain level can be considered constant through the whole surface, allowing therefore a good alignment among the peaks of the different spectra.

4.4 XPS ANALYSIS

As already explained, in order to stop the inevitable evaporation-condensation of copper, *Type D* samples were developed without exposed copper to the high temperature and low pressure environment inside the reaction chamber. X-ray Photoelectron Spectroscopy was therefore performed specifically to study the amount of copper and ruthenium present at the top surface of the samples after the annealing. The measurement process was executed on *Type A*, *Type D* and on a

sample not subjected to previous annealing. Precisely, was tested a *Type A* sample, despite this distinction has no practical meaning since the two sensed substrates are equivalent on the main surface before the annealing process. This process was performed setting the following parameters:

- Temperature at 1000°C
- Pressure at $2 \cdot 10^{-3}$torr
- 10 sccm of hydrogen
- 20 sccm of methane
- Annealing time 5 minutes
- Deposition time 10 minutes

Basically was performed a regular high temperature chemical vapor deposition in order to maintain the same conditions at the surface as if was performed a deposition aimed to graphene growth.

A typical XPS technique allows to study the surface of the samples because of its really low scanning depth of approximately 1nm to 10nm. As expected, the elements detected with X-ray photoelectron spectroscopy were copper, ruthenium and carbon (the amount of carbon on the sample is not reliable or removable, because it can come both from the graphene on the top of the sample and from the environment despite accurate cleaning). The crucial point was though to know the ratio between Cu and Ru on the surface of the samples, which only depends on the type of substrate, temperature and annealing time, and not from the presence or absence of graphene deposition process during the permanence at high temperature. The obtained spectra are shown in Figure 57 (sample which did not undergo to annealing) and Figure 58 (comparison between annealed *Type A* and *Type D* samples).

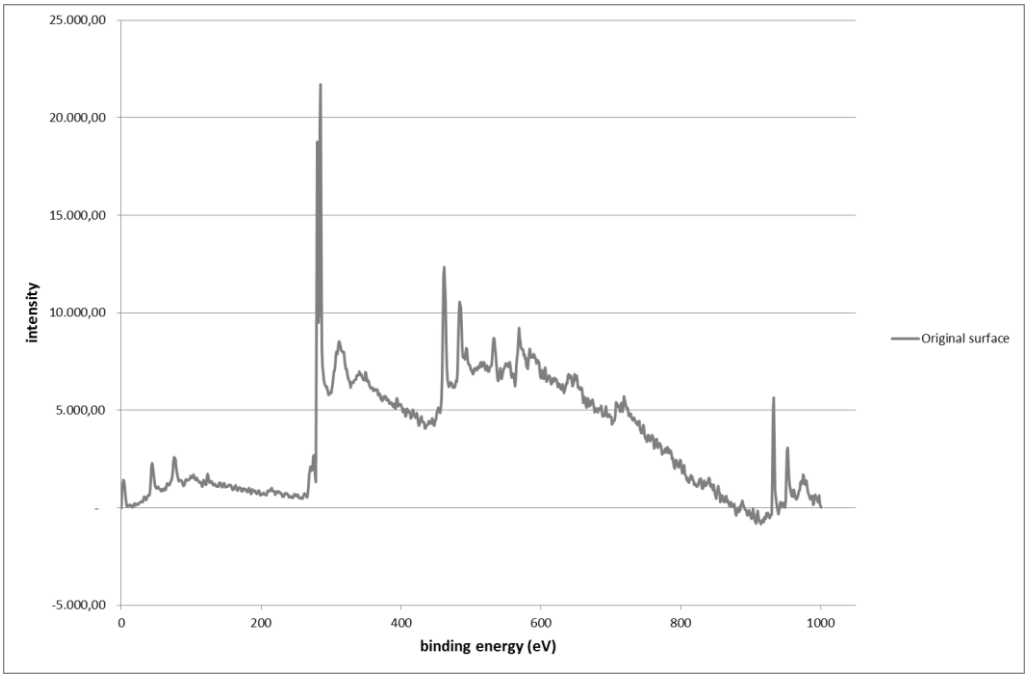

Figure 57 - XPS measurement of an original Type A or Type D electrodeposited substrate before annealing.

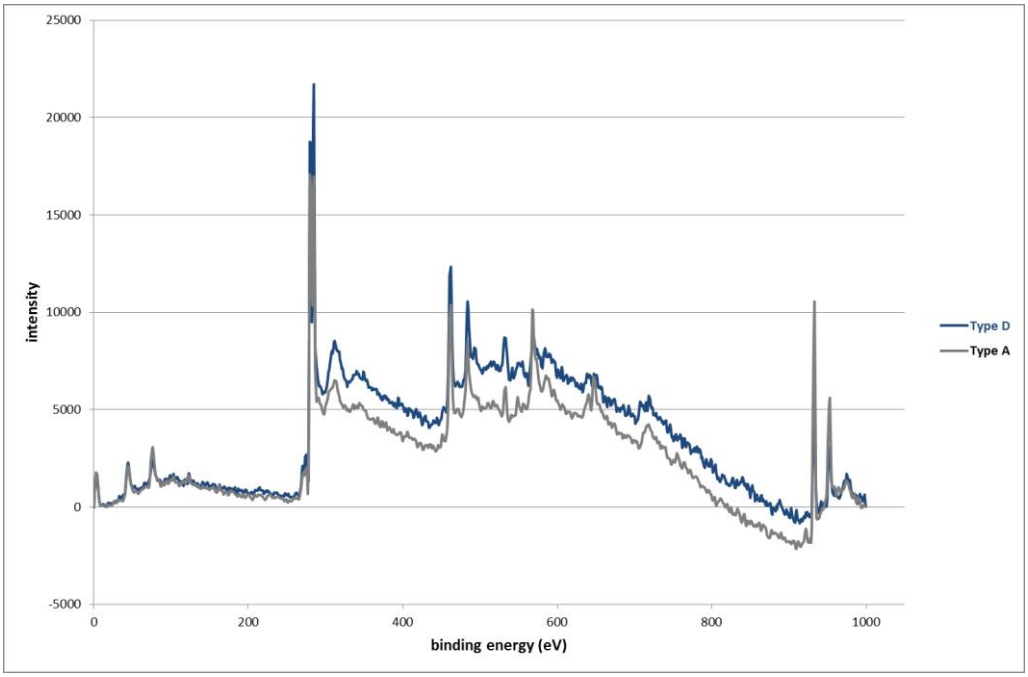

Figure 58 -Ccomparison between XPS diagrams of Type A and Type D samples after graphene growth; peaks at 280 eV belongs to Ru, at 285 eV and 284 eV belong respectively to C and Ru (superposition), and peaks at 933 eV and 953 eV come from Cu.

These graphs show peaks at 280 eV belonging to ruthenium, at 285 eV and 284 eV belonging respectively to carbon and ruthenium (these peaks are basically

superposed), and peaks at 933 eV and 953 eV coming again from copper. A magnification of these peaks from *Type A* and *Type D* samples is shown in Figure 59 and Figure 60.

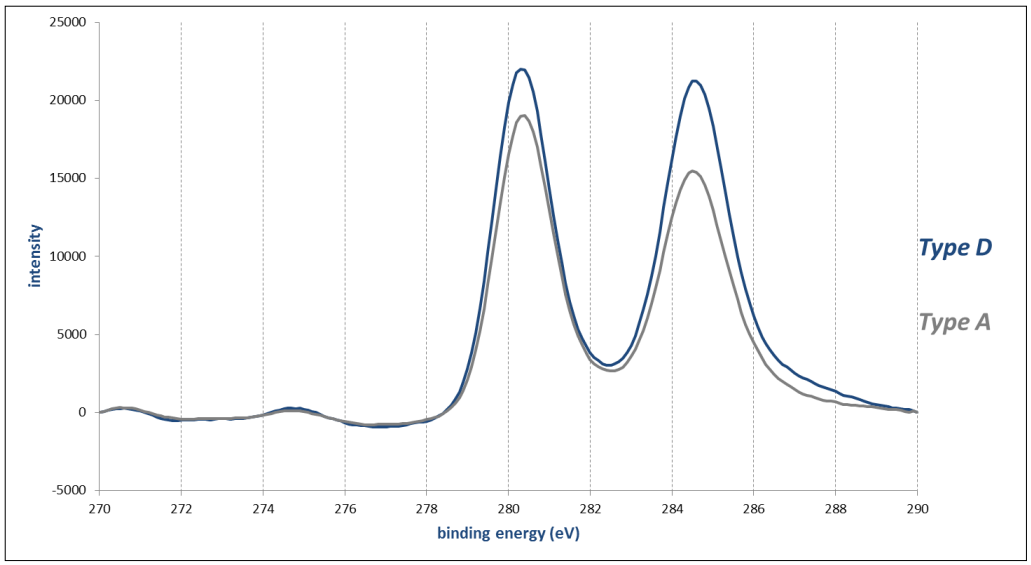

Figure 59 - Comparison between XPS diagrams of Type A and Type D samples after graphene growth, magnification of ruthenium and carbon peaks.

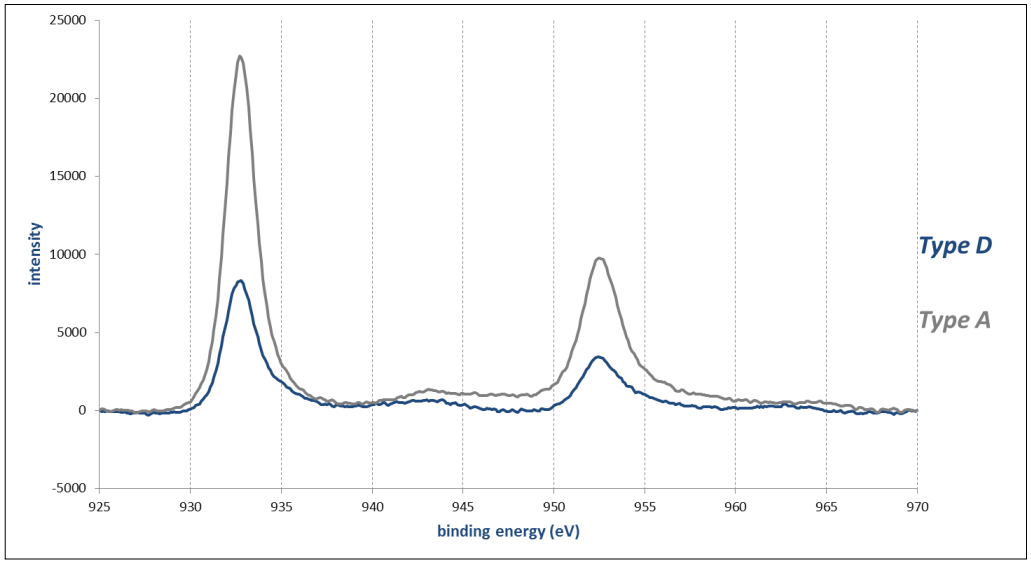

Figure 60 - Comparison between XPS diagrams of Type A and Type D samples after graphene growth (magnification of copper peaks).

The approximate composition of the surface can be then determined by dividing the individual peak areas (after appropriate background subtraction) by their respective atomic sensitivity factor (constant values related to each element's peak). The superposition between carbon (285 eV) and ruthenium (284 eV) peaks

is easily overcome since it exists a specific and unique relation (tabulated as for the sensitivity factors) among the areas of each peak of the same element. Knowing therefore the area of another Ru peak (the one placed at 280 eV) is possible to obtain the expected intensity for the peak at 284 eV and subtracting it from the total area, is easy to also find the intensity of the carbon peak at 285 eV.

Using these atomic sensitivity factors, the percentage quantity of copper and ruthenium (and carbon) on the surface of the sample was roughly estimated. Once the total composition of the substrate is known (Figure 62), a Ru-Cu ratio for each type of sample can be calculated (Figure 61).

	Not annealed	***Type A***	***Type D***
% Cu	6,93	22,35	16,48
% Ru	21,93	20,50	36,24
% C	71,14	57,15	47,28
Ru/Cu ratio	**3,16**	**0,92**	**2,20**

Figure 61 - Elemental percentage and highlighted Ru/Cu ratios for not annealed, type A and type D samples from XPS analysis.

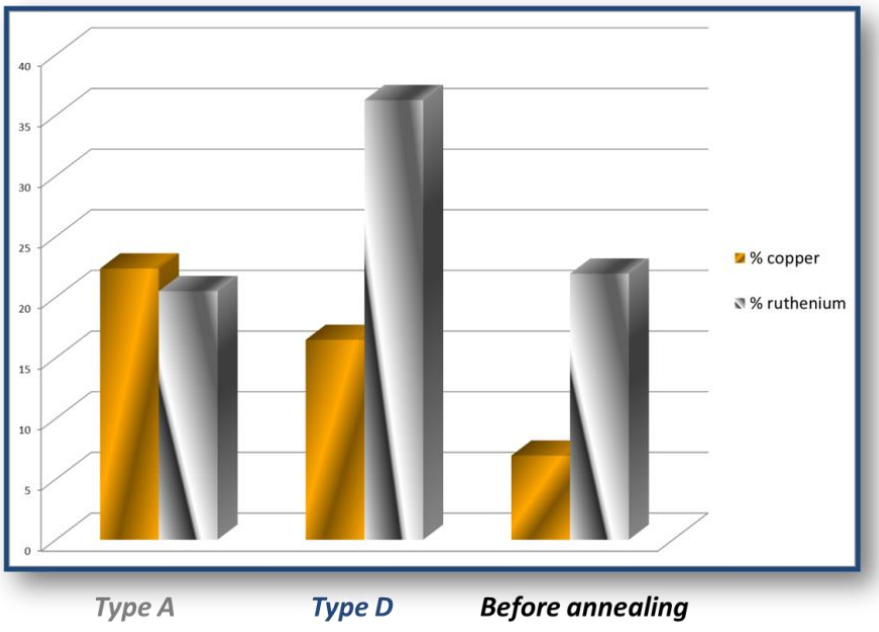

Figure 62 - Amount of copper and ruthenium in percentage on the surface of the various substrates.

A better graphical visualization in Figure 62 and the table above, can help to understand and prove the role of the ruthenium barrier against copper diffusion. As expected, the higher Ru-Cu ratio value is on the surface of the not annealed

sample that was not subjected to high temperatures and therefore copper diffusion through the ruthenium layer. *Type A* sample has the lowest value of Ru-Cu ratio because of the combined action of evaporation-recondensation from the not covered copper back side and grain boundary diffusion. These phenomena can indeed bring copper to the surface at the same time from the back and the core of the sample. An intermediate value of the Ru-Cu ratio was found in the *Type D* sample thanks to the blocking action performed by ruthenium to the detriment of evaporation-recondensation phenomena, thus the only mechanism left to increase the amount of copper on the surface of the substrate has to be grain boundary diffusion.

4.5 Sem analysis

To complete the work, on *Type A* and *Type D* samples was performed a SEM analysis (from Figure 63 to Figure 66) that shows the various substrates at various degrees of magnification after graphene deposition. In both cases graphene layer appears homogeneous and the surface shows particularly evident bulges on *Type A* substrate (average size of approximately 20 µm) probably because of the presence of larger amount of copper on the surface of these samples. On the contrary, the surface of *Type D* substrate shows much smaller bulges probably due to the fewer amount of copper covering the surface during the deposition process. It is even possible to notice traces of grooves forming the typical pattern coming from mechanical polishing of the electroformed copper.

Having noticed two brighter spots on the part to the lower right of Figure 63, was performed an EDX analysis to investigate the nature of these entities (Figure 67). With the term EDX spectroscopy (Energy Dispersive X-ray Analysis) or EDS spectroscopy (Energy Dispersive X-ray Spectrometry) is indicated an analytical methodology which exploit the emission of an X-ray beam hitting the sensed sample. This analysis is usually integrated in the SEM procedure and was used to determine the relative quantity of carbon on the surface of the substrate. The red curve represent the amount of carbon found on the substrate of *Type A* sample on the section of substrate denoted by the yellow line. The high amount of carbon at

the correspondence of the two bright spot led to think about the possibility of graphitic domains or organic impurities carbonized on the surface of the sample after high temperature deposition.

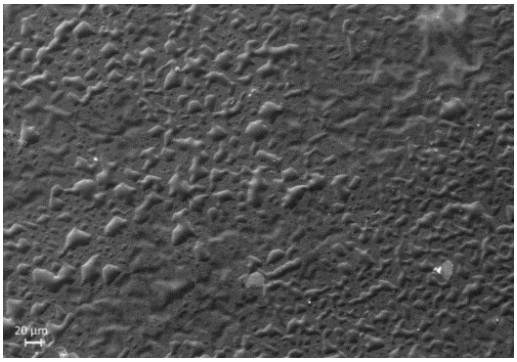

Figure 63 - SEM image of Type A sample showing the substrate after graphene deposition.

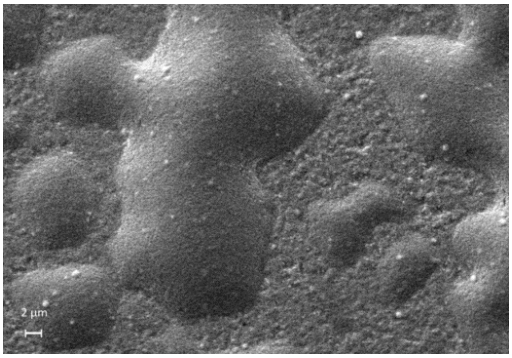

Figure 64 - SEM image of Type A sample displaying a magnification of the substrate after graphene deposition.

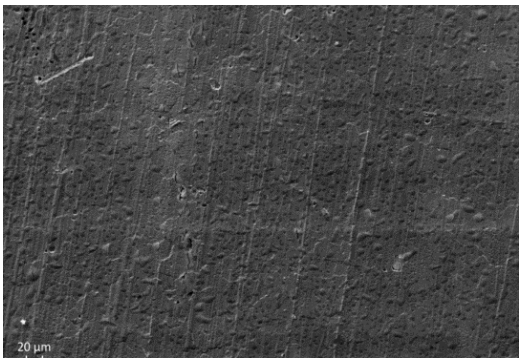

Figure 65 - SEM image of Type D sample showing the substrate after graphene deposition.

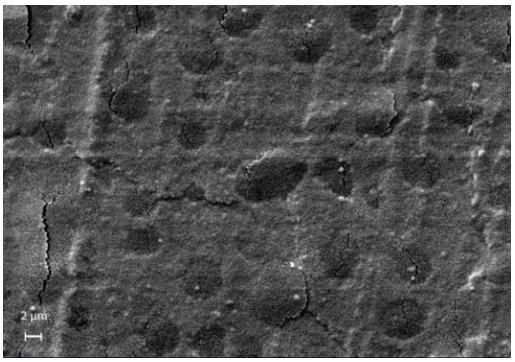

Figure 66 - SEM image of Type D sample showing a magnification of the substrate after graphene deposition.

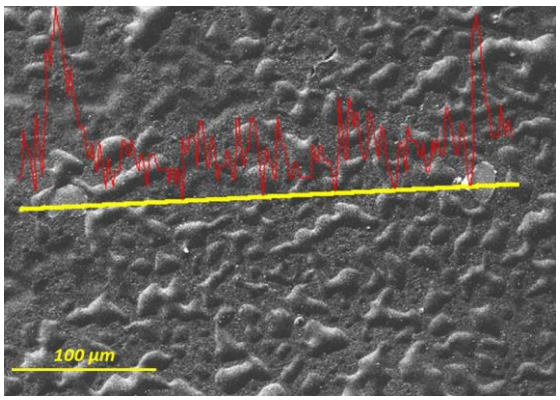

Figure 67 - EDX spectroscopy of the lower right part of a SEM image of Type A sample.

4.6 XRD ANALYSIS

Another characterization technique performed at Politecnico di Milano on the obtained samples was XRD. In X-ray diffraction analysis a sample is hit by a planar monochromatic X-ray wave varying gradually the impingement angle, then the diffracted signal is collected after the collision with the substrate. Diffraction effects are observed when crystalline and molecular structures are exposed to an electromagnetic radiation and phenomena like constructive and destructive interferences may arise. Constructive interference conditions are the basis to understand a diffraction pattern and are given by Bragg's law:

$$2d \sin \theta b = n\lambda$$

where $\boldsymbol{\lambda}$ is the wavelength of the X-ray, $\boldsymbol{d}$ the crystal lattice spacing, $\boldsymbol{\theta}$ the impingement angle and $\boldsymbol{n}$ is an integer number. In XRD therefore, a set of crystallographic lattice planes with distances $\boldsymbol{d_{hkl}}$ is irradiated by plane wave with a determined impingement angle. The subsequent phase shift of the wave depends on the configuration of the atoms inside the crystal and in order to obtain constructive interference, this conformation has to be a multiple number of the wavelength. It is therefore possible to determine the composition of a crystalline sample observing its diffraction pattern and knowing the wavelength of the X-rays used. In Figure 68 the working principle of the most common scanning procedure, the $\theta/2\theta$ scan, is exposed.

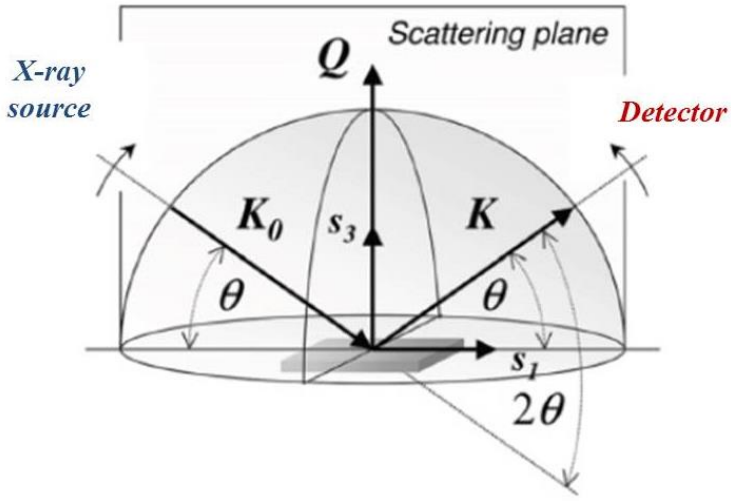

Figure 68 - Schematic representation of a θ/2θ scan.

In this configuration the sample is placed at the center of the instrument and the probing X-ray beam is directed to the sample surface at an angle $\boldsymbol{\theta}$. At the same angle (on the opposite side) the scattered radiation is monitored by the detector. The sample coordinate vectors $\boldsymbol{s_1}$ and $\boldsymbol{s_3}$ lie in the scattering plane defined by $\boldsymbol{K_0}$ and $\boldsymbol{K}$. During the scan the angle of the incoming and exiting beam are continuously varied, but they remain identical to each other throughout the whole scan in order to continuously collect the diffracted beam. the quantity measured throughout the monitoring is the intensity of the scattered beam entering the detector. The results are typically presented as a function of intensity and (2θ). As for our case, the sample was analyzed using $\boldsymbol{k_{alpha\ 1}}$ radiation with wavelength of 1,54Å, and the obtained XRD pattern is shown in Figure 69 and Figure 70. As presented, only ruthenium and copper peaks are detected in the two sample's spectra and no carbon peaks, therefore no graphitic peaks were detected for the analyzed samples, confirming again the fact that the chemical vapor deposited graphene was actually less than 10 layers, which is the lowest number of lattice planes needed for graphene in order to have a diffraction peak through XRD.

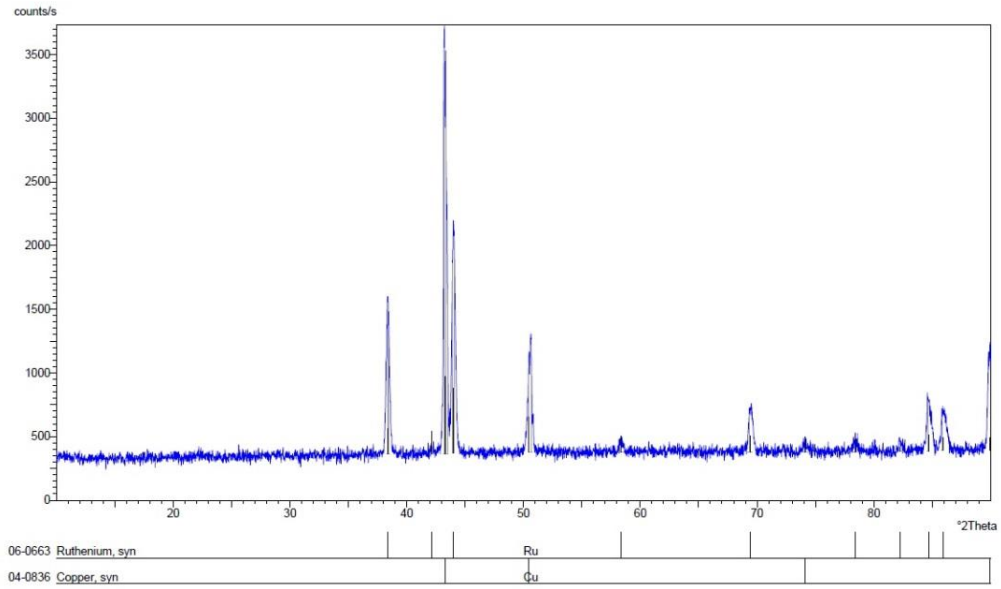

Figure 69 - XRD analysis of a Type A sample previously subjected to high temperature chemical vapor deposition of grapheme.

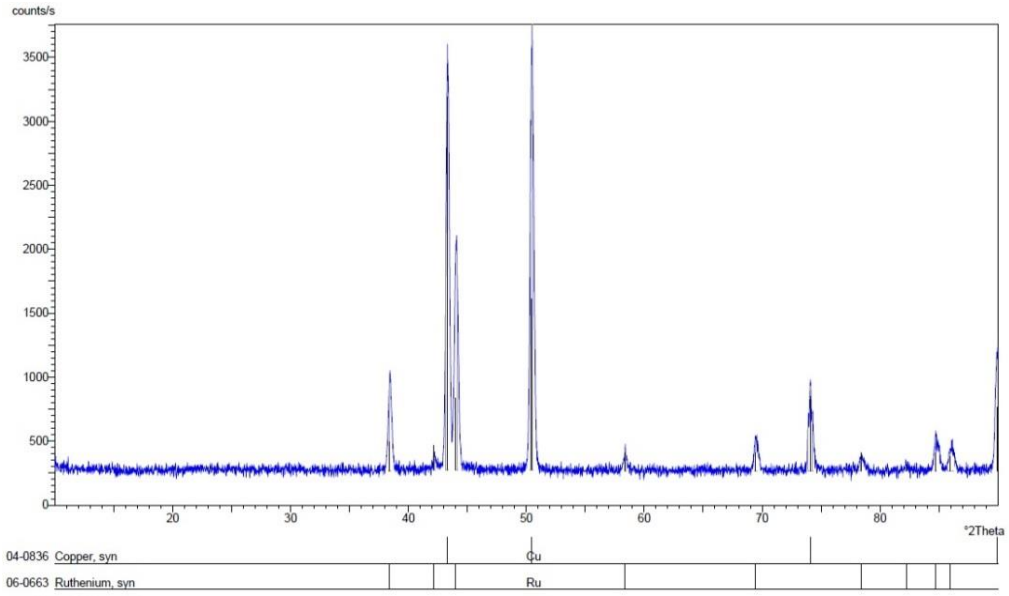

Figure 70 - XRD analysis of a Type D sample previously subjected to high temperature chemical vapor deposition of grapheme.

4.7 Final discussion

In conclusion these depositions and characterizations proved in first place that it is possible to grow graphene on an electrodeposited substrate, as stated by Raman measurement. Furthermore is possible to achieve a high graphene quality from *Type D* substrates. To explain this effect were obtained Ru-Cu ratios from surfaces of different substrates, since it is plausible that copper could somehow have an effect on graphene quality. *Type A* sample showed the lowest ratio because of the combined action of evaporation-recondensation and the grain boundary diffusion. These phenomena can indeed add copper to the surface from the back and from the core of the sample. An intermediate value of the Ru-Cu ratio was found in the *Type D* sample because of the prevention (or sensible reduction) of the copper evaporation from the back side, thus the only mechanism left to increase the amount of Cu on the surface of the substrate had to be grain boundary diffusion. A theory that could therefore explain the better quality of graphene on *Type D* sample must be related to the presence, the amount and the morphology of copper at the surface of the substrate. Since *Type B* (electroformed copper) and *Type C* (ruthenium on silicon oxide) presented lower quality graphene on their surfaces, the key is a combined effect between copper and

ruthenium. It is probable that after interdiffusion, once the copper has reached the surface of the sample, it is arranged in a more orderly way and can promote a good quality graphene growth acting as nucleation center for its growth [46]. Copper present at the surface coming from evaporation and redeposition though, may not have this particular effect, since *Type D* samples have a better quality graphene (better ratio between G and 2D peaks) despite a minor amount of copper on the surface. It is then likely that copper coming from evaporation-recondensation is less ordered and slightly masks the effect of Cu from grain boundary diffusion and this can lead to a slightly worse quality graphene after the deposition process on *Type A* samples.

5 CONCLUSION

The work presented in this thesis has been developed in two different stages at two different laboratories, respectively at the Department of Chemistry, Materials and Chemical Engineering "G. Natta" of the Politecnico of Milan and at the Department of Chemical and Biomolecular Engineering of the University of California, Berkeley.

This project was inspired by the recent developments in nanotechnological field, focusing on the wide applications that an exceptional material like graphene could have. Despite intensive studies on graphene for the past ten years, only few technologies are at the current day available for an industrial scale production. The goal of this thesis work was therefore to develop a suitable and cheaper fabrication process that could lead to final product whit adequate quality.

The first part was dedicated to the development of the substrates for the graphene growth. A two-step process produced a first samples typology (Type A) via electroforming of a copper foil on a steel substrate and, previous detachment, an electrodeposition of ruthenium on the obtained Cu substrate. During the progression of the work, were developed a total of four samples' typologies in order to investigate the mutual influence of copper and ruthenium on the graphene growth. Summarizing, were produced an electroformed copper layer covered on

one side by electrodeposited ruthenium (Type A), a simple electroformed copper substrate (Type B), an electrodeposited ruthenium substrate on silicon dioxide (Type C) and an electroformed copper substrate enclosed in electrodeposited ruthenium (Type D).

During the second stage of the project, was faced the crucial subject of graphene growth. The first attempts performing low temperature chemical vapor deposition were unsuccessful. This led to the development of an high temperature CVD which gave much better results, having recorded the presence of graphene. As the deposition process was tuned, has been also possible to increase the quality of the obtained graphene covering the back side of Type A samples with ruthenium in order to avoid excessive presence of copper on the surface through evaporation-recondensation phenomena (Type D substrates). The definitive deposition setting consisted in high temperature CVD at 1000°C with methane as carbon source.

The obtained specimens were characterized by means of Raman spectroscopy, XPS, SEM and XRD. This characterization techniques revealed the possibility of depositing high quality graphene via CVD process on electrodeposited ruthenium on electroformed copper substrate. Specifically was observed that a high quality in the deposited graphene layer can be reached thanks to grain boundary diffusion of copper through the ruthenium layer. An explanation for this effect has been proposed, and relates the presence of highly ordered copper spots coming from the diffused material to the quality of graphene. These high ordered domains can subsequently act as nucleation centers for the growth of a homogeneous graphene layer on the whole substrate.

In conclusion, this thesis work proposes a reliable and cheap graphene deposition process that, if implemented, could eventually lead to applications in industrial graphene synthesis.

REFERENCES

[1] A. Lavoisier, "Traité Élémentaire de Chimie."

[2] "The Noble prize in physics 2010," *The Nobel foundation*.

[3] H. Boehm, R. Setton, and E. Stumpp, "Nomenclature and terminology of graphite intercalation compounds," *Pure and appl. chem.*, vol. 66, no. 9, pp. 1893–1901, 1994.

[4] H. P. Boehm, A. Clauss, G. O. Fischer, and U. Hofmann, "Das Adsorptionsverhalten sehr dunner Kohlenstoff-Folien," *Zeitschrift fur anorganische und allgemeine Chemie*, vol. 316, no. 3–4, pp. 119–127, Jul. 1962.

[5] J. F. M. Gmitra, S. Konschuh, C. Ertler, C. Ambrosch-Draxl, "Band-structure topologies of graphene : Spin-orbit coupling effects from first principles," *Phys. Rev.*, no. December, 2009.

[6] P. Phillips, "Mottness," *Annals of Physics*, vol. 321, no. 7, p. 1650.

[7] A. K. Geim and A. H. Macdonald, "Graphene : Exploring carbon flatland".

[8] B. T. Kelly, "Physics of graphite," p. 477, 1981.

[9] A. K. G. A.H. Castro Neto, F. Guinea, K.S: Novoselov, "The electronic properties of graphene."

[10] Morozov, K.S. Novoselov, M.I. Katsnelson, F. Schedin, D.C. Elias1, J.A. Jaszczak, "Giant Intrinsic Carrier Mobilities in Graphene and Its Bilayer."

[11] S. Mikhailov and P. Intech, "Physics and Applications of Graphene - Theory," p. 5772, Mar. 2011.

[12] G. and M. D. Ado Jorio, Riichiro Salta, "Raman spectroscopy in graphene related systems," *Wiley-VCH Verlag GmbH & Co., Germany*, 2011.

[13] Eric Pop, Vikas Varshney, "Thermal properties of graphene: Fundamentals and applications," *MRS Bull.*, vol. 37, p. 1273, 2012.

[14] Y. Zhang, J. P. Small, W. V. Pontius, and P. Kim, "Fabrication and electric-field-dependent transport measurements of mesoscopic graphite devices," *Applied Physics Letters*, vol. 86, no. 7, p. 073104, 2005.

[15] P. Blake, B. Pd, N. Rr, B. Tj, D. Jiang, F. Schedin, P. La, and M. Sv, "Graphene-based liquid crystal device.," vol. 8, no. 6, p. 80649, 2008.

[16] Hernandez Y, Nicolosi V, Lotya M, Blighe FM, Sun Z, De S, "High-yield production of graphene by liquid-phase exfoliation of," vol. 3, no. 9, 2008.

[17] M. Lotya, Y. Hernandez, K. Pj, S. Rj, V. Nicolosi, K. Ls, B. Fm, Z. Wang, D. Gs, and C. Jn, "Liquid phase production of graphene by exfoliation of graphite in surfactant / water solutions" vol. 131, no. 10, p. 807449, 2009.

[18] X. Li, G. Zhang, X. Bai, X. Sun, X. Wang, E. Wang, and H. Dai, "Highly conducting graphene sheets and Langmuir-Blodgett films .," vol. 3, no. 9, 2008.

[19] W. S. H. J. and R. E. Offeman, "Preparation of Graphitic Oxide," *Journal of the American Chemical Society*, vol. 80, no. 6, 1958.

[20] Stankovich S, Dikin DA, Piner RD, Kohlhaas KA, Kleinhammes A, Jia Y, "Synthesis of graphene-based nanosheets via chemical reduction of exfoliated graphite oxide," *Carbon*, no. January, 2007.

[21] S. Stankovich, R. D. Piner, X. Chen, N. Wu, S. T. Nguyen, and R. S. Ruoff, "Stable aqueous dispersions of graphitic nanoplatelets via the reduction of exfoliated graphite oxide in the presence of poly(sodium 4-styrenesulfonate)," *Journal of Materials Chemistry*, vol. 16, no. 2, p. 155, 2006.

[22] H. B. Wang JJ, Zhu MY, Outlaw RA, Zhao X, Manos DM, "Synthesis of carbon nanosheets by inductively coupled radio-frequency plasma enhanced chemical vapor deposition," *Carbon*, vol. 42, no. 14, p. 2872, 2004.

[23] J. Hass et al, "The growth and morphology of epitaxial multilayer graphene," *J. Phys.: Condens. Matter*, vol. 20, p. 323202, 2008.

[24] F. Varchon, R. Feng, J. Hass, X. Li, B. N. Nguyen, C. Naud, P. Mallet, J.-Y. Veuillen, C. Berger, E. H. Conrad, and L. Magaud, "Electronic structure of epitaxial graphene layers on SiC: effect of the substrate.," *Physical review letters*, vol. 99, no. 12, p. 126805, Sep. 2007.

[25] K. Nakada, M. Fujita, G. Dresselhaus, and M. Dresselhaus, "Edge state in graphene ribbons: Nanometer size effect and edge shape dependence.," *Physical review. B, Condensed matter*, vol. 54, no. 24, pp. 17954–17961, Dec. 1996.

[26] X. Li, X. Wang, L. Zhang, S. Lee, and H. Dai, "Chemically derived, ultrasmooth graphene nanoribbon semiconductors.," *Science (New York, N.Y.)*, vol. 319, no. 5867, pp. 1229–32, Feb. 2008.

[27] D. V. et al Kosynkin, "Longitudinal unzipping of carbon nanotubes to form graphene nanoribbons," *Nature*, vol. 458, p. 872, 2009.

[28] L. Jiao, L. Zhang, X. Wang, G. Diankov, and H. Dai, "Narrow graphene nanoribbons from carbon nanotubes .," vol. 458, no. 7240, p. 7919, 2009.

[29] J. Cai, P. Ruffieux, R. Jaafar, M. Bieri, T. Braun, S. Blankenburg, M. Muoth, A. P. Seitsonen, M. Saleh, X. Feng, K. Müllen, and R. Fasel, "Atomically precise bottom-up fabrication of graphene nanoribbons.," *Nature*, vol. 466, no. 7305, pp. 470–3, Jul. 2010.

[30] R. S. E. and K. S. Coleman, "Graphene Film Growth on Polycrystalline Metals," *Accounts of Chemical Research*, vol. 46, 2013.

[31] J. H. Zhancheng Li, Ping Wu, Chenxi Wang, Xiaodong Fan, Wenhua Zhang, Xiaofang Zhai, Changgan Zeng, Zhenyu Li, Jinlong Yang, "Low-Temperature Growth of Graphene by Chemical Vapor Deposition Using Solid and Liquid Carbon Sources," *ACS Nano*, vol. 5, no. 4, p. 3390, 2011.

[32] Z. L. Wei Chen, Zhongli Fan, Gaofeng Zeng, "Layer-dependent supercapacitance of graphene films grown by chemical vapor deposition on nickel foam," *Journal of power sources*, vol. 225, no. March, p. 251, 2013.

[33] M. U. Prakash R. Somani , S. P. Somani, "Planer nano-graphenes from camphor by CVD," *Chemical Physics Letters*, vol. 430, 2006.

[34] X. Li, W. Cai, L. Colombo, and R. Rs, "Evolution of graphene growth on Ni and Cu by carbon isotope labeling" vol. 9, no. 12, p. 902515, 2009.

[35] H. Stelter, M. and Bombach, "Process Optimization in Copper Electrorefining," *Adv. Eng. Mater.*, vol. 6, pp. 558–562, 2004.

[36] A. Oriani, "Synthesis of indium phosphide for thin film solar cells," *Department of Chemistry, Materials and chemical engineering "G. Natta", Politecnico of Milan*, 2012.

[37] Y. H. Helen H. Lou, "Electroplating," *Encyclopedia of Chemical Processing*, 2013.

[38] H. Okamoto, "Cu-Ru (copper-ruthenium) phase diagram," *Journal of Phase Equilibria*, vol. 13, no. 4, pp. 440–440, Aug. 1992.

[39] J. H. Sinfelt, "Ruthenium-copper: a model bimetallic system for studies of surface chemistry and catalysis," *International Reviews in Physical Chemistry*, vol. 7, no. 4, 1988.

[40] C. Miao, C. Zheng, O. Liang, and Y. Xie, "Chemical Vapor Deposition of Graphene," no. Figure 2, 2009.

[41] C. Mattevi, H. Kim, and M. Chhowalla, "A review of chemical vapour deposition of graphene on copper," *Journal of Materials Chemistry*, vol. 21, no. 10, p. 3324, 2011.

[42] C. Ferrari, J. C. Meyer, V. Scardaci, C. Casiraghi, M. Lazzeri, F. Mauri, S. Piscanec, D. Jiang, K. S. Novoselov, S. Roth, and a K. Geim, "Raman spectrum of graphene and graphene layers.," *Physical Review Letters*, vol. 97, no. 18, p. 187401, Oct. 2006.

[43] M. O. Brien and B. Nichols, "CVD Synthesis and Characterization of Graphene Thin Films," *Sensors Peterborough NH*, vol. TR, no. January, p. 5047, 2010.

[44] P. W. Sutter, J.-I. Flege, and E. a Sutter, "Epitaxial graphene on ruthenium.," *Nature Materials*, vol. 7, no. 5, pp. 406–411, May 2008.

[45] T. Mohiuddin, A. Lombardo, R. Nair, A. Bonetti, G. Savini, R. Jalil, N. Bonini, D. Basko, C. Galiotis, N. Marzari, K. Novoselov, A. Geim, and A. Ferrari, "Uniaxial strain in graphene by Raman spectroscopy: G peak splitting, Grüneisen parameters, and sample orientation," *Physical Review*, vol. 79, no. 20, May 2009.

[46] J. Wintterlin and M. L. Bocquet, "Graphene on metal surfaces," *Surface Science*, vol. 603, no. 10–12, pp. 1841–1852, Jun. 2009.

TABLE OF FIGURES